Technische Universität Chemnitz

Sonderforschungsbereich 393

Numerische Simulation auf massiv parallelen Rechnern

Andrea Eppler

Klaus Bernert

Two-Stage Testing of Advanced Dynamic Subgrid-Scale Models for Large-Eddy Simulation on Parallel Computers

Preprint SFB393/99-13

Preprint-Reihe des Chemnitzer SFB 393

SFB393/99-13 **Juli 1999**

Contents

Authors' address:

Andrea Eppler
Klaus Bernert
TU Chemnitz
Fakultät für Mathematik
D-09107 Chemnitz

http://www.tu-chemnitz.de/sfb393/

Two-Stage Testing of Advanced Dynamic Subgrid-Scale Models for Large-Eddy Simulation on Parallel Computers

Andrea Eppler and Klaus Bernert

Chemnitz University of Technology, Chemnitz, D-09107, Germany

Abstract

The investigations of the present work are intended to contribute to improvements in dynamic subgrid-scale (SGS) modelling for large-eddy simulation (LES) on high-performance parallel computers. Overall, thirteen SGS models, viz. nine dynamic-type closures proposed in this study along with four subgrid parametrizations known from the literature, have been tested numerically in a two-stage approach. The effects of varying filters and model parameters have been analyzed and, as a result, superior variants have been selected.

Starting from problems encountered in dynamic subgrid-scale modelling, refined closure principles are introduced, and advanced dynamic SGS models originating from algebraic Smagorinsky, scale-similarity and linear-combination types are presented which have been derived from a generalized use of the Germano identity at tensor and scalar levels. A distinctive feature of the subgrid parametrizations proposed in this paper consists in the formulation of localized space- and time-dependent model coefficients which are either assigned to the individual tensor components of the SGS stresses (generalized anisotropic models with component-specific coefficients) or which are determined as scalar coefficients from physically meaningful relations taking subgrid-scale dissipation into consideration (realizable single-coefficient model versions). In addition, the approximate localization approach due to Piomelli *et al.* [Phys. Fluids **7**, 839 (1995)] has been adopted in most of the subgrid closures suggested here.

These models, combined with spatial filters of several types and widths, have been studied comparatively in a systematic two-stage testing procedure for a fully developed turbulent pipe flow. Model performance has been assessed in comparison with each other and with the known SGS parametrizations as well as with published experimental and numerical pipe-flow data available.

The first stage of model evaluation comprises *a priori* tests of the closures using a direct numerical simulation (DNS) database. The test quantities cover not only subgrid terms at tensor, vector and scalar levels but also the individual terms of the Germano identity at these levels and energy fluxes between several ranges of scales to gain a more detailed insight into interscale energy transfer. The *a priori*-test results for all the proposed SGS models and particularly for the versions of scale-similarity and combined types with component-specific coefficients proved to be superior to those of the known subgrid parametrizations and were inspected to find model/filter combinations designated for further investigations.

As the second testing stage, actual finite-difference large-eddy simulations have been performed primarily for the last-mentioned model/filter combinations, and sensitivity to variations in input parameters has been examined. Backscatter, which has been observed in about a third of the total number of grid points, was identified to be a crucial problem of the LES computations. In the *a posteriori* tests, the best predictive capability of all SGS closures implemented was established for the generalized anisotropic Smagorinsky-type model with coefficient clipping, whereas the scale-similarity and mixed models gave acceptable LES predictions of statistical first- and second-order one-point moments of the GS velocity field only if applied in conjunction with imposed backscatter limitations.

Among the employed filters of physical-space top-hat and spectral sharp-cutoff types, discrete top-hat kernels and especially approximations by means of Simpson's rule resulted in the overall closest agreement with the relevant comparative data in both testing stages.

I Introduction

Large-Eddy Simulation (LES) has been developed into a promising and potentially powerful technique for flow modelling and numerical simulation, which is gaining increasing importance in computing technological and geophysical turbulent and transitional flows as well as in investigating the dynamics of large-scale structures.
The underlying principle of directly solving the basic equations of motion for the large-scale (grid-scale, GS) turbulence components while modelling the interactions between grid-scale and subgrid-scale (SGS) components is motivated not only by special features of large eddies and fine-scale turbulence but also by the progressive advancement of computer technology and high-performance scientific computing.
In numerous applications to a variety of flow types ranging from "building block flows" to fairly complex real-world problems, results of LES-based studies have indicated the need for further research concerning all aspects of the method, i. e. the averaging operation for GS/SGS decomposition, the subgrid-scale model, the grid system and numerical schemes as well as the sensitive balance between them.

The investigations of the present work contribute to the model and filter components of LES within the framework of the dynamic modelling approach. Starting from problems encountered in dynamic subgrid-scale modelling, which are addressed below, a number of advanced dynamic SGS models (closure hypotheses for the subgrid-stress tensor in the filtered equations of motion for incompressible fluids) are proposed in this paper. Combined with several spatial filters, these models have been subjected to a systematic two-stage testing procedure for a particular well-documented "building block flow" to evaluate their performance in comparison with each other and with known subgrid parametrizations. The complementary approaches of *a priori* and *a posteriori* testing have been applied here because the former, as the first stage, gave valuable indications of model performance and filter influence and was efficiently used to select those SGS closures to be primarily studied in the more expensive large-eddy simulations, which provided the ultimate tests. The two main objectives of this investigation are (i) to identify advantages and limitations of the proposed dynamic subgrid-scale parametrizations including the inherent modelling principles and (ii) to find out the superior model/filter combinations for further research and future LES applications.

Characteristics and Problems of Dynamic SGS Modelling

A large class of extremely appealing and potentially efficient "refined adaptive subgrid-scale models" [1] is represented by the dynamic SGS models due to Germano [2], [3]. Owing to the basic idea of dynamically evaluating spatially and temporally varying model coefficients adjusted to local instantaneous flow dynamics rather than *ad hoc* specifying fixed model constants, this approach to SGS modelling offers a great potential for accurately simulating a wide range of flow types. These cover statistically unsteady, nonequilibrium and strongly inhomogeneous turbulent as well as laminar, transitional and intermittent flows. In addition, near-wall flow behaviour and backscatter energy transfer, the simulation of which still presents considerable challenges, can be addressed.

Starting from the definition of a spatial grid-filtering operation and a second test filter at a generally coarser level, dynamic procedures take advantage of an algebraic relation between subgrid-scale stresses arising from the application of these filters – the well-known Germano identity (see Sec. II.B.1). This tensor equation relates the test-filtered subgrid-scale stresses, the subtest-scale stresses and the associated resolved turbulent stresses. When replacing the former two by SGS parametrizations, the model coefficients involved can be evaluated from the Germano identity. This basic concept to dynamically determine space- and time-dependent model coefficients by exploiting the information on the smallest resolved scales aims at subgrid-scale models of universal applicability. They are designed to overcome limits of performance of classical SGS models without considerably increasing the models' complexity.

The most common approach to dynamic modelling in the line of Germano is based on the direct application of the test filter with a fixed width and the straightforward use of the tensorial

Germano identity to solve for the model coefficients as functions of space and time. Alternatively, modified approaches including ensemble averaging [4], averaging along fluid-particle trajectories in a Lagrangian frame of reference [5], [6], [7], [8] or starting from Taylor series expansions of the test-filtered quantities in the Germano identity with taking the limit for the test-filter width tending to zero [9] have been suggested, too.

However, in developing dynamic modelling procedures especially within the framework of the original methodology [2] considered below, several assumptions have been incorporated which indicate problems, inconsistencies and the need for further investigations with respect to mathematical and physical foundations as well as numerical implementation. Subsequently, five problems (P1 – P5) are specified:

(P1) As a first hypothesis in deriving dynamic SGS closures, subgrid- and subtest-scale stresses have been parametrized by the same functional dependence on large-scale quantities. This includes model coefficients that are assumed to be the same at the two different filter levels the stresses are related to. Though not stringent for evaluating the Germano identity, this supposition has frequently been taken as a basis and has been justified by scale-invariance arguments [2], [9], [10], [11], [12], [13], which in turn are motivated by the presumption of a well-developed inertial range [14], [15]. Limitations of this approach may be relevant to applications with substantially different widths and/or types of the grid filter and the filter associated with the consecutive application of grid- and test-filtering operations [4], [9]. Several attempts to account for scale dependence in dynamic Smagorinsky-type models are outlined in [5] and [11]. Especially, generalized formulations with individual coefficients for the subgrid- and subtest-scale stresses have been suggested by Meneveau [11], Moin [16], [17] and Ronchi *et al.* [12]. Multiple-scale filtering can provide additional information on how model coefficients and errors depend on scale [13].
Concerning the filters involved, to ensure compatibility of dynamic procedures with the self-similarity assumption, in [14], a re-interpretation of the grid- and test-filtering operations has been presented which enforces self-similarity of grid and test$*$grid filters independently of the test-filter type.

(P2) A serious problem in using the Germano identity to evaluate the model coefficients results from the fact that they appear inside the integral convolution operators representing test filtering applied to the subgrid-scale stresses. So, this identity leads to a system of integral equations for the coefficients to be determined. For the purpose of reducing these integral relations to algebraic ones, in previous formulations [2], [18], the spatial variability of the model coefficients in the test-filtered subgrid-scale stresses has been neglected, and the coefficients have been taken out of the filtering operation as if they were constants. An *a priori* assessment of this assumption for particular SGS parametrizations was conducted in [10].
Ghosal *et al.* [19] pursued an approach in the context of a variational formulation implying the numerically iterative solution of the ensuing Fredholm's integral equation of the second kind to determine the coefficient field at each time step. Thereby they generalized the dynamic procedure to fully inhomogeneous flows.
As a computationally efficient treatment of the problem, Piomelli *et al.* [20] proposed to estimate the model coefficients in the test-filtered subgrid-scale stresses by approximate values from previous time steps (or iterations) of the numerical solution process. Their approximate localization procedure resulted in a localized model formulation of general applicability.

(P3) Depending on the number of coefficients to be calculated for the subgrid- and subtest-scale stress models from the Germano identity (and, if necessary, from additional conditions), problems may arise concerning their unique determination. Thus, evaluating this tensor equation for a scalar model coefficient gives rise to the overspecification problem. It has been solved by contracting the Germano identity with several second-order tensors [2], [18], [20], in the original work [2] without giving reasons, later on substantiated by a local least-squares error-minimization technique [18] as well as by means of a nonlocal generalization based on a variational approach [19]. In a few publications, e. g. [21], [22], the use of tensorial model coefficients has been recommended.

(P4) Up to now, dynamic models of Smagorinsky type have generally been subjected to the instability/singularity problem. Ill-conditioned behaviour of such models may be attributed to negative values of the resulting total viscosity (sum of molecular and SGS turbulence viscosities), to model coefficients that frequently change their sign and exhibit strong spatial and temporal fluctuations, particularly in connection with pointwise vanishing or small denominators in the expressions for the coefficients. The problem has been reduced by applying various global or local spatial (in some cases also temporal) averages to the model coefficient as a whole [23] or to its numerator and denominator separately for the purpose of numerical stabilization, for example averages in statistically homogeneous directions or over neighbouring grid cells in [2], [15], [22], [24], [25], [26], [27], [28], [29], [30], [31], [32]. In addition, error minimization of the Germano identity along fluid-particle trajectories has been used to establish a Lagrangian dynamic SGS model including the solution of additional differential equations [5], [6], [7], [8]. Moreover, *a priori* bounds (lower and upper ones e. g. in [33], [34]) have been specified for clipping the dynamic model coefficients. Specifically, the total viscosity has been constrained to be nonnegative [20], [21], [29], [31], [32], [35], [36], [37], [38]. Physically meaningful lower bounds have also been derived from an entropy condition imposed on the total dissipation (sum of viscous, SGS and numerical dissipations $\geqslant 0$) [34], [39] or within the framework of the constrained minimization procedure [19].

(P5) A central issue has been the modelling of backscatter from subgrid to grid scales. With respect to dynamic models of eddy-viscosity/Smagorinsky type, contrary to molecular viscosities, there exist no constraints following from the basic laws of thermodynamics for SGS turbulence viscosities to be nonnegative. However, backscatter-related numerical instabilities encountered in case of negative total viscosities, as discussed for example in [19], [40], [41], point out limitations and drawbacks of eddy-viscosity approaches, which remain to be further investigated. It is common practice to limit the amount of backscatter by enforcing the above-mentioned lower bounds to the SGS turbulence viscosity and, correspondingly, to the dynamic Smagorinsky-model coefficients.
Alternative approaches to the modelling of local instantaneous reverse energy transfer in the context of dynamic procedures have mainly been provided by SGS models of scale-similarity and mixed types [29], [42], [43], [44], [45], [46], with artificial backscatter control included in [47], by the addition of stochastic forcing terms [40], or by the use of differential transport equations for subgrid-scale turbulence energies [12], [19], [48].

Scope of the Present Work

Motivated by the advantages and the adaptive potential of dynamic modelling procedures on the one hand and by the problems and deficiencies of popular dynamic SGS parametrizations on the other hand, in the present paper, nine refined dynamic subgrid-scale models are suggested.

Within the framework of the standard dynamic modelling approach by means of applying a test filter of nonvanishing width and directly evaluating the Germano identity to determine the model coefficients, the proposed models aim at

- the computationally efficient solution of conceptual problems of this approach, viz. the treatment of model coefficients inside the integral test-filtering operation (P2), overspecification (P3), and the instability/singularity problem (P4),
- a flexible capturing of the anisotropy and of the near-wall behaviour of the SGS-stress tensor,
- a proper approximation to local instantaneous backscatter energy transfer.

Moreover, some of the models have been designed to fulfil formal conditions imposed on the modelled SGS-stress tensor such as realizability for nonnegative filter functions in physical space [49], [50], [51] and to overcome limitations of the underlying nondynamic base parametrizations. Model development, which is outlined in Sec. II.B, is mainly based on

- the generalized use of the Germano identity at the tensor level of the SGS stresses and of deduced relations at the scalar level,

- the formulation of locally defined model coefficients either related to the individual components of the SGS-stress tensor or scalar ones which may be mathematically uniquely determined from physically motivated conditions,
- the approximate localization in the line of Piomelli *et al.* [20] to efficiently treat the model coefficients inside the integral convolution operators of the test-filtered subgrid-scale stresses.

With respect to the base parametrizations, in this study, three model types are included, which imply different approaches to backscatter modelling as well as to the approximation of local and nonlocal energy transfer processes in wavenumber space. The models under investigation are introduced and motivated in more detail in Sec. II.B. Combined with spatial filters of several widths and types, they have been evaluated for a fully developed turbulent pipe flow in a two-stage testing procedure.

The first stage comprises *a priori* tests of the proposed models in conjuntion with various grid and test filters using a DNS database which had been generated on the massively parallel computer Parsytec GC/PowerPlus-128 of Chemnitz University of Technology. The *a priori*-testing methodology and the computed test quantities are explained in Sec. III.A, the findings are presented in Sec. III.B. The *a priori*-test results have been analyzed to select representatives of the three model types and the most promising model candidates in particular, which were subjected to further testing.

As the second testing stage, actual large-eddy simulations have been performed applying these models with variations in input data such as model parameter bounds, grid density and filters.

Concerning the spatial filters involved in dynamic modelling, discrete approximations to the top-hat and to the spectral sharp-cutoff kernels defined in physical space and specified in Sec. II.C have been tested comparatively to study the effect of filters that qualitatively differ in the separation of grid and subgrid scales in physical and wavenumber spaces. Definiteness properties of the resulting SGS-stress tensor are also affected by this filter choice.

The test-flow conditions, especially the values of the Reynolds number, $Re_\tau = u_\tau R/\nu = 180$ and 1,050 for DNS and LES, respectively, have been selected to be comparable with published results of numerical and experimental pipe-flow investigations. Flow parameters and the basic LES equations are reviewed in Sec. II.A. The computer code is based on a second-order finite-difference discretization of the governing conservation equations in cylindrical coordinates on a 3D staggered-grid system. The numerical procedure, input data and details of filtering and model implementation are briefly described in Sec. II.D. Some aspects of parallelization are also addressed.

A survey of the large-eddy simulation runs performed is given in Sec. IV.A. The model- and filter-related results of the *a posteriori* tests concerning mean flow quantities and turbulence characteristics are discussed in Sec. IV.B, a comparison with experimental and numerical pipe-flow data being included. Finally, conclusions are drawn from the comparative evaluation of the investigated model/filter combinations (summarized in Sec. V), from the outcome of *a priori* and *a posteriori* tests as well as from the sensitivity of the LES results to variations in input data.

II Modelling and Numerical Procedure

II.A Flow Specification and Basic LES Equations

The numerical experiments of the present study are devoted to a fully developed turbulent flow of an incompressible fluid through a straight cylindrical pipe. The test flow is considered to be statistically steady as well as homogeneous in the axial and circumferential directions. This particular application has been chosen as a geometrically and fluid dynamically simple "building block flow", which is often encountered in the various engineering fields and for which numerical and experimental data are available for comparison.

In the DNS, which provided the database for the *a priori* tests, a Reynolds number of $Re_\tau = u_\tau\, R/\nu = 180$ based on pipe radius R and wall-friction velocity u_τ is implemented, corresponding to $Re_{CL} = u_{CL}\, R/\nu \approx 3{,}500$ in terms of centerline velocity u_{CL}. These test-flow conditions were selected to reproduce the ones of the pipe-flow direct numerical simulations described in [52], [53], [54], [55], [56] and agree with those of the experimental investigations performed by Adrian *et al.* [57], [58]. To be compatible with [52], the Reynolds number of the large-eddy simulations equals $Re_\tau = 1{,}050$, equivalent to $Re_{CL} \approx 25{,}000$.

The computational domain is represented by a circular cylinder defined by $(r, \varphi, z) \in [0, R] \times [0, 2\pi] \times [0, L]$, where r, φ, z denote cylindrical coordinates as usual. The length L is to be chosen sufficiently large as compared with the radius R in view of periodic boundary conditions to be applied in the longitudinal direction. Particularly, the spatial two-point correlation functions should be vanishingly small for separation distances of the order of $0.5\,L$ so that the largest flow structures can be captured. Following [52], the lengths $L = 10\,R$ and $L = 8\,R$ were specified for DNS and LES, respectively. The latter at least guarantees that the computed statistical one-point moments are not substantially influenced by this choice.

The direct and large-eddy simulations are based on the system of fundamental equations of fluid dynamics following from mass and momentum conservation principles for incompressible Newtonian fluids. Applying a linear filtering operation (see Secs. II.B.1 and II.C), denoted by an overbar and assumed to be commutative with respect to space and time derivatives, yields the governing LES equations which may be written in cylindrical $(r,\ \varphi,\ z)$-coordinates as follows

$$
\begin{array}{lcr}
\frac{\partial}{\partial r}(r\overline{u}\,) + \frac{\partial}{\partial \varphi}(\overline{v}\,) + \frac{\partial}{\partial z}(r\overline{w}\,) = 0\,, & & \\[6pt]
\frac{\partial \overline{u}}{\partial t} + \frac{1}{r}\Big\{ \frac{\partial}{\partial r}[r(\overline{u}\,\overline{u}\text{-}\tau_{11}+\overline{p})] + \frac{\partial}{\partial \varphi}[(\overline{v}\,\overline{u}\text{-}\tau_{21})] + \frac{\partial}{\partial z}[r(\overline{w}\,\overline{u}\text{-}\tau_{31})] \Big\} + \frac{1}{r}(\text{-}\overline{v}\,\overline{v}+\tau_{22}) & = & f_1\,, \\[6pt]
\frac{\partial \overline{v}}{\partial t} + \frac{1}{r}\Big\{ \frac{\partial}{\partial r}[r(\overline{u}\,\overline{v}\text{-}\tau_{12})] + \frac{\partial}{\partial \varphi}[(\overline{v}\,\overline{v}\text{-}\tau_{22}+\overline{p})] + \frac{\partial}{\partial z}[r(\overline{w}\,\overline{v}\text{-}\tau_{32})] \Big\} + \frac{1}{r}(\overline{v}\,\overline{u}\text{-}\tau_{21}) & = & f_2\,, \\[6pt]
\frac{\partial \overline{w}}{\partial t} + \frac{1}{r}\Big\{ \frac{\partial}{\partial r}[r(\overline{u}\,\overline{w}\text{-}\tau_{13})] + \frac{\partial}{\partial \varphi}[(\overline{v}\,\overline{w}\text{-}\tau_{23})] + \frac{\partial}{\partial z}[r(\overline{w}\,\overline{w}\text{-}\tau_{33}+\overline{p})] \Big\} & = & f_3\,,
\end{array} \tag{1}
$$

$$
\boldsymbol{\tau} = \boldsymbol{\tau}^{vis} + \boldsymbol{t}^{SGS}, \quad t_{ij}^{SGS} = -(\overline{u_i u_j} - \overline{u}_i\overline{u}_j), \quad \tau_{ij}^{vis} = 2\,\nu\,\overline{S}_{ij};
$$

$$
\overline{S}_{11} = \frac{\partial \overline{u}}{\partial r}, \quad \overline{S}_{22} = \frac{1}{r}\left(\frac{\partial \overline{v}}{\partial \varphi} + \overline{u}\right), \quad \overline{S}_{33} = \frac{\partial \overline{w}}{\partial z}, \quad \overline{S}_{12} = \overline{S}_{21} = \frac{1}{2}\left(\frac{1}{r}\frac{\partial \overline{u}}{\partial \varphi} + \frac{\partial \overline{v}}{\partial r} - \frac{\overline{v}}{r}\right),
$$

$$
\overline{S}_{23} = \overline{S}_{32} = \frac{1}{2}\left(\frac{\partial \overline{v}}{\partial z} + \frac{1}{r}\frac{\partial \overline{w}}{\partial \varphi}\right), \quad \overline{S}_{13} = \overline{S}_{31} = \frac{1}{2}\left(\frac{\partial \overline{w}}{\partial r} + \frac{\partial \overline{u}}{\partial z}\right).
$$

In (1), $\overline{u}_1 = \overline{u}$, $\overline{u}_2 = \overline{v}$, $\overline{u}_3 = \overline{w}$ represent the physical GS velocities in the radial, circumferential and axial directions. Throughout this paper, the subscripts r, φ, z will be used interchangeably with 1, 2, 3. For the pipe flow considered, a constant driving axial gradient of the statistically mean pressure (divided by the density), $d\langle p\rangle/dz = -2u_\tau^2/R$, is imposed, which was incorporated into the right-hand side f_3 so as to make the grid-scale pressure $\overline{p}$ periodic in the streamwise direction. Referring to the stresses (divided by the density), the notations τ_{ij}, τ_{ij}^{vis} are adopted for the total and viscous stress tensors, respectively; t_{ij}^{SGS} (with the superscript omitted below) denotes the (generalized) subgrid-scale stress tensor arising from filtering the nonlinear convective terms and representing the subgrid closure problem, which will be dealt with in the following subsection.

II.B Dynamic Subgrid-Scale Models

II.B.1 Modelling Principles

Dynamic approaches to subgrid modelling proceed from the definition of two spatial filtering operations – the grid filter denoted by an overbar and associated with kernel $\overline{G}$ of width $\overline{\Delta} > 0$,

$$\overline{f}(\mathbf{x},t) = \int_{R^3} \overline{G}(\mathbf{x},\mathbf{y},\overline{\Delta}) f(\mathbf{y},t)\, d\mathbf{y}\,, \tag{2}$$

and the test filter indicated by a hat and associated with kernel $\widehat{G}$ of width $\widehat{\Delta} > 0$, generally $\widehat{\Delta} \geqslant \overline{\Delta}$,

$$\widehat{f}(\mathbf{x},t) = \int_{R^3} \widehat{G}(\mathbf{x},\mathbf{y},\widehat{\Delta}) f(\mathbf{y},t)\, d\mathbf{y}\,, \tag{3}$$

where f represents some turbulent field. Consecutively applying $\overline{G}$ and $\widehat{G}$ yields a third filter

$$\widehat{\overline{G}}(\mathbf{x},\mathbf{y},\widehat{\overline{\Delta}}) = \int_{R^3} \widehat{G}(\mathbf{x},\mathbf{z},\widehat{\Delta})\, \overline{G}(\mathbf{z},\mathbf{y},\overline{\Delta})\, d\mathbf{z} \tag{4}$$

of width $\widehat{\overline{\Delta}} \geqslant \widehat{\Delta}$. As usual, the grid-filtering operation in case of LES is implicitly tied to the discretization method. For the filters considered in this study, the functions $\overline{G}$, $\widehat{G}$ and thus $\widehat{\overline{G}}$ are homogeneous in the sense that they depend only on the difference between the position arguments with the filter widths being constant and the right-hand sides of Eqs. (2), (3) as well as the analogous expression for $\widehat{\overline{f}}(\mathbf{x},t)$ representing convolution integrals. In addition, the kernels are required to be normalized so that constants are invariant under filtering. In deriving the governing LES equations, the filtering operators have to commute with differentiation, too.

The main idea in dynamic modelling, which is independent of any subgrid model and not restricted to a particular filter type, is based on the well-known Germano identity as an universal relation between the SGS stresses associated with $\overline{G}$- and $\widehat{\overline{G}}$-filter levels, i. e. between the subgrid-scale stresses $t_{ij} = -(\overline{u_i u_j} - \overline{u}_i \overline{u}_j)$, the subtest-scale stresses $T_{ij} = -(\widehat{\overline{u_i u_j}} - \widehat{\overline{u}}_i \widehat{\overline{u}}_j)$, and the related resolved turbulent stresses $\mathfrak{L}_{ij} = -(\widehat{\overline{u}_i \overline{u}_j} - \widehat{\overline{u}}_i \widehat{\overline{u}}_j)$:

$$T_{ij} = \mathfrak{L}_{ij} + \widehat{t}_{ij}\,, \quad i,j \in \{1,2,3\}\,, \tag{5}$$

interpreted by Germano as a consistency rule and a similarity rule [3]. For Eq. (5) not to result in a trivial identity, the filters are required to satisfy (see also [59])

$$\widehat{\overline{G}} \neq \overline{G}\,, \quad \widehat{\overline{\Delta}} > \overline{\Delta}\,. \tag{6}$$

In this paper, it is proposed not only to exploit the kinematic identity (5) at the tensor level of the stresses but also to found model development and evaluation on the following consequences at the vector and scalar levels:

- vector level – divergence of the subtest-scale stress tensor entering the $\widehat{\overline{G}}$-filtered Navier-Stokes equations (subtest forces)

$$\textstyle\sum_j \dfrac{\partial T_{ij}}{\partial x_j} = \sum_j \dfrac{\partial \mathfrak{L}_{ij}}{\partial x_j} + \sum_j \dfrac{\partial \widehat{t}_{ij}}{\partial x_j}\,, \quad i \in \{1,2,3\}\,, \tag{7}$$

- scalar level – terms representing the energetic interactions between large- and small-scale components associated with filter $\widehat{\overline{G}}$

$$\textstyle\sum_{i,j}\widehat{\overline{u}}_i\frac{\partial T_{ij}}{\partial x_j} = \sum_{i,j}\widehat{\overline{u}}_i\frac{\partial \mathfrak{L}_{ij}}{\partial x_j} + \sum_{i,j}\widehat{\overline{u}}_i\frac{\partial \widehat{t}_{ij}}{\partial x_j}\,, \tag{8}$$

- scalar level – the part of this interaction term corresponding to fine-scale dissipation at $\widehat{\overline{G}}$-level and representing the net energy transfer between the large-scale velocity field $\widehat{\overline{\mathbf{u}}}$ and the related small-scale field, $f02\_23 = \sum_{i,j}T_{ij}\widehat{\overline{S}}_{ij}$,

$$\textstyle\sum_{i,j}T_{ij}\widehat{\overline{S}}_{ij} = \sum_{i,j}\mathfrak{L}_{ij}\widehat{\overline{S}}_{ij} + \sum_{i,j}\widehat{t}_{ij}\widehat{\overline{S}}_{ij}\,, \tag{9}$$

  which is decomposed into the contributions from the energy flux $f12\_23 = \sum_{i,j}\mathfrak{L}_{ij}\widehat{\overline{S}}_{ij}$ between scales of motion larger than $\widehat{\overline{\Delta}}$ and those intermediate between $\overline{\Delta}$ and $\widehat{\overline{\Delta}}$ ("local contribution" according to [47]) and from the energy flux $f01\_23 = \sum_{i,j}\widehat{t}_{ij}\widehat{\overline{S}}_{ij}$ between scales of motion larger than $\widehat{\overline{\Delta}}$ and scales smaller than $\overline{\Delta}$ ("not-so-local contribution" according to [47]). (Here, the fluxes are defined to be positive in case of energy drain towards smaller scales. The flux notation has been chosen according to the boundaries of the two ranges of scales involved in energy transfer, where the numbers 0 and 3 represent the size of the smallest and largest scales of motion, respectively; 1 and 2 are assigned to the filter widths $\overline{\Delta}$ and $\widehat{\overline{\Delta}}$, respectively. To illustrate this further, the symbol $f01\_13 = \sum_{ij}t_{ij}\overline{S}_{ij}$ will be adopted to denote the energy flux between subgrid and grid scales at $\overline{G}$-level with the sign being opposite to that of the SGS dissipation.)
  Basically, the present investigation of large and small scales interactions at both $\overline{G}$- and $\widehat{\overline{G}}$-levels focuses on the SGS-dissipation term, while the SGS-diffusion part is not studied, mainly for reasons explained e. g. in [15] and [60].

Another important relation is given by the scalar equation that results from taking the trace of Eq. (5) and that connects the small-scale kinetic energy at $\widehat{\overline{G}}$-level, the test-filtered SGS energy of the grid level and the related resolved turbulence energy:

$$-\frac{1}{2}\textstyle\sum_i T_{ii} = -\frac{1}{2}\sum_i \mathfrak{L}_{ii} - \frac{1}{2}\sum_i \widehat{t}_{ii}\,. \tag{10}$$

Particular equations selected from the above consequences of the Germano identity have been used to mathematically uniquely and efficiently determine space- and time-dependent model coefficients of dynamic SGS parametrizations and to evaluate model performance.

Following the most common practice in modelling the subgrid- and subtest-scale stresses, they are approximated by the same type of model in terms of the respective large-scale quantities including identical model coefficients.
One of the key assumptions of the generalized-anisotropic model versions proposed in this paper consists in the use of individual model coefficients related to the particular tensor components of the SGS stresses. By introducing additional degrees of freedom, it is thus intended to avoid overspecification (P3) and to allow for a more flexible account of SGS-stress anisotropy, which is especially pronounced in wall-bounded turbulent shear flows. This type of coefficients is expected to exhibit reduced fluctuations and a more favourable numerical behaviour. The component-related model coefficients are assigned to the individual SGS stress-tensor components as spatially and temporally varying adaptive weighting factors, which, obviously, depend on the coordinate system chosen. As distinguished from tensor components, they will subsequently be denoted by indices in parentheses.
Also, alternative models are formulated with a scalar coefficient each calculated from physically meaningful conditions related to subgrid-scale dissipation.

Unlike SGS parametrizations with globally averaged expressions for their model coefficients as proposed by Germano [2], all the models suggested by the authors of the present work use locally defined coefficients, that is essentially without any kind of global averaging. These localized formulations are designed to achieve a greater capability of adequately reproducing local subgrid-scale stresses t_{ij} and SGS dissipation $\varepsilon_{SGS} = -f01\_13$ as well as local backscatter energy transfer $\varepsilon_+ = 1/2\,(\varepsilon_{SGS} + |\varepsilon_{SGS}|)$ [61] and to offer a wider range of applicability. For stability reasons, after having been calculated from their formulae, the model coefficients were suitably modified (see Sec. II.D.4).

In favour of the localized approach, it has been suggested in recent publications [23] to keep the important local information as much as possible in the dynamic model formulation. Improved results by using dynamic SGS closures with localized coefficients have already been obtained, for example, in [5], [19], [20]. The need for further investigations into dynamic model versions with locally formulated coefficients has been pointed out in [22] and, concerning intermittency of SGS dissipation, in [62].

With respect to the treatment of the model coefficients inside the test-filtered modelled SGS stresses $\widehat{t}_{ij}^{mod}$ in (5) or related equations, the approximate localization approach due to Piomelli and Liu [20] is mainly adopted since this technique is considered to be a computationally efficient alternative to solving the Fredholm's integral equation of the second kind. So either the subgrid-scale stress tensor as a whole or the model coefficients involved are replaced by approximate values calculated during the numerical solution procedure from the previous time step and subsequently marked with a superscribed asterisk.

As to the base model type, the tested closures comprise dynamic subgrid-scale parametrizations of algebraic Smagorinsky, scale-similarity and mixed types the coefficients of which are evaluated as space- and time-dependent parameters from algebraic equations without having to solve additional differential or integral equations. Compared with known dynamic SGS models, the closure assumptions introduced below are not substantially more complex.

For assessing model performance in both *a priori* and *a posteriori* tests, particularly with respect to reproducing flow features at scales between $\overline{\Delta}$ and $\widehat{\overline{\Delta}}$, Eqs. (5) and (7) – (10) can be used, too. In *a priori* tests, the average error in satisfying these equations with modelled subgrid and subtest-scale stresses as well as correlation coefficients between left- and right-hand sides are computable. The idea of explicitly evaluating the average square error of the Germano identity with particular models for t_{ij} and T_{ij} was introduced and tested in [13]. Furthermore, Meneveau and Katz proposed to apply this approach to dynamically choose among available SGS parametrizations in LES.

II.B.2 Smagorinsky-Type Models

Before turning to the proposed modified versions, three well-known SGS models which, for comparison, have been incorporated into the *a priori* and *a posteriori* tests of this investigation will be outlined first.

Model 1 (smag): The first base type for model development and evaluation originates from the traditional Smagorinsky model [63] for the deviatoric part of the (generalized) SGS-stress tensor as a function of the local grid-scale strain-rate tensor $\overline{S}_{ij}$. The model involves the classical eddy-viscosity assumption in physical space

$$t_{ij}^{mod} - \tfrac{\delta_{ij}}{3} \textstyle\sum_k t_{kk}^{mod} = 2\,\nu_{SGS}\,\overline{S}_{ij} \tag{11}$$

and the algebraic formulation of the subgrid-scale eddy viscosity

$$\nu_{SGS} = (f_D\, C_S\, \overline{\Delta})^2\, |\overline{S}|\,, \tag{12}$$

where $|\overline{S}| = (2\sum_{i,j}\overline{S}_{ij}\overline{S}_{ij})^{1/2}$, C_S denotes the empirical Smagorinsky constant, $\overline{\Delta}$ stands for a length scale representative of the subgrid-scale motion, and f_D means an *ad hoc* damping function which reduces the turbulent length and velocity scales near solid walls. For the pipe-flow application of the present study, $C_S = 0.1$ and a Van-Driest-type exponential wall function $f_D(r_+) = [1 - exp(-r_+^a/A_+^a)]^b$, $r_+ = (1-r)u_\tau/\nu$, $A_+ = 25$, with $a = b = 1$ or, alternatively,

$a = 3$, $b = 1/2$, are adopted. The specification of the SGS length scale in terms of unidirectional grid spacings is based here on the quadratic mean and is given in Sec. II.C; another definition in widespread use is the geometric-mean-based formula introduced in [64] and generalized to highly anisotropic grids in [65] and [66]. (For its derivation, the underlying hypotheses and intrinsic deficiencies of this absolutely dissipative model, see for example [23], [59], [67], [68], [69], [70], [71], [72], [73], [74], [75].)

Models 2 (lilly) and 3 (pio): As dynamic versions thereof, the popular models due to Lilly [18] and Piomelli, Liu [20] are tested, both starting from the usual hypotheses for the anisotropic parts of the (generalized) subgrid- and subtest-scale stresses, respectively,

$$t_{ij}^{mod} - \tfrac{\delta_{ij}}{3} \textstyle\sum_k t_{kk}^{mod} = C\beta_{ij}\,, \quad \beta_{ij} = 2\,\overline{\Delta}^2 |\overline{S}|\, \overline{S}_{ij}\,, \tag{13}$$

$$T_{ij}^{mod} - \tfrac{\delta_{ij}}{3} \textstyle\sum_k T_{kk}^{mod} = C\alpha_{ij}\,, \quad \alpha_{ij} = 2\,\widehat{\overline{\Delta}}^2 |\widehat{\overline{S}}|\, \widehat{\overline{S}}_{ij}\,, \tag{14}$$

and using the following equation resulting from the Germano identity (5)

$$\mathfrak{L}_{ij} - \tfrac{\delta_{ij}}{3} \textstyle\sum_k \mathfrak{L}_{kk} = T_{ij} - \tfrac{\delta_{ij}}{3} \sum_k T_{kk} - \widehat{t}_{ij} + \tfrac{\delta_{ij}}{3} \sum_k \widehat{t}_{kk} \tag{15}$$

to determine the model coefficient.
In the model due to Lilly [18], the coefficient appearing inside of the test-filtered subgrid-scale stresses in (15) was extracted from the test-filtering operation without taking account of its space dependence. To solve the overspecification problem (P3), Lilly introduced a least-squares minimization procedure. In addition, a spatial averaging operation $\langle \ldots \rangle$ in homogeneous flow directions was applied to both the numerator and denominator of the resulting expression for C in order to enhance computational stability. For the pipe flow considered in the present paper, this results in

$$C(r,t) = \Big\langle \textstyle\sum_{i,j} \mathfrak{L}_{ij} M_{ij} \Big\rangle_{\varphi,z} \Big/ \Big\langle \textstyle\sum_{k,l} M_{kl} M_{kl} \Big\rangle_{\varphi,z} \tag{16}$$

with $M_{ij} = \alpha_{ij} - \widehat{\beta}_{ij}$.
The approach followed by Piomelli and Liu [20] subsequently termed approximate localization approach is characterized by using an estimated value C^* for the model coefficient inside the integral convolution operator of $\widehat{t}_{ij}^{mod}$ in Eq. (15). The estimate C^* is computed during the numerical solution procedure from previous time (or iteration) steps. This approximate localization idea has been adopted in [38], [76], and [77]. Further, contracting (15) with α_{ij} to locally minimize the sum of the squares of the residual gives the localized model coefficient

$$C(\mathbf{x},t) = \Big(\textstyle\sum_{i,j} (\mathfrak{L}_{ij} + \widehat{C^* \beta_{ij}}) \alpha_{ij} \Big) \Big/ \textstyle\sum_{k,l} \alpha_{kl} \alpha_{kl}\,. \tag{17}$$

In accordance with [20], the resulting subgrid-scale eddy viscosity was bounded from below to guarantee nonnegative values of the total viscosity $\nu + \nu_{SGS} \geqslant 0$. An additional local averaging of the model coefficient over the test-filtering volume as performed by the last-mentioned authors was found to be not necessary for reasons of stability and is, therefore, not included in the computations of the present work.

Model 4 (smagc): As distinguished from the known dynamic models presented above, the modelling approach suggested by the authors of this paper introduces generalized Smagorinsky-type closures for the subgrid- and subtest-scale stresses,

$$t_{ij}^{mod} = C_{(ij)}\, \beta_{ij}\,, \tag{18}$$

$$T_{ij}^{mod} = C_{(ij)}\, \alpha_{ij}\,, \tag{19}$$

containing component-related space- and time-dependent model coefficients $C_{(ij)}(\mathbf{x},t) = C_{(ji)}(\mathbf{x},t)$. Contrary to the popular subgrid parametrizations of this base type, modelling is thus extended to the whole of the SGS-stress tensor instead of just the deviatoric part. Consequently, the GS pressure, the SGS normal stresses and hence the subgrid-scale kinetic energy are directly computable, and realizability of the modelled subgrid-stress tensor can be verified.

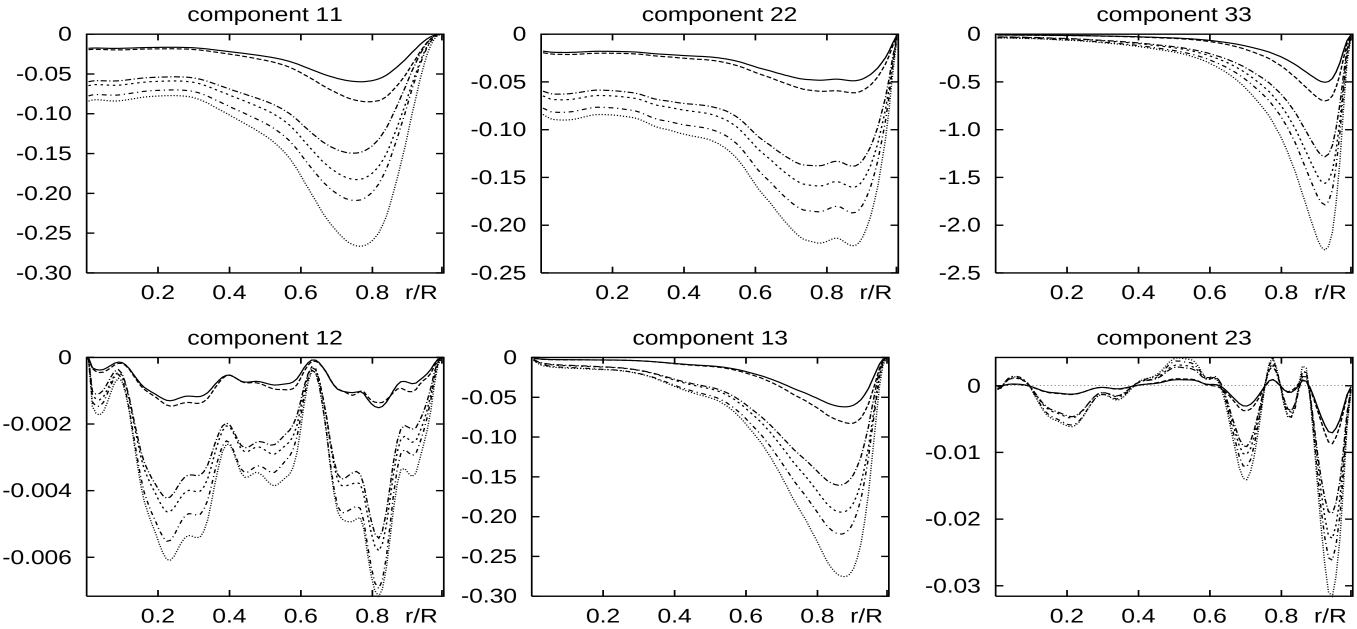

Figure 1: Mean values of stresses $\mathcal{L}_{ij}/u_\tau^2$ —— , t_{ij}^{def}/u_τ^2 - - - , $\mathfrak{L}_{ij}^T/u_\tau^2$ -·-·- , $\mathfrak{L}_{ij}/u_\tau^2$ ---- , $\mathcal{L}_{ij}^T/u_\tau^2$ -·-·- , T_{ij}^{def}/u_τ^2 ········ (computed with top-hat type grid and test filters from DNS data) versus radial coordinate r/R

Using component-specific model coefficients is intended to generalize the scalar turbulence viscosity and the classical linear stress/strain relationship to overcome their limitations.
Inserting Eqs. (18), (19) into the tensorial Germano identity (5) and adopting the approximate localization approach [20] to replace the model coefficients in $\widehat{t}_{ij}^{mod}$ by $C^*_{(ij)}$-values calculated in the preceding time step yields

$$C_{(ij)} = \left(\mathfrak{L}_{ij} + \widehat{C^*_{(ij)}\beta_{ij}}\right)\Big/\alpha_{ij}\,. \tag{20}$$

The model (18), (20) was implemented in the effective-viscosity form $t_{ij}^{mod} = 2\,\nu_{(ij)}^{SGS}\,\overline{S}_{ij}$, $\nu_{(ij)}^{SGS} = C_{(ij)}\,\overline{\Delta}^2\,|\overline{S}|$, with the model coefficients bounded from below according to $\nu + \nu_{(ij)}^{SGS} \geqslant 0$. A clipping of the coefficients with respect to upper bounds was also tested.

II.B.3 Scale-Similarity-Type Models

Because of well-known deficiencies and limitations of the classical Smagorinsky base model regarding the gradient-type of the closure, the generally unsatisfactory approximation to the local SGS stresses, the underlying assumption of local equilibrium between SGS turbulence energy production and dissipation, as well as the primary account of the nonlocal component of energy transfer in wavenumber space and also in view of the instability/singularity problem connected with negative SGS eddy viscosities, subgrid-scale parametrizations of scale-similarity type have been incorporated into the tests as alternatives.

The modelling principle due to Bardina [78] is physically based on scale similarity of turbulence, which has been confirmed by the results of numerous experimental and numerical investigations of turbulent flow. The outcome of the direct numerical simulation of turbulent pipe flow performed in the present study also shows a remarkable similarity between turbulence characteristics of different length scales not only with respect to statistical means as functions of the radial coordinate (Fig. 1) but even at the level of instantaneous quantities along axial ($r = const.$, $\varphi = const.$) and radial ($\varphi = const.$, $z = const.$) lines (Fig. 2). This applies to the individual terms of the Germano identity (dashed lines in Fig. 1), to the subgrid- and subtest-scale stresses and equally to the following stresses computable from the resolved-scale field:

$\mathcal{L}_{ij} = -(\overline{\overline{u}_i\overline{u}_j} - \overline{\overline{u}}_i\overline{\overline{u}}_j)$ (modified) Leonard stresses according to [79] ,

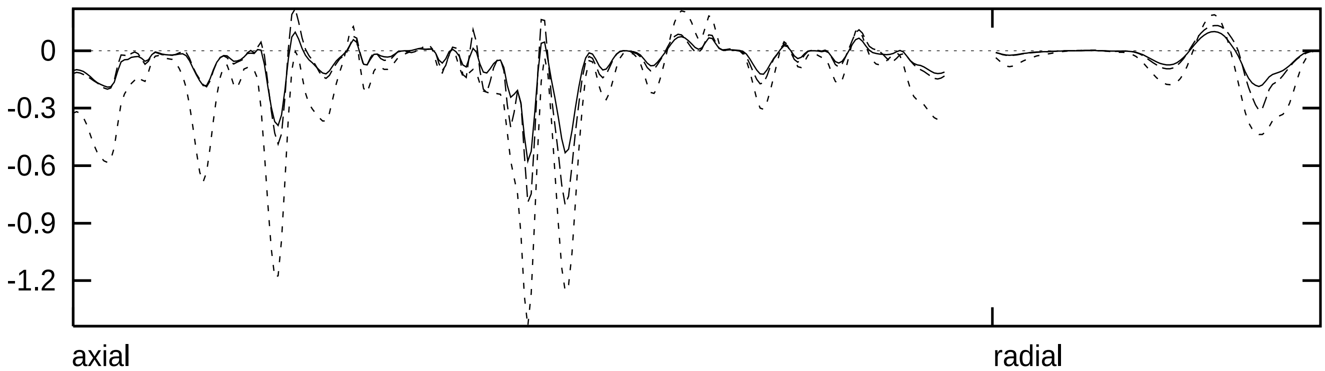

Figure 2: Instantaneous values of stresses $\mathcal{L}_{13}/u_\tau^2$ —— , t_{13}^{def}/u_τ^2 - - - , $\mathfrak{L}_{13}/u_\tau^2$ ---- (computed with top-hat type grid and test filters from DNS data) along an axial line and along a radial line

$$
\begin{aligned}
\mathcal{L}_{ij}^T &= -(\widehat{\overline{\overline{u}_i\overline{u}_j}} - \hat{\overline{\overline{u}}}_i\hat{\overline{\overline{u}}}_j)\,,\\
\mathfrak{L}_{ij} &= -(\widehat{\overline{u}_i\overline{u}_j} - \hat{\overline{u}}_i\hat{\overline{u}}_j) \quad \text{resolved turbulent stresses}\,,\\
\mathfrak{L}_{ij}^T &= -(\widehat{\overline{\overline{u}}_i\overline{\overline{u}}_j} - \hat{\overline{\overline{u}}}_i\hat{\overline{\overline{u}}}_j)\,.
\end{aligned}
$$

Figures 1 and 2 particularly suggest the use of the (modified) Leonard stresses $\mathcal{L}_{ij}$ as parametrization tensor for t_{ij}, whereas the GS strain-rate tensor $\overline{S}_{ij}$ can be shown to be less appropriate from the similarity point of view.

In modelling the terms representing the interactions between GS and SGS components within the framework of the scale-similarity concept, importance is primarily attached to local energy transfer in wavenumber space between turbulence components of roughly equal size with postulating similarity between the interacting components. Accordingly, closures of this type are aimed at approximating the major interactions between the smallest resolved (GS) and the largest unresolved (SGS) scales (transfer field) in such a way that the latter are represented by differences between single- and double- (or multiple-) filtered velocities. Ultimately, this leads to parametrizations of t_{ij} in terms of (generalized) stresses computable from the resolved-scale fields such as $\mathcal{L}_{ij}$ or $\mathfrak{L}_{ij}$. The resulting closure hypotheses stand out for improved approximations at the tensor level of local stresses [43], [44] and for advantages concerning the modelling of transitional and laminar flow regions ("behaviour across different flow regimes" [47]) as well as of wall-bounded flows (asymptotic near-wall behaviour of the modelled SGS-stress tensor, reproduction of typical near-wall structures [43], [47], [60]). Above all, however, models of this type are not purely dissipative and admit deterministic backscatter simulation [80] without resorting to negative turbulence viscosities, which may give rise to numerical instabilities. Whereas classical nondynamic scale-similarity models turned out to be not dissipative enough, their dynamic counterparts were found to be superior also in this respect. In the context of dynamic SGS modelling, scale-similarity-based parametrizations have met with renewed interest in recent publications [29], [42], [43], [45], [46], [47], [60], [70], [81], which often showed these models to be effective and sufficiently dissipative even without adding a supplementary Smagorinsky-type model component.

Further work is still needed to give a conclusive evaluation of the *a posteriori* performance of dynamic similarity models with respect to the approximation of SGS dissipation and backscatter as well as regarding the conceptual weakness of a mismatch in characteristic length scales between the modelled and defined SGS-stress fields [47], [82], [83].

Model 5 (leo): As the starting point and a simple candidate for testing scale-similarity closures, the following nondynamic base parametrization in terms of the (modified) Leonard stresses

$$t_{ij}^{mod} = D\,\mathcal{L}_{ij} \tag{21}$$

with the model constant $D = 1$ is used. Scale-similarity arguments due to Bardina applied to the individual stress components ensuing from the classical decomposition of the SGS-stress tensor (into Leonard, cross and true SGS Reynolds stresses) along with Galilean invariance considerations formed the background of the original model [78], which is formulated here for the total (generalized) SGS-stress tensor. (The resulting parametrization (21) is, obviously, Galilean invariant irrespective of the value of D.)

Model 6 (sc1): On the pattern of model 4 (smagc), by adopting Eqs. (18), (19), the tensorial Germano identity (5) and the approximate localization approach applied to the whole SGS-stress tensor inside of the test-filtering operation, the similarity-like dynamic model

$$t_{ij}^{mod} = \mathfrak{D}_{(ij)} \, (\mathfrak{L}_{ij} + \widehat{t}_{ij}^{*}) \, , \quad \mathfrak{D}_{(ij)} = \beta_{ij} / \alpha_{ij} \, , \tag{22}$$

is straightforwardly derived, where, essentially, the parametrization tensor and the numerator of the model coefficient are interchanged as compared with model 4 (smagc).

The following dynamic SGS models are proposed by taking a (generalized) scale-similarity closure as a basis formulated in terms of the (modified) Leonard stresses for the subgrid-scale stresses and, analogously, in terms of $\mathcal{L}_{ij}^{T}$ for the subtest-scale stresses

$$t_{ij}^{mod} = D_{(ij)} \, \mathcal{L}_{ij} \, , \quad T_{ij}^{mod} = D_{(ij)} \, \mathcal{L}_{ij}^{T} \, . \tag{23}$$

The component-related coefficients $D_{(ij)}$ are evaluated by means of the tensorial Germano identity (5).

Model 7 (sc2): If the model coefficients of the test-filtered SGS stresses involved are treated in the way proposed in [2], [18] with their spatial variability being neglected in $\widehat{t}_{ij}^{mod}$, the scale-similarity model coefficients

$$D_{(ij)} = \frac{\mathfrak{L}_{ij}}{\mathcal{L}_{ij}^{T} - \widehat{\mathcal{L}}_{ij}} = - \frac{\mathfrak{L}_{ij}}{\widehat{\bar{\bar{u}}_i \bar{\bar{u}}_j} - \widehat{\bar{\bar{u}}}_i \widehat{\bar{\bar{u}}}_j} \tag{24}$$

are obtained. The resulting dynamic model may also be rewritten in terms of the resolved stresses as the parametrization tensor

$$t_{ij}^{mod} = \mathfrak{D}_{(ij)} \, \mathfrak{L}_{ij} \, , \quad \text{where} \quad \mathfrak{D}_{(ij)} = \frac{\overline{\bar{\bar{u}}_i \bar{\bar{u}}_j} - \bar{\bar{u}}_i \bar{\bar{u}}_j}{\widehat{\bar{\bar{u}}_i \bar{\bar{u}}_j} - \widehat{\bar{\bar{u}}}_i \widehat{\bar{\bar{u}}}_j} \, . \tag{25}$$

Model 8 (sc3): Replacing the subgrid-scale stresses inside the test-filtered part of the Germano identity (5) by approximate values t_{ij}^{*} yields the SGS model

$$t_{ij}^{mod} = D_{(ij)} \, \mathcal{L}_{ij} \, , \quad D_{(ij)} = \frac{\mathfrak{L}_{ij} + \widehat{t}_{ij}^{*}}{\mathcal{L}_{ij}^{T}} \, , \tag{26}$$

which was finally implemented in terms of the parametrization tensor of model 6 (sc1)

$$t_{ij}^{mod} = \mathfrak{D}_{(ij)} \, (\mathfrak{L}_{ij} + \widehat{t}_{ij}^{*}) \, . \tag{27}$$

The related model coefficients

$$\mathfrak{D}_{(ij)} = \mathcal{L}_{ij} / \mathcal{L}_{ij}^{T} \, , \tag{28}$$

as compared with (22), are gradient-free and contain the (modified) Leonard stresses and their counterpart assigned to the $\widehat{\bar{G}}$-level.

For all the models with component-specific coefficients introduced above, realizability [49], [50], [51] in case of nonnegative filter functions in physical space cannot be proven and is, indeed, partly violated. Therefore, a simple "clipping" approximation [50] has been tested to additionally impose the weak realizability conditions

$$-t_{ii}^{mod} \geqslant 0 \qquad \forall i \in \{1,\, 2,\, 3\} \, , \tag{29}$$

$$(t_{ij}^{mod})^2 \leqslant t_{ii}^{mod} \, t_{jj}^{mod} \quad \forall i, j \in \{1,\, 2,\, 3\} \, , \tag{30}$$

on the modelled subgrid-scale stress tensor.

Going on from the preceding generalized anisotropic scale-similarity models, the following one-parameter versions with a scalar coefficient each are put forward as alternatives designed to obey the realizability constraints for the filter types mentioned above. To get an expression for the scalar model coefficient, the subgrid-scale energy dissipation is taken into consideration on account of the model's primary function. Specifically, the coefficient of the following three parametrizations is determined in such a way that the resulting model produces the same SGS dissipation as its counterpart with component-specific coefficients.

Model 9 (ss1): Starting from

$$t_{ij}^{mod} = \mathfrak{D}\,(\mathfrak{L}_{ij} + \widehat{t}_{ij}^{*})\,, \quad \mathfrak{D} \geqslant 0\,, \tag{31}$$

the SGS dissipation identical with that of model 8 (sc3) is enforced by setting

$$\mathfrak{D}\,\textstyle\sum_{k,l}(\mathfrak{L}_{kl} + \widehat{t}_{kl}^{*})\,\overline{S}_{kl} = \textstyle\sum_{i,j}\mathfrak{D}_{(ij)}(\mathfrak{L}_{ij} + \widehat{t}_{ij}^{*})\,\overline{S}_{ij}\,. \tag{32}$$

The resulting model coefficient

$$\mathfrak{D} = \left[\frac{\left(\sum_{i,j}\mathfrak{D}_{(ij)}(\mathfrak{L}_{ij} + \widehat{t}_{ij}^{*})\overline{S}_{ij}\right)}{\left(\sum_{k,l}(\mathfrak{L}_{kl} + \widehat{t}_{kl}^{*})\overline{S}_{kl}\right)}\right]_{+} \tag{33}$$

may be evaluated by defining $\mathfrak{D}_{(ij)}$ according to Eq. (28) and is restricted to nonnegative values as indicated by the subscript "+". This model retains the realizability property of the SGS-stress tensor for nonnegative filters in physical space provided that a positive semi-definite initial guess is chosen for $-t_{ij}^{*}$.

Model 10 (ss2): For the resolved-stress-related model

$$t_{ij}^{mod} = \mathfrak{D}\,\mathfrak{L}_{ij}\,, \quad \mathfrak{D} \geqslant 0\,, \tag{34}$$

to generate the same subgrid-scale dissipation as model 7 (sc2) and to be realizable, the model coefficient has to be taken as

$$\mathfrak{D} = \left[\left(\textstyle\sum_{i,j}\mathfrak{D}_{(ij)}\mathfrak{L}_{ij}\overline{S}_{ij}\right) \big/ \left(\textstyle\sum_{k,l}\mathfrak{L}_{kl}\overline{S}_{kl}\right)\right]_{+}\,, \tag{35}$$

where $\mathfrak{D}_{(ij)}$ is defined according to (25).

Model 11 (ss3): By direct analogy, the dynamic Leonard-stress-based parametrization

$$t_{ij}^{mod} = D\,\mathcal{L}_{ij}\,, \quad D \geqslant 0\,, \tag{36}$$

can be derived by equating its SGS dissipation with that caused by model 7 (sc2), which leads to

$$D = \left[\left(\textstyle\sum_{i,j}D_{(ij)}\mathcal{L}_{ij}\overline{S}_{ij}\right) \big/ \left(\textstyle\sum_{k,l}\mathcal{L}_{kl}\overline{S}_{kl}\right)\right]_{+} \tag{37}$$

with $D_{(ij)}$ being taken from Eq. (24).

Model 12 (ss4): As a modified approach to establishing a scalar model coefficient, it is proposed to use the scalar-level equation (9), which results from the Germano identity and is related to the fine-scale dissipation associated with $\widehat{\overline{G}}$-level. Supposing

$$t_{ij}^{mod} = D\,\mathcal{L}_{ij}\,, \quad T_{ij}^{mod} = D\,\mathcal{L}_{ij}^{T}\,, \quad D \geqslant 0\,, \tag{38}$$

and adopting approximate values t_{ij}^{*} from the previous time step in evaluating the test-filtered SGS stresses of (9), another dynamic model of scale-similarity type is obtained, given by $t_{ij}^{mod} = D\,\mathcal{L}_{ij}$ and

$$D = \left[\left(\textstyle\sum_{i,j}(\mathfrak{L}_{ij} + \widehat{t}_{ij}^{*})\,\widehat{\overline{S}}_{ij}\right) \big/ \left(\textstyle\sum_{k,l}\mathcal{L}_{kl}^{T}\,\widehat{\overline{S}}_{kl}\right)\right]_{+}\,. \tag{39}$$

If applied in conjuntion with nonnegative filters in physical space, models 9 (ss1) to 12 (ss4) not only satisfy conditions (29) and (30) but, by construction, ensure realizability in the stronger sense that the matrix representing $-t_{ij}^{mod}$ is positive semi-definite.

II.B.4 Mixed-Type Model

The third class of SGS closures investigated comprises mixed parametrizations consisting in a linear combination of a Smagorinsky-type model with a scale-similarity model. By supplementing a model which is absolutely dissipative in its classical version and mainly intended for representing the global energy drain with a model which is capable of predicting backscatter and is superior in approximating the local SGS stresses, it is attempted to benefit from the advantages of either type as well as to put less burden on the dynamic coefficient related to the Smagorinsky part (reduced fluctuations, e. g. [13], [29], [45], [84]). With regard to spectral energy transfer, the component that is local in wavenumber space and its nonlocal component are essentially modelled separately by this type of closure. Especially, when using a very coarse grid, the Smagorinsky term is required to represent the interaction of the grid scales with the distinctly smaller subgrid scales [10], [85]. Improved results have been attained in both *a priori* and *a posteriori* tests by applying recent models of mixed type such as those proposed by Zang *et al.* [29], Vreman *et al.* [46], Salvetti, Banerjee *et al.* [45], [84], Horiuti [10], Liu *et al.* [44] and Meneveau, Katz [13] (dynamic mixed nonlinear model).

Model 13 (comb): As a representative of dynamic mixed-type parametrizations, the following model was tested, which combines the generalized Smagorinsky closure including component-related coefficients with a similarity part proportional to the (modified) Leonard stresses.
Proceeding from parametrizations similar to the models proposed in [29] for the subgrid- and subtest-scale stresses, respectively,

$$t_{ij}^{mod} = C_{(ij)}\,\beta_{ij} + \mathcal{L}_{ij}\,, \quad T_{ij}^{mod} = C_{(ij)}\,\alpha_{ij} + \mathcal{L}_{ij}^{T}\,, \tag{40}$$

the tensorial Germano identity (5) and the approximate localization approach [20] are employed to deduce the coefficients of the Smagorinsky submodel as

$$C_{(ij)} = \frac{\mathfrak{L}_{ij} - \mathcal{L}_{ij}^{T} + \widehat{t_{ij}^{*}}}{\alpha_{ij}}\,. \tag{41}$$

Within the framework of the resulting mixed model, which may also be written as

$$t_{ij}^{mod} = \frac{\beta_{ij}}{\alpha_{ij}}\left(\mathfrak{L}_{ij} + \widehat{t_{ij}^{*}} - \mathcal{L}_{ij}^{T}\right) + \mathcal{L}_{ij}\,, \tag{42}$$

SGS parametrization is effectively restricted to the part of the (generalized) SGS-stress tensor which contains subgrid velocities, i. e. the (modified) cross stresses + (modified) true SGS Reynolds stresses = unresolved residual stresses according to the notation in [79], while the remaining component $\mathcal{L}_{ij}$ is explicitly calculated by definition from the GS velocity field.

II.C Grid and Test Filters

As introduced in Sec. II.B.1, the averaging operation that is applied as grid and test filter in the *a priori* tests and that is used for filtering the GS quantities in the large-eddy simulations is of the form

$$\tilde{f}(\mathbf{x},t) = \int_{R^3} \tilde{G}(\mathbf{x}-\mathbf{y},\tilde{\Delta})\,f(\mathbf{y},t)\,d\mathbf{y}\,, \tag{43}$$

where the tilde stands for grid and test filtering, respectively. The filtering kernel $\tilde{G}$ is defined to be the product of one-dimensional filter functions

$$\tilde{G}(\mathbf{x}-\mathbf{y},\tilde{\Delta}) = \prod_{i=1}^{3} \tilde{G}_i(x_i - y_i, \tilde{\Delta}_i) \tag{44}$$

with individual widths $\tilde{\Delta}_i$ in the ith direction. The latter are usually related to the unidirectional grid spacings Δx_i by $\overline{\Delta}_i = 2\,\Delta x_i$ and $\widehat{\Delta}_i = 2\,\overline{\Delta}_i = 4\,\Delta x_i$. From these, the scalar filter width $\tilde{\Delta}$

	a_0	a_1	a_2	a_3	α_1	α_2
f1	0.5	0.5	0	0	0	0
f2	2/3	1/3	0	0	0	0
f3a	0.499455	0.776523	0.343418	0.0663499	−0.0014544	0.6872
f3b	0.5	0.8056734	0.4684092	0.1627358	0	0.936818
F1	0.25	0.5	0.25	0	0	0
F2	1/6	2/3	1/6	0	0	0
F3	0.035365	0.07763	0.0266322	0.0556008	−1.301218	0.496446

Table I: Filter coefficients

used as subgrid-scale length scale is chosen here in the cylindrical coordinates as the quadratic mean

$$\tilde{\Delta} = \left(\frac{1}{3}\left((\tilde{\Delta}_r)^2 + (r\,\tilde{\Delta}_\varphi)^2 + (\tilde{\Delta}_z)^2\right)\right)^{\frac{1}{2}} . \tag{45}$$

In agreement with other published works concerning LES of wall-bounded flows [2], [10], [20], [36], [61], [80], [86], [87] and in view of unresolved issues, filtering is performed only in the two directions where the flow is statistically homogeneous, i. e. no filtering is applied in the radial direction, which is distinguished by insufficient spatial resolution and the complicating wall effects. Accordingly, $\widehat{\Delta}_r$ was set equal to 0.

As the basic filter types, the top-hat (or box) filter in physical space and the spectral sharp-cutoff filter are considered (for their definition, advantages and disadvantages, see e. g. [15] and [88]). These filter functions are associated with different properties concerning their support in physical and wavenumber spaces and thus the GS/SGS separation. Furthermore, the tensor $-t_{ij}$ resulting from the application of the (nonnegative) top-hat kernel is positive semi-definite, as opposed to its nonrealizable counterpart associated with the spectral sharp-cutoff filter.

The clearest separation of small and larger scales of a fluctuating function is attained with the spectral sharp-cutoff filter **fsc** in wavenumber space defined by the one-dimensional transfer function

$$\tilde{\mathcal{G}}_i(k\,\tilde{\Delta}_i) = \begin{cases} 1 & \text{if } k\,\tilde{\Delta}_i \leqslant \pi\,, \\ 0 & \text{otherwise}\,, \end{cases} \tag{46}$$

with k representing an one-dimensional wavenumber. When a LES is performed in physical space, it may be not possible or too expensive to use the sharp-cutoff filter. Lele [89] examines the following class of discrete one-dimensional filters of 5-point-implicit–7-point-explicit type, working on uniformly spaced grids:

$$\tilde{f}_j + \sum_{l=1}^{2} \alpha_l\,\frac{\tilde{f}_{j-l} + \tilde{f}_{j+l}}{2} = \sum_{l=0}^{3} a_l\,\frac{f_{j-l} + f_{j+l}}{2}\,, \tag{47}$$

where f_j denotes the value of f at node j, $\tilde{f}_j$ is the corresponding filtered value, and the subscripts $j-l$, $j+l$ indicate neighbouring node values in direction i. The most common filters belonging to this class are of 3-point-explicit type and approximate the top-hat kernel in physical space

$$\tilde{G}_i(\xi, \tilde{\Delta}_i) = \begin{cases} \frac{1}{\tilde{\Delta}_i} & \text{if } |\xi| \leqslant \frac{\tilde{\Delta}_i}{2}\,, \\ 0 & \text{otherwise}\,, \end{cases} \tag{48}$$

by means of simple explicit integration rules – the trapezoidal rule (filter **f1**) and Simpson's rule (filter **f2**). For the coefficients of the filters, see Table I.

If the function f in (47) is defined on the interval $[0, L_i]$ of the independent variable x_i, the filter transfer function associated with (47) is given by

$$\tilde{\mathcal{G}}_i(k\,\Delta x_i) = \frac{\sum_{l=0}^{3} a_l\,\cos(k\,l\,\Delta x_i)}{1 + \sum_{m=1}^{2} \alpha_m\,\cos(k\,m\,\Delta x_i)}\,, \tag{49}$$

where $k = 2\pi n/L_i$ represents a scaled wavenumber with n denoting an integer. The first picture in Fig. 3 shows the grid-filter transfer functions of f1 and f2 as continuous functions of $k\,\Delta x_i$ along with the tranfer function $\overline{\mathcal{G}}_i$ of the sharp-cutoff grid filter. Obviously, the simple 3-point filters are far away from the sharpness of filter fsc, and the same applies to all the other explicit filters of class (47).

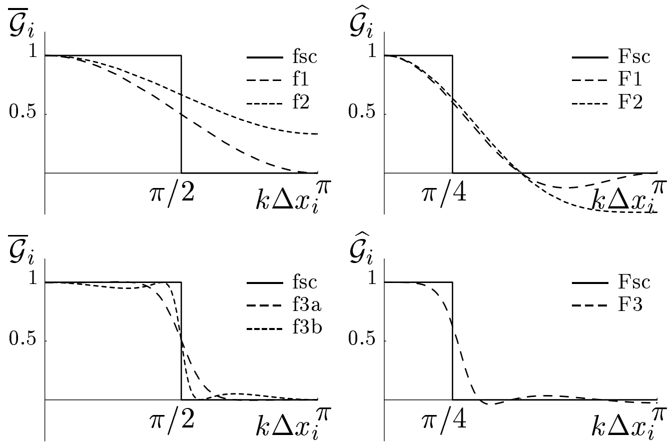

Figure 3: Filter transfer functions

The two implicit filters **f3a** and **f3b** in Table I try to use the full potential of (47) to approximate the transfer function of the sharp-cutoff kernel at the grid level.
Filter f3a can be deduced from (47) under the following conditions: fourth order accuracy, $\overline{\mathcal{G}}_i(0) = 1\,,\ \overline{\mathcal{G}}_i(1.2) = 0.95\,,\ \overline{\mathcal{G}}_i(\pi - 1.2) = 0.05\,,\ \overline{\mathcal{G}}_i(\pi) = 0\,,\ \overline{\mathcal{G}}_i''(\pi) = 0\,.$ Filter f3b is described in [90], it is a linear combination of a least-squares approximation to the sharp-cutoff grid filter with one of the sixth-order formulas constructed in [89].

For the corresponding test filters to be realized within the framework of (47), the coefficients are specified according to the lower part of Table I. Filters **F1** and **F2** again use the trapezoidal and Simpson's rules quadrature to approximate the top-hat filter, **F3** is a discrete approximation to the sharp-cutoff filter at the test level **Fsc**. It is derived from (47) by imposing the constraints: fourth order accuracy, $\widehat{\mathcal{G}}_i(0) = 1\,,\quad \widehat{\mathcal{G}}_i(\pi/4 - 0.25) = 0.95\,,\quad \widehat{\mathcal{G}}_i(1.1) = 0\,,\quad \widehat{\mathcal{G}}_i(1.7) = 0.03\,,$ $\widehat{\mathcal{G}}_i(2.5) = 0\,.$

If consecutively applied, grid and test filters $\overline{G}_i$, $\widehat{G}_i$ yield the filter $\widehat{\overline{G}}_i$, the width of which enters some of the models investigated. To evaluate $\widehat{\overline{\Delta}}_i$, for spectral sharp-cutoff filters $\overline{G}_i$ and $\widehat{G}_i$ with $\widehat{\Delta}_i \geqslant \overline{\Delta}_i$, it is used that $\widehat{\overline{G}}_i \equiv \widehat{G}_i$ and $\widehat{\overline{\Delta}}_i = \widehat{\Delta}_i$. For the class of top-hat filters, $\widehat{\overline{G}}_i$ is easily shown to be a "trapezoid" filter. Considering the least-squares approximation by a third top-hat filter, its width was defined as $\widehat{\overline{\Delta}}_i^{\,2} = \overline{\Delta}_i^{\,2} + \widehat{\Delta}_i^{\,2}$ (see also [46]).

II.D Numerical Procedure

II.D.1 Discretization in Space and Time, Initial and Boundary Conditions

Equations (1) are discretized on a staggered grid system in the cylindrical coordinates. The dimensionless grid spacings follow from the number of unknowns in the three directions: $\Delta r/R = 1/N_r$, $r\,\Delta\varphi/R = 2\pi\, r/(R\,N_\varphi)$, $\Delta z/R = L/(R\,N_z)$. $(N_r,\ N_\varphi,\ N_z)$ was set to $(96, 128, 256)$ for the DNS and to one of the triples $(8, 32, 64)$, $(16, 64, 128)$, $(32, 128, 256)$ for LES so as to match the spatial resolution characteristics of the simulations reported in [52]. For comparison, the spatial Kolmogorov microscale normalized by the pipe radius R is estimated to be about $2.2 \cdot 10^{-3}$ in the LES test flow and $8.7 \cdot 10^{-3}$ in case of the DNS Reynolds number.
The difference scheme is of second order in space and characterized by favourable conservation

properties. Time integration is performed as described in [52] using the Euler/Leapfrog technique with some necessary modifications. With respect to the velocity, the algorithm is explicit in r- and z-directions but implicit in φ-direction to avoid strong time-step restrictions resulting from the flat cells near the axis of the coordinate system. Because of the convective part of the momentum balance, the equations to be solved in φ-direction are not diagonal dominant. Thus, an algorithm which solves cyclic tridiagonal equation systems with pivoting has to be applied to enable maximal time increments Δt.
Mass conservation is guaranteed by adopting a splitting method resulting in a Poisson equation for the pressure correction, which is solved via FFT at every time step.

Periodic boundary conditions are implemented in the circumferential (φ-) and axial (z-) directions.
With respect to wall-boundary conditions, a no-slip condition for the velocity components is imposed at $r = R$. In the large-eddy simulations, corresponding to the small mesh numbers in the radial direction, the wall layer is not resolved, but approximate wall-boundary conditions are applied instead to evaluate the wall-shear stresses. Based on the law of the wall and using an analytic expression for the measured radial profile of the mean axial velocity, the shear stresses $\tau_{r\varphi}$ and τ_{rz} in positions at the wall are calculated according to the shifted boundary condition model due to Piomelli *et al.* [91] (without having introduced a streamwise displacement as yet).
At the axis, where the singularity of the coordinate system is located, a number of assumptions was needed to make the simulations feasible. Special features of the computed near-axis behaviour of some dependent variables are probably related to this.
For the axial velocity, which in the mean attains a maximum at $r = 0$, a zero-gradient boundary condition is adopted. The axis-boundary values of the remaining two velocity components are calculated in LES from the arithmetic mean of the corresponding grid-point values in the circumferential cell layer nearest to the axis. On the finest grid used in DNS, however, von-Neumann-type boundary conditions are also prescribed for the radial and azimuthal velocity components and, generally, for the subgrid turbulence viscosities as well.
Axis-boundary conditions for the SGS stresses in case of scale-similarity and mixed-type models are specified in terms of GS velocities at the axis so as to be compatible in the statistical mean with expressions for the axis values of $<t_{rr} - t_{\varphi\varphi}>$, $<t_{r\varphi}>$, $<t_{rz}>$ and $<t_{\varphi z}>$ following from the kinematics of homogeneous axisymmetric turbulence [92] as well as from the statistically averaged dynamic equations for the GS velocity field taking statistically steady and (with respect to φ and z) homogeneous flow conditions into account. Axis-boundary values for t_{zz} and one of the other two SGS normal stresses have been provided by means of an averaging procedure from values in neighbouring grid points adjacent to the axis.

For the very first simulation, initial conditions were based on measured mean velocity profiles with random perturbations superimposed chosen to fit measured rms values. Later on, simulations were started from data fields of previous runs on the present grid or using interpolated results obtained on coarser grids.

The time-step size Δt in the difference method was chosen as large as possible within the stability limits, maximally this is a value of 0.0004 for the DNS at its final stage and 0.005, 0.0015, 0.0004 for the LES on the three different grids.

According to [52], to prevent the simulated flow from becoming laminar, the DNS was started with a Reynolds number of $Re_\tau = 1{,}000$, which was gradually reduced to its final value of 180 during the first 2,500 time steps.
Afterwards, the direct numerical simulations were continued for 12 nondimensional time units until a statistically steady state was established, and then the flow statistics were collected.
In the large-eddy simulations, the flow was integrated forward in time for six characteristic time scales.

II.D.2 Parallelization

The numerical procedure described above was implemented on a GC/PowerPlus-128, which belongs to the MIMD class of parallel computers. Following the domain decomposition technique, the computational grid is partitioned into subgrids containing all points within a fixed z-range. Moreover, each processor stores a copy of flow variables from the nearest points of the two adjacent processors in order to reduce data transmission during the computations.
The chosen decomposition is favourable to solving the equation systems in φ-direction for $\overline{u}$, $\overline{v}$, $\overline{w}$ and u, v, w, respectively, because no data exchange between the processors is needed. To solve the Poisson equation for the pressure, FFT can be applied in φ- and z-directions. In our case, an outer "parallel" FFT [93] is adopted in z-direction. The inner FFT in φ-direction and the solution of the remaining tridiagonal equation systems can be realized on the subgrids without any interprocessor communication.

II.D.3 Filtering

The underlying storage management is advantageous to implementing explicit 3-point filters. In case of implicit filters, there arise two problems. The first is the problem of solving a set of cyclic pentadiagonal equations on a single processor. It is a problem of linear algebra which is not desired to be discussed here. The second problem concerns filtering in z-direction. The question is how to solve a set of equations with the structure mentioned above on a multiprocessor system. It was accomplished using a special procedure for a data exchange of each processor with each other. As a result, the quantities to be filtered are rearranged, and each processor has the complete data within a fixed φ-range. The program that solves the cyclic pentadiagonal equations on a single processor can be used now to filter in z-direction. A second exchange step stores all filtered quantities in their original positions.

II.D.4 Model Implementation

In calculating the local model coefficients $C_{(ij)}, D_{(ij)}$ and $\mathfrak{D}_{(ij)}$ as quotients of two tensor components, a special approach was chosen in order to avoid excessively fluctuating coefficients and to prevent peak coefficient values from entering into the modelled SGS stresses. To illustrate the numerical behaviour of these model coefficients, some instantaneous raw data computed in LES for $\mathfrak{D}_{(13)}$ of model 8 (sc3) in the grid points of a cross-section $z = const.$, linearly arranged with increasing r along the abscissa, are plotted in Fig. 4. Among the proposed SGS closures with component-specific coefficients, the computed coefficient values of this model are distinguished by the smallest range of variations, the lowest frequence and smallest magnitude of peaks.
In case of extremely small or vanishing denominators occuring in the expression for the model coefficients, a local mean value was adopted which was calculated from the values of the model coefficients in those neighbouring grid points where the quotient lies within a permissible interval. If it failed to determine such a local mean, an user-prescribed global mean (in terms of the radial coordinate) was used instead. Though this additional flow-dependent input is required, it is, however, available from the results of preceding *a priori* tests or large-eddy simulations, respectively, and entered the pipe-flow computations of the present work in less than 0.1 % of the total number of grid points.
After this procedure, the model coefficients were subjected to an additional cutting with the bounds specified as a function of model and filters and corresponding to a range of ± one to three times the mean (scale-similarity and combined models) or ± 10 times the mean for model 4 (smagc). For the upper bound to $\mathfrak{D}_{(13)}$ of model 8 (sc3), confer the horizontal dashed line in Fig. 4. The lower bound to $\mathfrak{D}_{(ij)}, D_{(ij)}$ of models 6 (sc1) to 8 (sc3) and to $\mathfrak{D}$ or D, respectively, of models 9 (ss1) to 12 (ss4) was set to zero in applications of nonnegative filters in physical space.

For the former group of models with component-related coefficients, the values of the coefficients associated with the SGS shear stresses were, if necessary, diminished further by the

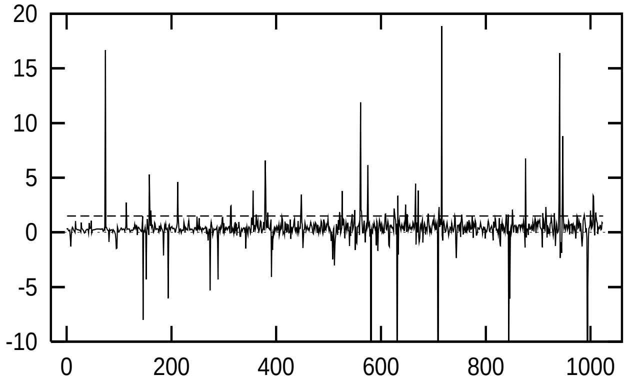

Figure 4: Original component-related model coefficient $\mathfrak{D}_{(13)}$ of parametrization 8 (sc3) computed with top-hat type grid and test filters from LES data in the grid points of a cross-section $z = const.$, linearly arranged with increasing r along the abscissa

"clipping" approximation to ensure the realizability condition (30).

Since backscatter turned out to be of crucial influence in the large-eddy simulations, *a priori* and *a posteriori* tests of the proposed scale-similarity and combined models with an artificially limited amount of backscatter were performed in addition. Several modifications have been tested. Common to all, the modelled flux $f01\_13^{mod} = -\varepsilon_{SGS}^{mod} = \sum_{i,j} t_{ij}^{mod}\overline{S}_{ij}$ is considered and, generally, expressed in terms of a scalar subgrid-scale turbulence viscosity as introduced in (11). For models 9 (ss1) to 12 (ss4) with a scalar coefficient each, the model coefficient was clipped from above in such a way that only backscatter values ε_{+}^{mod} corresponding to a nonnegative scalar total (hypothetical SGS + molecular) viscosity were retained.
In models 7 (sc2), 8 (sc3) and 13 (comb), similar to model 4 (smagc), the component-related backscatter $[t_{ij}^{mod}\overline{S}_{ij}]_{-}$ was limited to values associated with nonnegative component-specific total viscosities. The resulting upper bounds were imposed on the model coefficients under the same condition as for models 9 to 12, i. e. in those grid points where the modelled total flux $f01\_13^{mod}$ showed backscatter strong enough to result in a negative scalar total viscosity (model 13) or, alternatively, where $f01\_13^{mod}$ indicated backscatter of any intensity (models 7 and 8). For model 6 (sc1), yet another modification was tested. Here, the model coefficients and hence the SGS stresses were, if necessary, multiplied by a common nonnegative weighting factor less than unity in order to bound the backscatter part of $f01\_13^{mod}$, again according to a nonnegative total viscosity.

When calculating the modelled subgrid-scale stresses, a special treatment was required for those models that contain the test-filtered SGS stresses $\widehat{t_{ij}^{*}}$ (or test-filtered values of their generalized Smagorinsky-type parametrization $C_{(ij)}^{*}\beta_{ij}$ in case of model 4). In the *a priori* tests, two approaches were followed. First, $\widehat{t_{ij}^{*}}$ was computed by definition using DNS data of the present time step (method **dt***). However, since this information was not available in the actual large-eddy simulations, as an alternative, stored approximate values t_{ij}^{*} were adopted instead which had been generated according to the model formulation from DNS data of previous time steps (method **mt***). This imitates the approximate localization approach applied in LES by means of the model's SGS-stress predictions obtained for the preceding time step. To initialize t_{ij}^{*}, the (modified) Leonard stresses were used in most of the *a priori* and *a posteriori* tests.

III *A priori* Tests

III.A Methodology

As a first stage of evaluating the models presented above, *a priori* tests have been performed using DNS data for the pipe test flow, $Re_\tau = 180$ equivalent to $Re_{CL} \approx 3{,}500$, in the domain $[0, R] \times [0, 2\pi] \times [0, L],\ L = 10\,R$.
According to the basic principle of this approach to model testing as pioneered by Clark *et al.* [94] for statistically homogeneous turbulence and employed e.g. in [2], [10], [42], [44], [45], [47], [60], [71], [80], [83], [95], [96], [97], [98], [99], [100], [101], [102], [103], several test quantities containing subgrid terms are computed from DNS data by their definition on the one hand and using the model formulation on the other hand. (If necessary, these quantities are marked with the superscripts *def* and *mod*.) A comparison between the corresponding results is made here on both an instantaneous and a statistical level. With respect to the former, the "exact" and modelled values of the test quantities along specified axial and radial lines ($r = const.$, $\varphi = const.$) and ($\varphi = const.$, $z = const.$), respectively, are visualized for a point-by-point comparison at a particular time instant. Concerning statistical evaluation, 40 data files from DNS separated by $\Delta t = 0.1$ nondimensional time intervals are accumulated in order to provide statistically independent samples.
By averaging the quantities calculated from these instantaneous DNS fields and by spatial averaging over the homogeneous directions, statistical one-point data are generated and plotted as functions of the radial coordinate: mean values (subsequently denoted by $<\ldots>$) and rms values as well as correlation coefficients and L_1-norms of differences between the "exact" values and those obtained with the different models.

In total, 53 tensor, 18 vector, and 83 scalar test quantities have been analyzed in more than 200 *a priori* tests, which were performed on the local superscalar cluster HP9000/889 K460.
The test quantities chosen comprise the subgrid terms at the tensor level of the SGS stresses t_{ij} along with the anisotropy tensor $b_{ij} = (t_{ij} - 1/3\,\delta_{ij} \sum_k t_{kk})/\sum_l t_{ll},\ i,j \in \{1,2,3\}$; the SGS force terms at the vector level $\sum_j \partial t_{ij}/\partial x_j\ ,\ i \in \{1,2,3\}$; and the subgrid terms at the scalar level $\sum_{i,j} \overline{u}_i\, \partial t_{ij}/\partial x_j$; as well as the individual terms of the Germano identity at tensor, vector and scalar levels in Eqs. (5), (7) – (9). On account of the energetic primary function of SGS models, the energy fluxes $f01\_13$, $f01\_23$, $f02\_23$, $f12\_23$ (defined in Sec. II.B.1) and $f01\_12 = f01\_13 - f01\_23$ between several regions of scales bounded by the characteristic widths $\overline{\Delta}$ and $\widehat{\overline{\Delta}}$ of the filters $\overline{G}$ and $\widehat{\overline{G}}$, respectively, are included in the evaluation. In addition, kinetic energies of fine-scale structures related to both these filters, $-1/2 \sum_i t_{ii}$, $-1/2 \sum_i T_{ii}$, and the resolved turbulence energy, $-1/2 \sum_i \mathfrak{L}_{ii}$, have been computed. Of particular interest in this context is the models' capability to reproduce outscatter (ε_--) and backscatter (ε_+-) contributions to energy transfer between grid and subgrid scales associated with $\overline{G}$-level.
Following the methodology of statistical *a priori* testing in the line of Meneveau [104], some necessary conditions for the SGS-stress statistics to correctly predict the mean velocity and pressure as well as second-order moments of the resolved velocity have also been scrutinized.
As distinguished from the LES calculations, the *a priori* tests reported in the following subsection are based on the fine DNS grid with $96 \times 128 \times 256 \approx 3.15$ million nodes in order to avoid additional data manipulations prior to grid- and test-filtering procedures and to get highly resolved test quantities. For comparison, reference tests have additionally been carried out with data sampled on the medium LES grid (consistent *a priori* tests in the terminology of [47]).

Despite some critical assessments of this testing methodology including difficulties in interpreting the results [2], [15], [104], [105], [106] and regardless of the need for further research efforts in the field of SGS-model testing, *a priori* tests offer considerable promise as a first step towards examining model capabilities and serve as an efficient tool for studying the effects of filters [107] without having to solve differential equations. Specifically, DNS data yield valuable information on spatiotemporal behaviour of the quantities to be modelled and on their dependence on the filters used. In addition, the *a priori* investigations of the present study provided

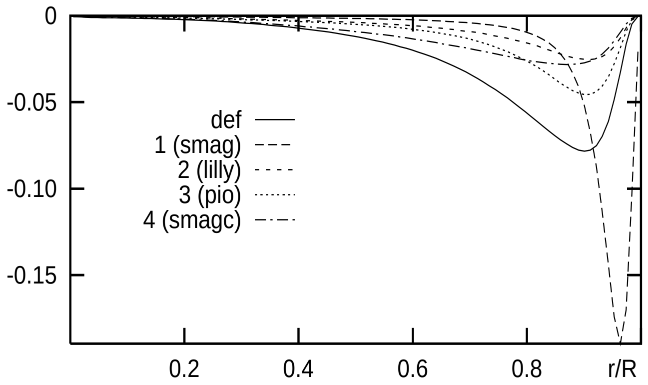

Figure 5: Mean values of defined SGS stress t_{rz}^{def}/u_τ^2 and corresponding modelled stress t_{rz}^{mod}/u_τ^2 for Smagorinsky-type SGS models as functions of the radial coordinate r/R

guidelines how to specify bounds for dynamically determined model coefficients and were useful in reducing the number of SGS models to be tested thoroughly in LES by selecting the most promising candidates. In this respect, *a priori* tests proved to be a supporting complementary approach to the more expensive large-eddy simulations in SGS-model development and verification.

On the other hand, when evaluating the *a priori*-test results, one has to take into account that quantities derived from DNS data and from LES results are related to different Reynolds numbers in this study and that the complex dynamical GS/SGS interactions do not exist in *a priori* tests. Thus, *a priori* tests alone do not provide conclusive evaluation of a SGS model. Rather, the model's performance in LES, i. e. its net effect on the computed GS field, will ultimately be the decisive factor.

III.B Results

A comparative evaluation of the models' performance in *a priori* tests on the fine DNS grid will first be outlined for a reference filter combination using the top-hat filter approximated by Simpson's rule at the grid and test levels, $\overline{G}_i$ = f2 and $\widehat{G}_i$ = F2, $i \in \{2, 3\}$. The influence of filter variations will be discussed in the second part of this subsection.

III.B.1 Model Performance

In assessing model performance at tensor, vector and scalar levels, a comprehensive comparison with the results of the well-known Smagorinsky-type subgrid models 1 (smag), 2 (lilly) and 3 (pio) is not possible without resorting to further assumptions since the actual GS pressure, SGS normal stresses and quantities derived therefrom are not directly accessible for these closures. Specifically for these parametrizations, the modelled subgrid terms have been evaluated against their defined counterparts computed from the deviatoric SGS-stress-tensor part.

Starting with the **tensor level** of the local subgrid stresses, the mean subgrid terms pertaining to the SGS normal stresses are hardly captured by models 1 (smag) to 3 (pio) associated with an extremely low level of these modelled quantities. (For the standard Smagorinsky model, these findings are consistent with the channel-flow *a priori*-test results in [83].) Applying the generalized anisotropic Smagorinsky-type model 4 (smagc) to the DNS data, the mean SGS normal stresses $<t_{rr}^{def}>$ and $<t_{\varphi\varphi}^{def}>$ as functions of the radial coordinate are reproduced satisfactorily or moderately well, respectively, in terms of both their magnitude and their radial profile. For the statistically mean subgrid-scale stress $<t_{zz}^{def}>$, which, in the present application, assumes the largest absolute values of all the SGS-stress-tensor components, the peak value is considerably underestimated in its absolute magnitude by this model. Accordingly, the values

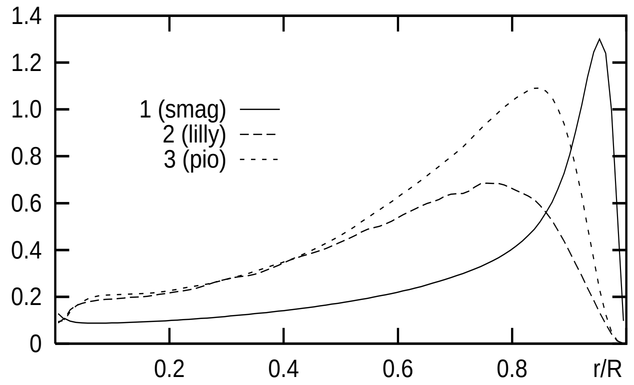

Figure 6: Mean values of scalar subgrid eddy viscosity ν_{SGS}/ν for Smagorinsky-type SGS models as functions of the radial coordinate r/R

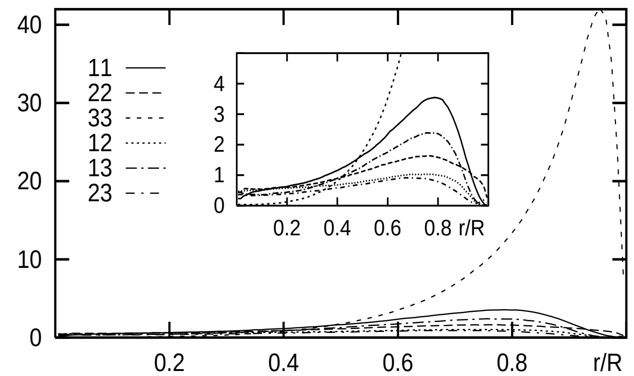

Figure 7: Mean values of component-specific subgrid eddy viscosities $\nu_{(ij)}^{SGS}/\nu$ for Smagorinsky-type SGS model 4 (smagc) as functions of the radial coordinate r/R. Insert: The same functions plotted for a smaller range of ordinates

given by model 4 (smagc) for the SGS energy corresponding to the grid filter $\overline{G}$ as well as that for the fine-scale energy associated with the $\widehat{\overline{G}}$-level exhibit a markedly lower maximum than the related defined energies.
With respect to the SGS shear stresses, the differences between the *a priori* predictions of the tested models are especially pronounced for t_{rz}, the component most relevant to pipe flow (Fig. 5). The absolute values of $<t_{rz}^{def}>$ are clearly underpredicted by all dynamic Smagorinsky-type parametrizations, whereas the classical model 1 (smag) yields an underestimation roughly within $0 < r/R < 0.9$ yet excessively large absolute values of $<t_{rz}^{mod}>$ within the remaining radial subrange with the peak being located too close to the wall. In spite of this poor local agreement between modelled and defined $<t_{rz}>$-values, the Smagorinsky model, nevertheless, provides a reasonable overall approximation to the integral $\int_0^R <t_{rz}> dr$, which (along with the corresponding integral of the GS part of the rz-Reynolds stress in the integrated shear-stress balance) directly contributes to the value of the mean longitudinal velocity component at the axis.

The ensemble means of the associated scalar SGS turbulence viscosity due to closures 1 (smag), 2 (lilly) and 3 (pio) vary in their values and profiles according to Fig. 6, where for model 1 this quantity, again, peaks at a smaller distance from the wall.
Fig. 7 illustrates the finding that in case of component-specific Smagorinsky-type model coefficients there are substantial differences between the individual subgrid eddy viscosities $\nu_{(ij)}^{SGS}$. For the pipe-flow application, the SGS viscosity related to the component t_{zz}^{mod} displays a pronounced peak extremely exceeding the level of the other SGS viscosities.

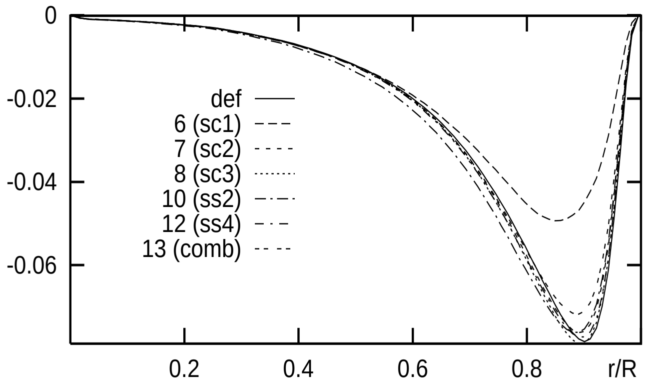

Figure 8: Functions as in Fig. 5 for scale-similarity- and mixed-type SGS models

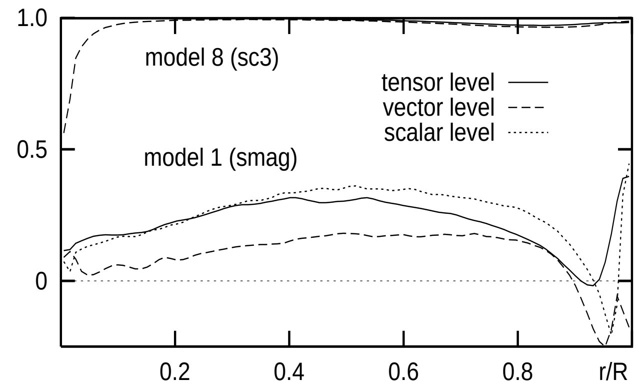

Figure 9: Representative correlations between defined and modelled subgrid terms at tensor, vector and scalar levels for Smagorinsky SGS model 1 (smag) (lower curves) and for scale-similarity SGS model 8 (sc3) (upper curves) as functions of the radial coordinate r/R

The *a priori*-test results obtained with the scale-similarity- and combined-type parametrizations, apart from model 6 (sc1), are generally distinguished from the Smagorinsky-type predictions by a fairly good qualitative and quantitative agreement between the mean subgrid terms computed from definition and using the model formulation. At the tensorial level, this applies to all the SGS-stress components and is exemplified for t_{rz} in Figs. 8 (mean values) and 9 (tensor-level correlation). This important subgrid stress is best reproduced by models 8 (sc3), 7 (sc2) and 12 (ss4) while remarkably underestimated by model 6 (sc1). The other two, smaller SGS shear stresses, $t_{r\varphi}$ and $t_{\varphi z}$ (both not shown), are particularly well approximated by closures 7 (sc2), 8 (sc3) and 13 (comb). With respect to the SGS normal stresses (not shown), model 6 (sc1) and also model 9 (ss1) yield the largest absolute values of these components as well as an overestimation of the mean subgrid energy at $\overline{G}$-level, whereas this quantity is typically slightly underpredicted by all the other scale-similarity and combined models. For the dominant SGS normal stress, t_{zz}, the best *a priori*-test results have been established with models 13 (comb), 8 (sc3) and 9 (ss1).
Considering SGS-stress anisotropy, the tensor b_{ij} and especially its greatest (zz-) component is *a priori* well captured by the scale-similarity and combined-type closures. Contrary to this, the degree of anisotropy of the SGS normal stresses $t_{\varphi\varphi}$ and t_{zz} in the near-wall region is grossly underestimated by the Smagorinsky-type model 4 (not shown).

According to their performance in the *a priori* tests, the proposed dynamic models of scale-similarity and mixed types are essentially classified into three groups: Models 8 (sc3), 7 (sc2) and 13 (comb) with component-specific coefficients are rated as the most promising parametrizations characterized by an excellent *a priori* correspondence between defined and modelled test quantities at all levels. For these models, the average absolute values of the differences between defined

	t_{11}	t_{22}	t_{33}	t_{12}	t_{13}	t_{23}	$\sum_j \frac{\partial t_{1j}}{\partial x_j}$	$\sum_j \frac{\partial t_{2j}}{\partial x_j}$	$\sum_j \frac{\partial t_{3j}}{\partial x_j}$	$\sum_{i,j} \overline{u}_i \frac{\partial t_{ij}}{\partial x_j}$
	.0358	.0327	.1562	.00009	.0221	.00032	.1515	.0017	.1815	2.6215
1 (smag)	.0398	.0427	.0826	.00008	.0213	.00035	.4947	.0257	.4332	4.1662
2 (lilly)	.0398	.0427	.0825	.00009	.0152	.00035	.4961	.0258	.1273	1.5789
3 (pio)	.0376	.0436	.0810	.00008	.0113	.00026	.4902	.0256	.0852	0.9683
4 (smagc)	.0019	.0046	.0644	.00004	.0112	.00011	.0161	.0012	.1123	0.9395
5 (leo)	.0082	.0050	.0388	.00002	.0039	.00004	.0517	.0005	.0463	0.6645
6 (sc1)	.0070	.0096	.0301	.00003	.0053	.00006	.0385	.0010	.0752	0.7546
6 (sc1)*	.0016	.0022	.0066	.00002	.0022	.00002	.0109	.0006	.0323	0.3539
7 (sc2)	.0025	.0010	.0134	.00001	.0007	.00002	.0203	.0003	.0149	0.2092
8 (sc3)	.0017	.0008	.0096	.00001	.0007	.00001	.0140	.0002	.0115	0.1654
9 (ss1)	.0024	.0041	.0055	.00003	.0031	.00011	.0198	.0010	.0240	0.3844
10 (ss2)	.0044	.0008	.0132	.00003	.0020	.00010	.0412	.0009	.0262	0.3896
11 (ss3)	.0035	.0006	.0124	.00002	.0009	.00005	.0283	.0006	.0157	0.2255
12 (ss4)	.0040	.0011	.0122	.00002	.0007	.00004	.0302	.0006	.0108	0.1812
13 (comb)	.0010	.0009	.0048	.00001	.0011	.00002	.0111	.0003	.0236	0.2670

Table II: Representative average L_1-norms of differences between defined and modelled subgrid terms at tensor, vector and scalar levels for the SGS models tested and the reference filter combination (* corresponds to $\widehat{G}_i \equiv \overline{G}_i \equiv$ f2; the head of the table contains the definition of the subgrid terms and, below, their average L_1-norms with the subgrid stresses computed according to definition)

and modelled subgrid stresses (L_1-norms of the error at the tensor level, see Table II) are very small, and the qualitative close agreement between defined and modelled subgrid terms at the tensor level is reflected in correlation coefficients of nearly 1.0 (see Fig. 9 for the t_{rz}-correlation coefficients and Table III). The *a priori* performance of the nondynamic SGS closure 5 (leo) comes close to that of the group one models. In the second place, the parametrizations 12 (ss4) and 11 (ss3) in terms of the (modified) Leonard stresses with scalar coefficients follow, which give typical tensor-level correlations of about 0.95. The third group comprises the resolved-stress-related models 9 (ss1) and 10 (ss2) resulting in average SGS-stress correlation coefficients roughly between 0.8 and 0.9.
Model 6 (sc1), if combined with top-hat grid and test filters of the usual filter-width ratio $\widehat{\Delta}_i/\overline{\Delta}_i = 2$, belongs to the third group. However, for the special choice of the box test-filter width $\widehat{\Delta}_i = \overline{\Delta}_i$ (see Sec. III.B.2), this model may rather be assigned to the second group (* in Tables II and III).

At the **vector level** of the divergence-type subgrid terms entering the filtered momentum equations, the correlations are typically reduced against the tensor level. In Fig. 9, correlation coefficients are plotted for the third component of the divergence vector along with those at the scalar level. While the vector- and scalar-level correlations for the best group of models are only slightly lower than their counterparts at the tensor level, the former are significantly decreased for the parametrizations of the second group and even more diminished for the group three models. These correlations of the proposed dynamic scale-similarity and combined SGS models are contrasted with considerably lower correlation coefficients for the Smagorinsky-type closures, especially for the known models 1 (smag), 2 (lilly) and 3 (pio) (Table III).
Among the vector-level test quantities, the divergence of the SGS stresses entering the $\overline{w}$-equation turned out to be noticeably sensitive to the subgrid-scale model used in the *a priori* tests. Due to larger derivatives $d\langle t_{rz}^{mod}\rangle/dr$ within about $0.9 < r/R < 1.0$ (Fig. 5), the classical Smagorinsky model generated substantially more pronounced peaks closer to the wall in the mean value of this quantity, whereas its profile obtained with the three dynamic Smagorinsky-type parametrizations and with model 6 (sc1) exhibits too low extrema as compared with the defined curve. Superior to these results, the streamwise force component is more accurately reproduced by the dynamic scale-similarity and linear-combination models 7 (sc2) to 13 (comb),

	t_{11}	t_{22}	t_{33}	t_{12}	t_{13}	t_{23}	$\sum_j \frac{\partial t_{1j}}{\partial x_j}$	$\sum_j \frac{\partial t_{2j}}{\partial x_j}$	$\sum_j \frac{\partial t_{3j}}{\partial x_j}$	$\sum_{i,j} \overline{u}_i \frac{\partial t_{ij}}{\partial x_j}$
1 (smag)	.2013	.1303	.2336	.0645	.2234	.0163	.0995	.0869	.2225	.2462
2 (lilly)	.2020	.1323	.2330	.0663	.2298	.0193	.1224	.0877	.2258	.2540
3 (pio)	.4024	.3046	.3440	.2795	.5265	.1680	.2515	.1764	.3815	.4004
4 (smagc)	.6592	.6886	.7889	.7007	.7299	.7884	.2574	.3218	.4532	.4558
5 (leo)	.9873	.9935	.9875	.9885	.9831	.9910	.9779	.9867	.9730	.9726
6 (sc1)	.7877	.8402	.8681	.8153	.8167	.9009	.2867	.3867	.4817	.4807
6 (sc1)*	.9510	.9670	.9665	.9531	.9496	.9762	.5801	.6811	.7430	.7449
7 (sc2)	.9943	.9984	.9945	.9910	.9888	.9941	.9725	.9831	.9689	.9684
8 (sc3)	.9962	.9986	.9959	.9901	.9899	.9933	.9713	.9811	.9691	.9689
9 (ss1)	.8166	.8026	.8565	.8524	.8722	.8705	.3287	.3889	.4840	.4900
10 (ss2)	.8579	.8559	.8972	.8821	.8954	.9023	.3834	.4527	.5504	.5547
11 (ss3)	.9394	.9344	.9551	.9530	.9576	.9594	.5450	.6174	.7171	.7226
12 (ss4)	.9424	.9396	.9611	.9564	.9637	.9631	.5662	.6381	.7473	.7531
13 (comb)	.9770	.9917	.9858	.9881	.9869	.9929	.8461	.8987	.9152	.9145

Table III: Representative average correlation coefficients between defined and modelled subgrid terms at tensor, vector and scalar levels for the SGS models tested and the reference filter combination (* corresponds to $\widehat{G}_i \equiv \overline{G}_i \equiv$ f2)

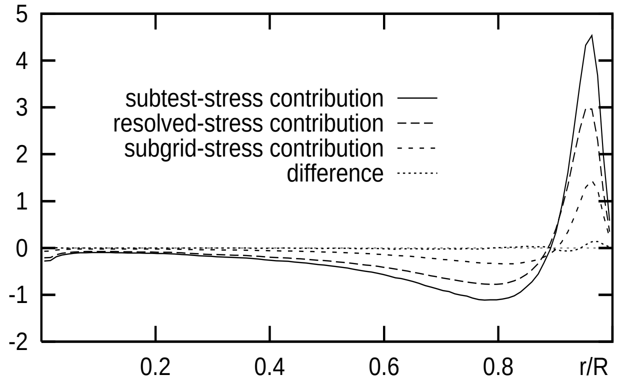

Figure 10: Terms in the third equation of the statistically mean vector-level Germano identity (7) (normalized by u_τ^2/R) with the subgrid- and subtest-scale stresses computed from SGS model 12 (ss4)

above all closures 8 (sc3), 7 (sc2) and 12 (ss4). Similar findings characterize model performance at the **scalar level** (Fig. 9, Tables II and III).

In the *a priori* tests of those models which include an evaluable parametrization of the subtest-scale stresses, the deviations from the statistically mean Germano identity at tensor, vector and scalar levels computed with the modelled subgrid- and subtest-scale stresses have been monitored. For model 12 (ss4), the coefficients of which have been derived from the scalar-level Germano identity (9), the individual terms in the third equation of the averaged vector-level Germano identity (7) are plotted along with the difference between left- and right-hand sides in Fig. 10.

The analysis of **energy transfer** reveals that all (total and component-related, forward and backward) energy fluxes and the mean flux $<f01\_13> = -<\varepsilon_{SGS}>$ between grid and subgrid scales (Fig. 11) with its forward scatter and backscatter (Fig. 12) contributions in particular are fairly well approximated by the scale-similarity and mixed-type parametrizations 7 (sc2) to 13 (comb) in the *a priori* tests. This applies to both their radial distribution and their magnitude with the latter being typically slightly underestimated by these models.

The absolutely largest "local" fluxes between the supertest range and adjacent ranges of

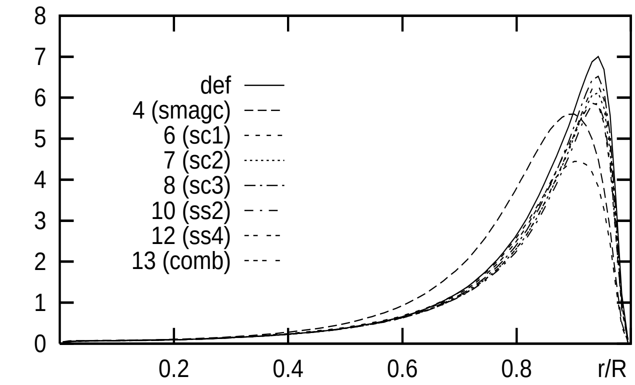

Figure 11: Mean values of flux $f01\_13 = -\varepsilon_{SGS}$ (normalized by u_τ^3/R) for Smagorinsky-, scale-similarity- and mixed-type SGS models as functions of the radial coordinate r/R

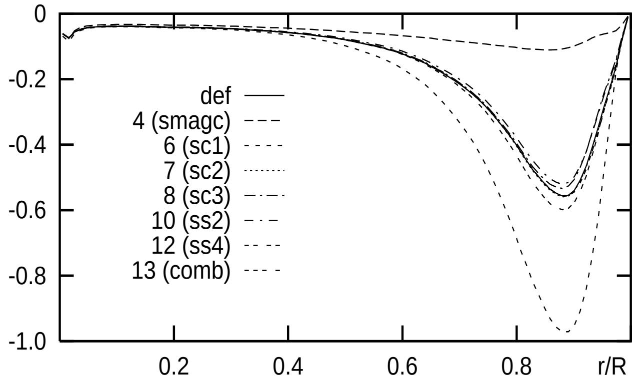

Figure 12: Mean values of backscatter contribution to flux $f01\_13 = -\varepsilon_{SGS}$ (normalized by u_τ^3/R) for Smagorinsky-, scale-similarity- and mixed-type SGS models as functions of the radial coordinate r/R

smaller scales, $f02\_23$ and $f12\_23$, which have been computed for models with evaluable subtest-stress parametrization, are faithfully reproduced by the concerned closures of scale-similarity type such as 12 (ss4) (Fig. 13). The smaller flux $f01\_13 = -\varepsilon_{SGS}$ (Figs. 11, 14) between grid and subgrid scales associated with $\overline{G}$-level and the smallest flux $f01\_12$ (Figs. 14, 15) of "local" nature between subgrid scales and the adjacent part of the grid scales intermediate between $\overline{\Delta}$ and $\widehat{\overline{\Delta}}$ (as well as their forward scatter parts) are generally slightly underestimated by models 7 (sc2) to 13 (comb), which are thus considered to be somewhat underdissipative. The approximation of the latter flux has been identified as a minor deficiency of the proposed scale-similarity models in the *a priori* tests. In this regard, the mixed model 13 (comb) provides the most accurate results (Fig. 15).
Total backscatter (Fig. 12) as well as the inverse scatter part of $f01\_12$ computed from the DNS data according to models 7 (sc2) to 12 (ss4) are also found to be at most insignificantly lower in their absolute values than the defined counterparts. Here, the predictions by models 7 (sc2) and 12 (ss4) are nearly identical with the defined curve, while the linear-combination model 13 (comb) gives rise to a slightly excessive amount of backscatter.
For the "not-so-local" flux contribution $f01\_23$ (Fig. 13) between subgrid scales and the supertest range, which in its maximum ranks next to $f01\_13$, the quality of approximation with models 7 (sc2) to 13 (comb) is similar to that of the latter flux.

By comparison, the energy transfer study for the Smagorinsky-type model 4 (smagc) indicates a more pronounced underestimation of the maximum amount of mean net SGS dissipation and of the maximum mean forward scatter part of $f01\_13$ with the peak occuring at a greater distance from the wall than in the defined curve (Fig. 11). Due to the involved backscatter

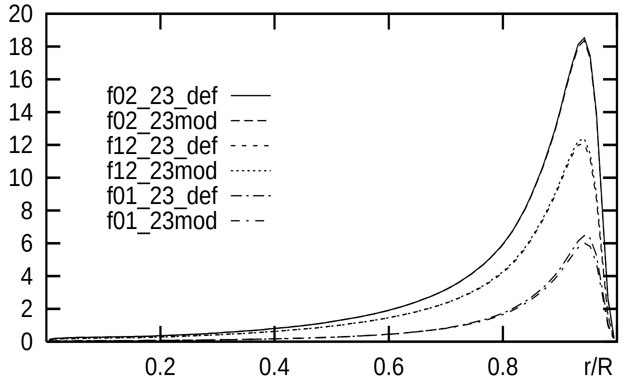

Figure 13: Mean values of flux $f02\_23$ and of the "local" $f12\_23$ and "not-so-local" $f01\_23$ contributions (normalized by u_τ^3/R) with the subgrid- and subtest-scale stresses computed from definition and using SGS model 12 (ss4)

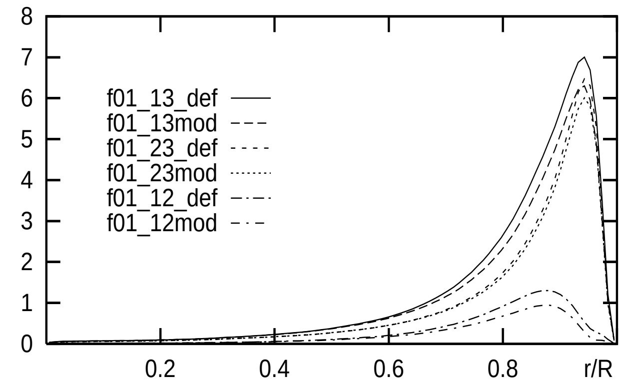

Figure 14: Mean values of flux $f01\_13$ and of the "not-so-local" $f01\_23$ and "local" $f01\_12$ contributions (normalized by u_τ^3/R) with the subgrid-scale stresses computed from definition and using SGS model 12 (ss4)

limitation according to nonnegative component-related total viscosities, the amount of backscatter is severely underpredicted by this model, mainly within $0.6 < r/R < 1$ (Fig. 12). With respect to fluxes between other ranges of scales, the model yields too low a peak in the mean "local" fluxes $f02\_23$ and $f12\_23$. Above all, however, the maximum value of the mean modelled "not-so-local" contribution $f01\_23$ is noticeably smaller than its defined counterpart, while the mean "local" $f01\_12$ flux (Fig. 15) is strongly overestimated by parametrization 4 (smagc).

Related to common modelling assumptions but different backscatter treatment, closure 6 (sc1) as against 4 (smagc) gives qualitatively similar *a priori*-test results for energy fluxes with widely differing backscatter. For model 6 (sc1), the mean "local" flux $f01\_12$ (Fig. 15) is less overpredicted, and an extremely overestimated backscatter (Fig. 12) along with the smallest amount of net SGS dissipation (Fig. 11) among all the proposed closures are indicative of model performance.

For models 4 (smagc), 6 (sc1), 8 (sc3), 9 (ss1), 12 (ss4) and 13 (comb), which, in their parametrization tensor or coefficient formulation, contain the test-filtered SGS stresses t_{ij}^* (or the Smagorinsky-type model coefficients in the test-filtered $C_{(ij)}^*\beta_{ij}$-form), these were calculated from the best information available according to method dt* in the reference *a priori* tests (Tables II and III). On applying the more realistic method mt*, model performance, as expected, declines. Typically, the correlation coefficients were reduced by 1 % (model 12) up to 8 % (model 9) for the SGS normal stresses, by 1 % (models 12 and 13) up to 6 % (model 4) for the SGS shear stresses, and by 3 % (model 12) up to 15 % (model 9) at the vector/scalar level. For the promising model 8 (sc3), a reduction of 2 to 3 % and 6 to 7 % in tensor and vector/scalar level

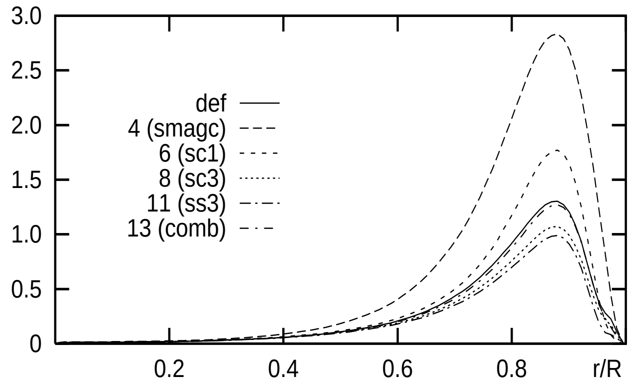

Figure 15: Mean values of flux $f01\_12$ (normalized by u_τ^3/R) for Smagorinsky-, scale-similarity- and mixed-type SGS models as functions of the radial coordinate r/R

correlations, respectively, was established.

Of the other model parameters that have been varied in the *a priori* tests, the backscatter limitation applied to models 6 (sc1) to 8 (sc3) and 13 (comb) with component-related coefficients had the strongest effect. This modification essentially involved a deterioration of the representative average correlation coefficients and L_1-error norms at all levels, and it enabled only a few improvements to be achieved just for model 6 (sc1), which was found to produce excessive backscatter. In contrast to that, the total-flux-related backscatter manipulation of models 9 (ss1) to 12 (ss4) with a scalar coefficient each resulted in only weak changes as against the respective reference tests.

Concerning realizability of the models with component-specific coefficients in combination with top-hat-type filters, to enforce condition (30), the modelled shear stresses have been modified in at most 25 % (model 6), 9 % (model 13) and no more than 5 % (models 7 and 8) of the total number of grid points. For the Smagorinsky-type model 4 (smagc), as expected, condition (30) is violated in a larger percentage of the computational points (35 % and more). In comparison with the original model versions without any realizability modification, this correction did not give a definite global improvement in the *a priori* model performance. For models 4 (smagc), 7 (sc2), 8 (sc3) and 13 (comb), it caused a slight increase in the correlation coefficients pertaining to the SGS shear stresses and to the vector and scalar levels, whereas the mean L_1-distances of these modelled subgrid terms from their defined counterparts grew larger for models 7 and 8 and were only partly decreased for models 4, 6 and 13.

As another parameter variation, in models of Smagorinsky type, 1 (smag) to 4 (smagc), and models with a Smagorinsky ingredient, 6 (sc1) and 13 (comb), the scalar SGS length scale $\overline{\Delta}$ in proportion to the grid size ($\overline{\Delta}_i$ in terms of Δx_i) has been chosen equal to once or twice the latter for comparison. Adopting models 2 (lilly), 3 (pio), 6 (sc1) and 13 (comb), the modelled SGS stresses and all quantities derived therefrom are independent of or hardly influenced by the ratio of the subgrid length scale to the grid spacing. A weak sensitivity to variations in this quantity appeared for model 4 with $\overline{\Delta}$ entering the modelled subgrid stresses via β_{ij}, the dynamic coefficients $C_{(ij)}$ and the upper bounds chosen for them. For the classical Smagorinsky model 1, where the modelled subgrid stresses depend on the square of the SGS length scale, the *a priori*-test results – especially those for the SGS shear stresses and the scalar-level subgrid term – suggest to prefer the value 1 for the ratio considered.
In addition, in this model's empirical wall-damping function for the SGS length scale, the exponents $a = 3$, $b = 1/2$ (fitted to the wall-limiting behaviour of SGS stresses) caused an increase in near-wall ν_{SGS}-values as well as in some of the L_1-error norms and gave no definitive improvement upon the values $a = b = 1$ in the *a priori* tests on the DNS grid.

The comparative consistent *a priori* tests performed on the medium LES grid ($16 \times 64 \times 128$ nodes) using the reference filter combination essentially yielded similar results in terms of qualitative behaviour regardless of some noticeable quantitative differences. As compared with the finer DNS grid, tensor-level correlations for the proposed models are typically diminished here by 0.5 % (model 8) up to about 40 % (model 4). Proceeding from tensor to vector level, correlations on the coarser grid do not decrease as much as on the finer DNS grid; their values are 37 % below (model 4), 1 % below (model 8) up to even 74 % above (model 9) the corresponding vector-level values in Table III. For the subgrid terms at the scalar level, correlation coefficients are smaller by 23 % for model 4 (smagc), by 1 % for model 8 (sc1) or greater up to 11 % for model 9 (ss1) than their counterparts on the DNS grid.

III.B.2 Filter Influence

For the purpose of a comparative evaluation of the implemented filters, all the SGS models have been combined with the approximated top-hat filters f1, f2 and F1, F2, respectively. Especially the scale-similarity and mixed parametrizations require a filtering with sufficient localization in physical space as provided by the top-hat type [10], [15], [47]. Following the recommendations related to consistency between model and filter in [103], the Smagorinsky-type model 4 (smagc) has been coupled with spectral sharp-cutoff-type filters as well, and so has the Leonard-stress-free model 6 (sc1). In addition to the 5-point-implicit–7-point-explicit approximations f3a, f3b and F3, the "exact" sharp-cutoff filter (46) with $\widehat{\Delta}_i = 2\,\Delta x_i$, $4\,\Delta x_i$ and $8\,\Delta x_i$, $i \in \{2,\, 3\}$, implemented via FFT, has been tested.

The influence of variations in grid and test filters with respect to their widths and types clearly came out in the *a priori*-test results for most of the test quantities, and, generally, it was even more pronounced than the effect of changing model parameters.
Considering the widths of the filters involved in the Germano identity (and assuming grid and test filters to be of the same type), according to (6), the dynamic modelling procedure adopted in this paper requires $\widehat{\overline{\Delta}}_i > \overline{\Delta}_i$, a relation that implies $\widehat{\Delta}_i > \overline{\Delta}_i$ for filters of sharp-cutoff type in spectral space, which satisfy Reynolds' averaging postulates. Within this class of filters, the most common ratio $\widehat{\Delta}_i/\overline{\Delta}_i = 2$ has been chosen here. As distinguished from filters generating a spectrally sharp GS/SGS separation, for graded filters with spectral overlapping between GS and SGS components, even $\widehat{\Delta}_i = \overline{\Delta}_i$ is admissible. So, in applying approximations to the top-hat filter, the case $\widehat{G}_i \equiv \overline{G}_i$ has also been examined in particular *a priori* tests.

For all the dynamic SGS parametrizations proposed in Sec. II.B except models 11 (ss3) and 12 (ss4), qualitatively and quantitatively superior results (in terms of both correlations and relative L_1-error norms) were achieved by means of box-type grid and test filters with $\widehat{\Delta}_i = \overline{\Delta}_i = 2\,\Delta x_i$. This applies individually to the trapezoidal and Simpson's rule approximations of the top-hat filter and is especially marked for models 6, 9, 10 and 13, which contain test-filtering in both their parametrization tensor and the dynamic coefficients.
As compared with the variant $\widehat{\Delta}_i = 2\,\overline{\Delta}_i$ and $\widehat{\overline{\Delta}}_i^{\,2} \approx 5\,\overline{\Delta}_i^{\,2}$, this test-filtering over a smaller interval, $\widehat{\Delta}_i = \overline{\Delta}_i$ and $\widehat{\overline{\Delta}}_i^{\,2} \approx 2\,\overline{\Delta}_i^{\,2}$, enables less local information to be averaged out and a more pronounced similarity between $\overline{G}$- and $\widehat{\overline{G}}$-filtered quantities to be attained. Concerning the proposed scale-similarity models, the special case $\widehat{G}_i \equiv \overline{G}_i$ for box-type filters means that a smaller and more intermittent range of scales (between $\overline{\Delta}_i$ and $\widehat{\overline{\Delta}}_i$) is incorporated into modelling and that the resolved-stress and the (modified) Leonard-stress tensors coincide, $\mathfrak{L}_{ij} \equiv \mathcal{L}_{ij}$.
The *a priori*-test results in [107] also suggest that, for scale-similarity and mixed models, the second filter type in the computation of the parametrization tensor should be as similar as possible to the grid filter. With respect to the width, it was concluded in [107] that in applications along with high-order finite-difference schemes, it may be more appropriate to use the (modified) Leonard stresses, i. e. the second filter of the same width as the grid filter, instead of the resolved-stress tensor and a test filter of width $\widehat{\Delta}_i = 2\,\overline{\Delta}_i$.

For all the subgrid-scale models tested herein, the top-hat filter approximated by Simpson's rule and for models 4 (smagc), 6 (sc1) to 8 (sc3), 9 (ss1), 10 (ss2) and 13 (comb), the choice $\widehat{G}_i \equiv \overline{G}_i \equiv$ f2 with $\widehat{\Delta}_i = \overline{\Delta}_i = 2\,\Delta x_i$ in particular yielded the overall closest agreement between

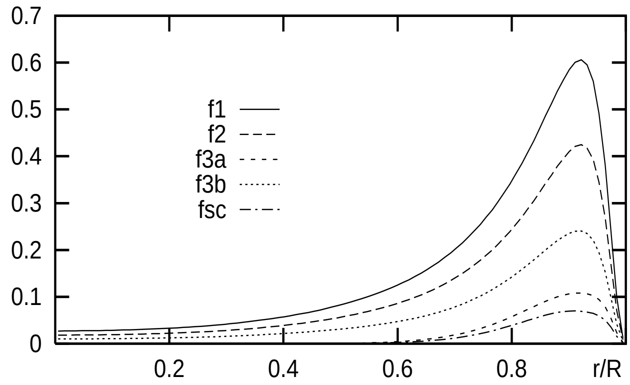

Figure 16: Mean values of defined subgrid-scale energy (normalized by u_τ^2) for top-hat- and sharp-cutoff-type grid filters $\overline{G}_i$ of width $2\,\Delta x_i$ on the DNS grid as functions of the radial coordinate r/R

modelled and defined quantities both in a qualitative and a quantitative sense. The most striking improvement in performance by changing the test filter from $\widehat{G}_i \equiv$ F2 to $\widehat{G}_i \equiv \overline{G}_i \equiv$ f2 was observed with model 6 (sc1) (see * in Tables II and III).
Overall, in nearly every respect, the best *a priori* test of the model/filter combinations under study was established for model 8 (sc3) – followed by models 7 (sc2), 13 (comb) and 6 (sc1) – all applied along with the filters $\widehat{G}_i \equiv \overline{G}_i \equiv$ f2. This particular filter/filter combination typically produced the smallest absolute values of defined (and also numerous modelled) "local" energy fluxes $f01\_12$, $f01\_13$, $f02\_23$, $f12\_23$, subgrid- and subtest-scale stresses and energies as well as forward scatter and backscatter contributions to net SGS dissipation within the class of discrete approximations to the top-hat filter.

Adopting sharp-cutoff-type grid and test filters instead with $\widehat{\Delta}_i = 2\,\overline{\Delta}_i$, the performance of models 4 (smagc) and 6 (sc1) deteriorates as is mainly indicated by a strong decrease in the level of correlations and a considerable increase in the average L_1-distances between defined and modelled subgrid terms compared with the reference filter combination. This may be attributed to the spectrally sharp GS/SGS separation, which results in lower absolute values of defined subgrid stresses and energies arising only from small-scale turbulence components below the cutoff and being modelled by means of a spectrally disjoint range of larger scales. Contrary to the top-hat type, cutoff filters exhibit an oscillating physical-space behaviour with varying sign, which, in [15] and [47], is considered a cause of reduced correlation between local flow features. For the "exact" sharp-cutoff filter, the grid-/test-filter combination with widths $\overline{\Delta}_i = 4\,\Delta x_i$, $\widehat{\Delta}_i = 8\,\Delta x_i$ turned out to be more favourable with respect to the correlation coefficients and relative L_1-error norms than the variant of smaller grid and test filtering with $\overline{\Delta}_i = 2\,\Delta x_i$, $\widehat{\Delta}_i = 4\,\Delta x_i$. The latter, among all the filter combinations tested for the two models mentioned above, gave the smallest defined and modelled energies of subgrid-scale motion (Fig. 16) and at the subtest-scale level in addition to appreciably smaller absolute values of defined subgrid- and subtest-scale stresses than box-type filters of the same width. Concerning energy transfer, it characteristically generated the smallest defined fluxes $f01\_23$ as well as $f01\_13 = -\varepsilon_{SGS}$ with the absolutely largest forward scatter and backscatter contributions.
With regard to the 5-point-implicit–7-point-explicit sharp-cutoff approximations, they are comparable in computing time with the FFT realization of (46), and, on the DNS grid, the filter combination $\overline{G}_i =$ f3a, $\widehat{G}_i =$ F3 seems to imitate the pair of original sharp-cutoff filters of widths $\overline{\Delta}_i = 2\,\Delta x_i$ and $\widehat{\Delta}_i = 4\,\Delta x_i$ more closely than $\overline{G}_i =$ f3b, $\widehat{G}_i =$ F3 (for SGS energy, see Fig. 16).

IV Large-Eddy Simulations – *A posteriori* Tests

IV.A Simulation Overview

In the second and indispensable stage of evaluation, the proposed subgrid models have been thoroughly tested *a posteriori* by performing large-eddy simulations for the fully developed turbulent pipe flow, $Re_\tau = 1{,}050$ equivalent to $Re_{CL} \approx 25{,}000$, in the domain $[0, R] \times [0, 2\pi] \times [0, L]$, $L = 8\,R$. To study model performance in LES, the effect of filters and computational grids as well as the sensitivity of numerical results to variations in model parameters, in total, over 80 simulations have been analyzed. The findings will be presented in the following subsection mainly for the medium LES grid and a filter choice corresponding to the reference filter combination defined in Sec. III.B.

As suggested by the outcome of the *a priori* tests, simulation efforts have been focused on scale-similarity models of the first group with component-specific coefficients and, among them, model 8 (sc3) in particular. Of the remaining models with scalar coefficients, the Leonard-stress-related model 12 (ss4) and the resolved-stress-based parametrization 10 (ss2) as representatives of the groups 2 and 3, respectively, have been primarily tested in LES. In another series of simulations, the generalized Smagorinsky-type model 4 (smagc) has been applied in combination with various test filters including those of sharp-cutoff type. For comparison, simulation results obtained with the known models 1 (smag) to 3 (pio) and 5 (leo) are again incorporated in the evaluation, which was performed against numerical [52] and experimental [108], [109], [110] pipe-flow data.

The LES input quantities were largely chosen to match the values assigned in the reference *a priori* tests. In addition, model parameters such as bounds for the dynamic model coefficients, the subgrid-scale length scale in relation to the grid size for Smagorinsky-type model components and the exponents of the Van-Driest-type wall-damping function of the classical Smagorinsky model have been varied. Furthermore, in employing models with component-specific coefficients along with top-hat filters, the "clipping" approximation for realizability (30) was optionally activated. Concerning the proposed models of scale-similarity type, LES results are presented with the backscatter modifications (outlined in Sec. II.D.4) included. For the promising model 8 (sc3), these *a posteriori* tests are supplemented with simulation runs without any backscatter-related modification and those performed with filter variations. The favourable effect of grid refinement was demonstrated for model 6 (sc1), by way of example.

The large-eddy simulations reported here have been started from the same initial data field for each of the Smagorinsky-type models 1 (smag) to 4 (smagc) and of the scale-similarity-/ combined-type models 5 (leo) to 13 (comb), and they have been carried out for six characteristic time scales. Statistical data evaluation, which has been conducted by applying the same methods to the GS velocity field as used in the *a priori* tests, is based on 45 LES realizations separated by $\Delta t = 0.12$ nondimensional time units. Here, the initial time development of the simulated flow has been excluded from the computation of statistical quantities.

The analyzed statistics comprise not only first- and second-order one-point moments of the GS velocity field, which will be discussed in the following subsection, but also higher-order turbulence characteristics (third- and fourth-order moments) as well as spatial two-point autocorrelation functions of GS velocities in various directions and the associated one-dimensional energy spectra, which will only partly be outlined here.

IV.B Results

IV.B.1 Model Performance

The LES results obtained on the medium grid using the Simpson's rule approximations to the top-hat filter, f2 and F2, showed small to great quantitative and, in parts, also qualitative differences in the analyzed statistics for SGS models or model groups 4 (smagc), 6 (sc1), and 7

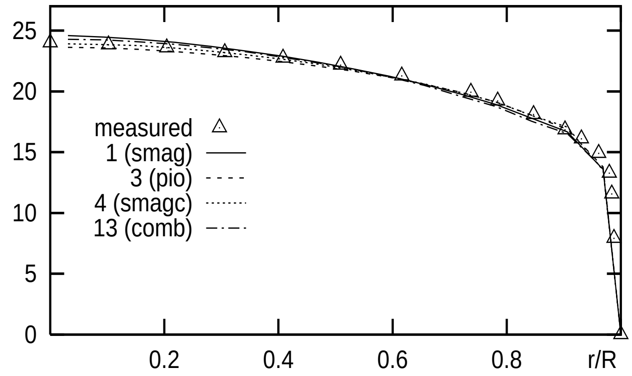

Figure 17: Mean values of axial velocity component, $<w>/u_\tau$, for Smagorinsky- and mixed-type SGS models as functions of the radial coordinate r/R

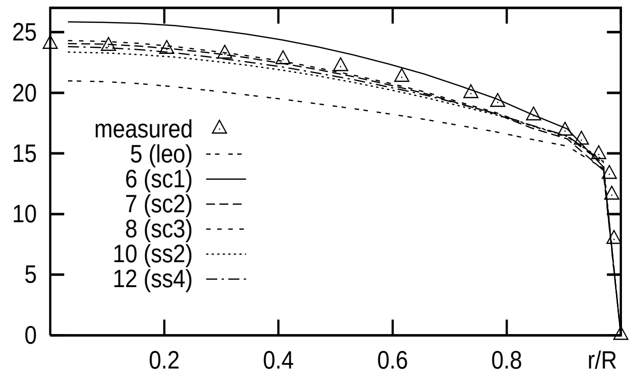

Figure 18: Mean values of axial velocity component, $<w>/u_\tau$, for scale-similarity-type SGS models as functions of the radial coordinate r/R

(sc2) to 13 (comb) in comparison with each other and with the known subgrid closures 1 (smag) to 3 (pio) and 5 (leo). For the classical Smagorinsky model 1 (smag), the findings presented here closely agree with those in [52].

The computed radial profiles of the **mean axial velocity component**, $<\overline{w}>=<w>$, have been evaluated against experimental pipe-flow data by Browne and Dinkelacker [108]. Among the Smagorinsky-type models, the base model 1 (smag) gave slightly overestimated $<w>$-values near the axis (Fig. 17). In this respect, improved $<w>$-curves have been established by means of the dynamic model versions 3 (pio) and, first of all, 2 (lilly) (not drawn). The mean axial velocity obtained with the latter model nearly coincides with that of the proposed model 4 (smagc), which, applied along with the test filter $\widehat{G}_i$ = f2 of width $2\,\Delta x_i$, provided the best $<w>$-predictions of all the SGS models tested. Deviations can be noticed in the underresolved near-wall region, which, for the Smagorinsky model 1, was treated with an $O(r_+)$ exponential wall-damping function, whereas no supplementary near-wall modifications have been incorporated into all the other parametrizations. With respect to the scale-similarity-type models, the amount of backscatter in LES has been found to have a strong effect on the resulting mean axial velocity profile. To illustrate this, the $<w>$-profile computed with the nondynamic scale-similarity model 5 (leo) is depicted in Fig. 18. This curve is similar to the mean axial velocities produced by the original formulations of models 7 (sc2) and 8 (sc3) without any backscatter-related modification (not drawn). For these $<w>$-profiles, the value on the axis is much too small, and the curves as functions of the radial coordinate are too flat. This is connected with too large an integral of the absolute value of the rz-Reynolds shear stress (sum of GS part and mean SGS stress) $-\int <u\,(w-<w>)>dr = -\int <\overline{u}\,(\overline{w}-<\overline{w}>)>dr + \int <t_{rz}>dr$ with respect to r from 0 to R and also within radial subranges excluding the near-wall region.
The latter results are contrasted with the $<w>$-predictions by models 6 (sc1) to 13 (comb)

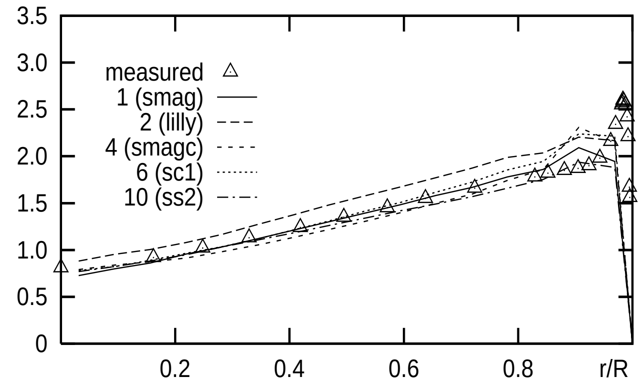

Figure 19: Rms values of axial velocity component, w_{rms}/u_τ, for Smagorinsky- and scale-similarity-type SGS models as functions of the radial coordinate r/R

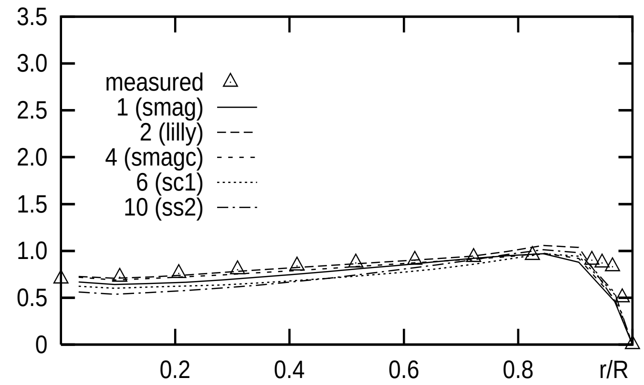

Figure 20: Rms values of radial velocity component, u_{rms}/u_τ, for Smagorinsky- and scale-similarity-type SGS models as functions of the radial coordinate r/R

with an artificially limited amount of backscatter as described in Sec. II.D.4. For models 7 (sc2) to 12 (ss4), the computed $<w>$-profiles within the radial subrange $0 \leqslant r/R \leqslant 0.5$ compare satisfactorily well with the measured one. The mean axial velocity values obtained with models 9 (ss1) to 12 (ss4) with a scalar coefficient each are generally located below the experimental data with the largest deviations occuring roughly within $0.5 \leqslant r/R \leqslant 0.9$ (see representatives 10 and 12 in Fig. 18).

Within the group of SGS closures with scale-similarity part, the mixed model 13 (comb) enabled slightly superior $<w>$-predictions to be achieved within this radial subrange (Fig. 17), whereas parametrizations 7 (sc1) to 12 (ss4) resulted in too strong a decrease in the $<w>$-profile in the direction towards the wall.

The exceptional behaviour of model 6 (sc1) is evident from the mean axial velocity profile, which, from the axis to the near-wall region, lies above the $<w>$-values measured in experiment and those predicted by all the other models tested (Fig. 18).

Velocity rms values have been computed from the three GS velocity components (without having included an estimate for the SGS contributions) and have been compared with experimental data for rms values of the statistical velocity fluctuations u_{rms}, v_{rms} taken from [109] and w_{rms} from [108]. The measured rms values of the axial velocity component, w_{rms}, are reasonably well reproduced by models 1 (smag), 6 (sc1) and 10 (ss2) in particular (Fig. 19). In connection with the empirical wall-boundary conditions and the current coarse resolution of the near-wall region, the peak close to the wall is, however, not captured adequately. The w_{rms}-level generated by model 2 (lilly) is typically higher than the measured one, while all the other models produced values mostly below the experimental curve, which additionally includes the contributions from the subgrid scales. Similarly, the levels of the measured radial and circumferential velocity rms

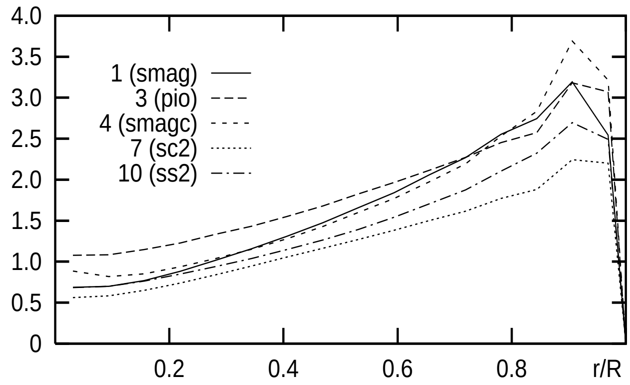

Figure 21: Mean values of GS energy, $<E_{GS}>/u_\tau^2$, for Smagorinsky- and scale-similarity-type SGS models as functions of the radial coordinate r/R

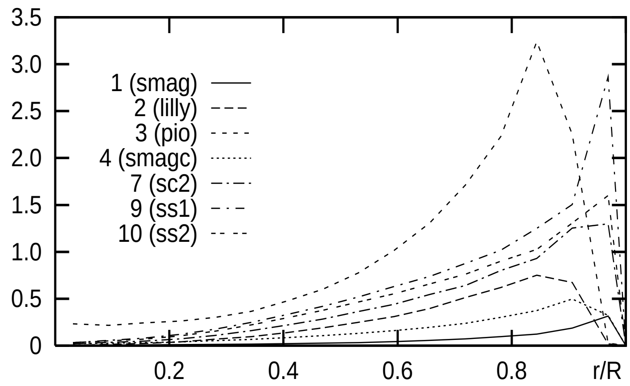

Figure 22: Mean values of SGS energy, $<E_{SGS}>/u_\tau^2$, for Smagorinsky- and scale-similarity-type SGS models as functions of the radial coordinate r/R

values are generally slightly underpredicted within the subrange $0 \leqslant r/R \leqslant 0.7$ with the agreement between measured and computed values being fairly close for the Smagorinsky-type models 1 (smag) to 4 (smagc). In Fig. 20, rms values of the radial velocity component are displayed; the v_{rms}-level is not much higher, and the quality of approximation is comparable with that of u_{rms}.

In **GS and SGS energies**, remarkable differences can be observed between the mean values obtained with the different models. The computed mean GS energy, which is defined here to be the statistically averaged fluctuating part of grid-scale energy (GS part of kinetic turbulence energy), $<E_{GS}> = 1/2\,(<\overline{u}^2 + \overline{v}^2 + \overline{w}^2> - <w>^2)$, is plotted in Fig. 21. Within the radial subrange $0 \leqslant r/R \leqslant 0.7$, the highest $<E_{GS}>$-levels have been generated by models 2 (lilly) (not drawn) and 3 (pio). The largest near-wall peak values of this quantity have resulted from the application of models 4 (smagc) and 6 (sc1) (not drawn), followed by the known Smagorinsky-type models 1 (smag) to 3 (pio). Lower mean values of the energy of grid-scale motion have been established with models 9 (ss1) to 12 (ss4) (see representative 10 in Fig. 21) and with model 13 (comb). The lowest $<E_{GS}>$-level is typical of models 7 (sc2) and 8 (sc3) (not drawn).

The even more pronounced differences in magnitude and radial distribution of the mean subgrid-scale energy, $<E_{SGS}> = -1/2\sum_i<t_{ii}>$, are obvious from Fig. 22. It indicates that, with some models and the current spatial resolution, a relatively large maximum amount of turbulent kinetic energy is present in the unresolved scales. For the known Smagorinsky-type models 1 (smag) to 3 (pio), $<E_{SGS}>$ has been approximated according to the estimate given by Lilly [67]: $<E_{SGS}> = <\nu_{SGS}^2>/(C_\nu\overline{\Delta})^2$ with $C_\nu = 0.094$. Adopting model 3 (pio), this estimate caused the largest peak of $<E_{SGS}>$ located at the greatest distance from the wall as well as the largest SGS-energy level from the axis to the near-wall region. Compared with

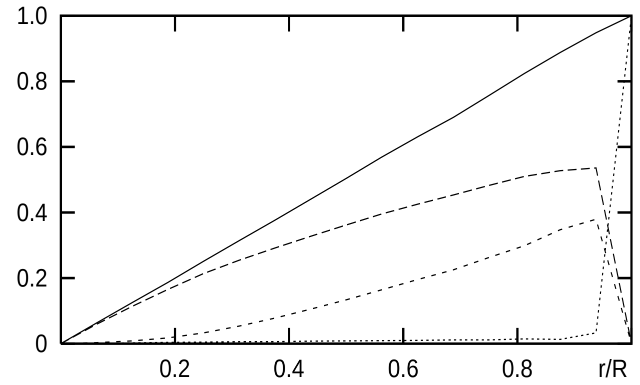

Figure 23: Decomposition of the statistically averaged total rz-shear stress $-\tau_{rz}^{sum}/u_\tau^2$ —— for SGS model 8 (sc3) into the contributions from the grid-scale part of the rz-Reynolds stress $-\tau_{rz}^{GS}/u_\tau^2$ – – – , the mean rz-subgrid-scale stress $-t_{rz}^{SGS}/u_\tau^2$ - - - - , and the associated mean viscous stress $-\tau_{rz}^{vis}/u_\tau^2$ ········

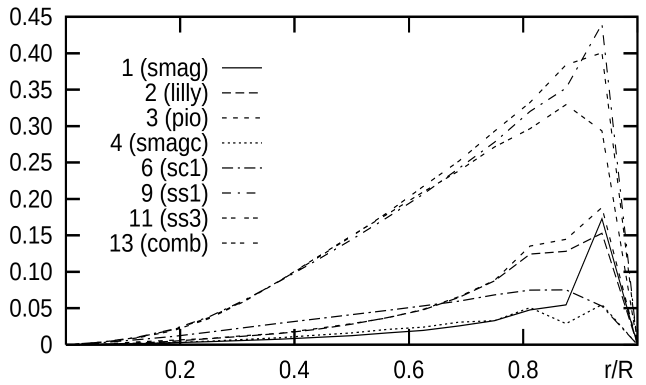

Figure 24: Mean values of $-t_{rz}^{SGS}/u_\tau^2$ for Smagorinsky-, scale-similarity- and mixed-type SGS models as functions of the radial coordinate r/R

that, the maximum of $<E_{SGS}>$ turned out to be smaller and closer to the wall for the group of models 9 (ss1) to 12 (ss4). Among these parametrizations with a scalar coefficient each, 9 (ss1) gave an exceptionally large peak value of $<E_{SGS}>$ which in its magnitude comes close to that resulting from model 3 (pio). Scale-similarity- and combined-type-models 6 (sc1) to 8 (sc3) and 13 (comb) rank next (see representative 7 in Fig. 22). The lowest level of computed or estimated subgrid energy is discernible for the Smagorinsky-type closures 2 (lilly), 4 (smagc) and, above all, 1 (smag). In the near-wall region, the $<E_{SGS}>$-curves for the proposed models 7 (sc2) to 13 (comb) as against the known Smagorinsky-type parametrizations 1 (smag) to 3 (pio) take far higher values up to the wall and have their maximum at roughly $r/R \approx 0.97$.

Based on LES data for model 8 (sc3), Fig. 23 represents the radial profile of the statistically averaged **total rz-shear stress**, $<\tau_{rz}^{sum}>$, along with the individual contributions from the grid-scale part of the rz-Reynolds stress and the mean values of the associated subgrid-scale and viscous stresses, which add up to the linear profile characteristic of the fully developed steady-state turbulent pipe-flow considered: $<\tau_{rz}^{sum}> = -<\overline{u}\,(\overline{w} - <\overline{w}>)> + <t_{rz}> + \nu\, d<w>/dr$. The magnitude of the individual contributions shown in Fig. 23 is exemplary of the results attained with models 7 (sc2) to 13 (comb), while larger GS shear-stress contributions and considerably smaller **SGS stresses** $<t_{rz}>$ (Fig. 24) within nearly the whole radial range including the near-wall region have generally been obtained with the Smagorinsky-type models 1 (smag) to 4 (smagc) and with model 6 (sc1). Fig. 24 especially illustrates the low $<t_{rz}>$-level resulting from models 4 (smagc) and 6 (sc1) and, for the remaining proposed dynamic scale-similarity parametrizations, the nearly uniform growth of $-<t_{rz}>$ up to its near-wall

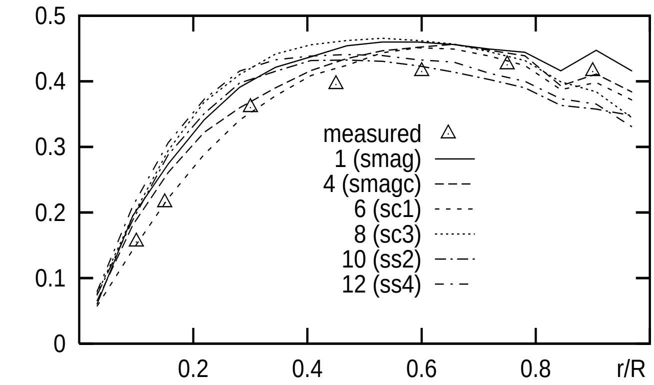

Figure 25: Correlation coefficient C_{rz} between axial and radial velocity components for Smagorinsky- and scale-similarity-type SGS models as function of the radial coordinate r/R

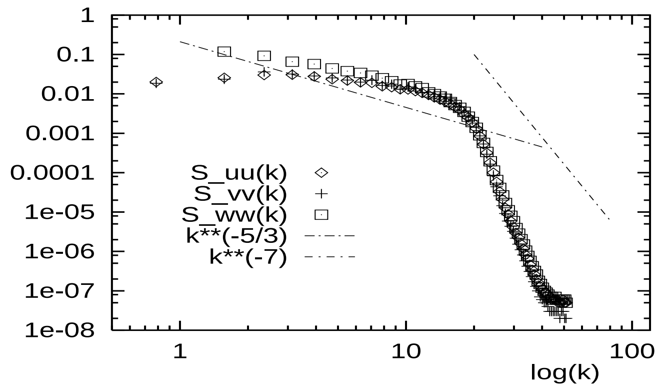

Figure 26: Streamwise one-dimensional (normalized) energy spectra $S_{\alpha\alpha}(k)\, R/u_\tau^2$ of the GS velocities for SGS model 8 (sc3) in the radial position $r/R \approx 0.2$ versus wavenumber k (log-log plot)

maximum at $r/R \approx 0.94$.

To evaluate the **correlation coefficient** (spatial one-point correlation function normalized by the rms values) between the axial and radial velocity components, from the great number of available and widely differing experimental results for this quantity, measured data by Sabot [110] have been employed for comparison with the values of $C_{rz} = <\overline{u}\,(\overline{w} - <\overline{w}>)>/(u_{rms}\, w_{rms})$ computed from the GS velocity field. The measured values drawn in Fig. 25 are moderately well reproduced, at least by models 6 (sc1) and 4 (smagc). Here, for most of the SGS parametrizations used, the computed correlations within the radial subrange $0 \leqslant r/R \leqslant 0.6$ typically exceed their experimental counterparts. This is connected with (for this range) mostly too small velocity rms values u_{rms}, w_{rms} computed from the GS field.

With respect to the analyzed statistical one-point moments of higher order, the **skewness** of the three GS velocities has been described quite well as against experimental data adopted from [110]. However, in view of the chosen number of realizations from which to evaluate statistics, the GS velocity **flatness** values near the axis were greatly varying from one simulation to the next.

Among the computed two-point statistics, especially the **two-point autocorrelation functions** in the radial direction of the axial velocity component proved to be sensitive to the SGS model. Differences between the results obtained for the models or model groups under study can also be seen in the associated streamwise one-dimensional (normalized) **energy spectra** of the three GS velocities. A typical visualization of these spectra in the radial position $r/R \approx 0.2$ is given for model 8 (sc3) in Fig. 26, where a log-log spectral plot is presented. It is common to the spectra for all the models tested that they have too steep a slope within the high-wavenumber range and lack a well-developed $k^{-5/3}$-behaviour. The spectra resulting from model 4 (smagc) and the proposed scale-similarity- and combined-type parametrizations, 6 (sc1) to 13 (comb), if backscatter is limited artificially, exhibit a characteristic "kink" at the high-wavenumber end. This is most pronounced for model 6 (sc1), which was found to underpredict SGS dissipation and to overpredict backscatter.

Of the tested variations in models and LES input parameters, the backscatter treatment turned out to have great influence. Without any backscatter limitation, scale-similarity-type models caused numerical instabilities in some applications or they typically resulted in clearly too flat radial profiles of mean axial velocity, in larger near-wall velocity rms values and considerable amounts of average GS and SGS energies. Specifically, the maxima of these energies as well as those of the absolute values of the GS part of the rz-Reynolds stress and of the associated mean SGS stress come close to each other in both magnitude and radial position.
A quantitative analysis of backscatter reveals that the SGS stresses computed according to definition from DNS data give rise to a reverse energy flow on the DNS grid in about 34 % and on the medium LES grid in roughly 30 % to 31 % of the total number of grid points. Applying the proposed parametrizations, modelled backscatter was observed in the *a priori* tests on the DNS grid in nearly 30 % (model 9) to 36 % (model 6) and on the medium LES grid in 24 % (model 9) to 36 % (model 6) of the total number of computational points. As against that, in LES, approximately 32 % (model 9) up to 40 % (model 6) of the grid points encountered backscatter. Considering the different models, the backscatter part computed according to definition is underestimated in the *a priori* tests using the proposed models with a scalar coefficient by 1 % (model 12) to 7 % (model 9), and it is recovered extremely well by models 7 (sc1), 8 (sc2) and 13 (comb). Closure 6 (sc1), when compared with all the other parametrizations tested, was found to generate a backward energy flux in the largest part of the computational points and to overpredict the defined backscatter fraction.
In addition, the LES results indicated the general tendency for the Leonard-stress-related models 7 (sc2), 11 (ss3) and 12 (ss4) to produce more backscatter than the resolved-stress-related closures 8 (sc3), 9 (ss1), 10 (ss2) and the linear-combination model 13 (comb). Among the models with component-specific coefficients, in the *a priori* tests closure 8 (sc3) and in LES parametrizations 13 (comb) and 8 (sc3) brought about backscatter occuring in the smallest fraction of the grid points.
With respect to the amount, an inverse energy flux corresponding to a negative total viscosity was established in the *a priori* tests in no more than 2 % or at most 7 % (model 6) of the total number of grid points, while in LES (at a greater Reynolds number) as much as over 20 % to almost 30 % of the discretization points on the same grid experienced backscatter of this intensity.

Realizability modifications for models with component-related coefficients applied along with box-type filters have been performed in LES in a far greater fraction of the computational points than in the *a priori* tests on the DNS grid, viz. in 15 % to 18 % (models 7, 8 and 13) and in about 45 % (models 4 and 6) of the total number of grid points. As a result of these modifications, the absolute values of $< t_{rz} >$ clearly decreased, and the GS part of the rz-Reynolds stresses increased (by smaller values) so that there was a general tendency towards a rise in the mean axial velocity values at the axis and, mostly, up to the near-wall region. Accordingly, the performance of the considered models in LES improved (model 4) or declined (model 6), respectively, by applying additional realizability modifications.

In large-eddy simulations similar to the *a priori* tests, the variation of the ratio of the SGS length scale $\overline{\Delta}$ to the grid size $(\overline{\Delta}_i/\Delta x_i)$ in the Smagorinsky part of models 2 (lilly), 3 (pio), 6 (sc1) and 13 (comb) had hardly any observable effect on the results, especially for the mean axial velocity profile, the velocity rms values and the rz-shear stress balance. Adopting for this ratio the value 2 instead of 1, no stable simulations were accomplished for model 4 (smagc), and the computed mean and rms values of velocity deteriorated for model 1 (smag).
With regard to the near-wall reduction of the SGS length scale in this model, the Van-Driest-type wall-damping function with the exponents $a = 3$, $b = 1/2$ gave a more pronounced peak in SGS

turbulence viscosity close to the wall but altogether, on the LES grid, no decisive improvements upon the $O(r_+)$ damping.

Not only in this underresolved near-wall region, the impact of grid density became apparent. In changing from coarse to medium LES grid, the expected qualitative behaviour of SGS stresses as well as those of GS and SGS parts of kinetic turbulence energy in terms of grid size has been observed, and significant improvements in the computed statistics were achieved. On the finest as compared with the medium LES grid, for model 6 (sc1), a partial increase in performance with respect to the mean axial velocity profile succeeded. According to local hardware facilities currently available, thorough large-eddy simulations with all the considered models on the finest LES grid were, however, beyond reach in the present study. Therefore, *a posteriori* tests of the proposed SGS closures on finer grids and, above all, in properly resolved near-wall flow regions remain to be performed.

IV.B.2 Filter Influence

In a series of large-eddy simulations, for model 8 (sc3) as a representative, four combinations of discrete box-type filters at the grid-level (applied in calculating model coefficients from the GS field) and at the test level (entering the parametrization tensor and the coefficients) have been tested comparatively: $\overline{G}_i \equiv$ f1 has been coupled with $\widehat{G}_i \equiv$ F1 and with $\widehat{G}_i \equiv$ f1. Analogously, for the Simpson's rule approximation, $\overline{G}_i \equiv$ f2 and $\widehat{G}_i \equiv$ F2 (reference filter combination) or $\widehat{G}_i \equiv$ f2 have been chosen alternatively.
Mean velocity profiles proved to be rather insensitive to these filter variations and nearly coincided for the first two filter combinations (trapezoidal-rule quadrature) equally as for the latter two (Simpson's-rule quadrature), which yielded $<w>$-curves in slightly closer agreement with experiment. For both types of discrete approximations to the top-hat kernel, by adopting $\widehat{G}_i \equiv \overline{G}_i$ compared with the test filter of greater width, a larger SGS and, conversely, a smaller GS energy were predicted together with larger absolute values of the mean SGS stress $<t_{rz}>$ and smaller absolute values of the GS contribution to the rz-Reynolds stress. Specifically, for the filters $\widehat{G}_i \equiv \overline{G}_i \equiv$ f1, the maximum of the mean SGS energy reaches that of the mean GS energy in magnitude and radial position, and for $\widehat{G}_i \equiv \overline{G}_i \equiv$ f2 the same applies to the maximum absolute values of $<t_{rz}>$ and of the GS part of the rz-Reynolds stress.
In all, for the considered model, the reference filter combination resulted in the smallest absolute values of mean SGS energy, $<E_{SGS}>$, and SGS stress $<t_{rz}>$ and offered the best comparison with experimental flow data available.

For model 4 (smagc), simulations succeeded by adopting the test filters of width $\widehat{\Delta}_i = 2\,\Delta x_i$ along with setting $\widehat{\overline{\Delta}}_i^{\,2} = 5\,(\Delta x_i)^2$ (top-hat type) and $\widehat{\overline{\Delta}}_i^{\,2} = 4\,(\Delta x_i)^2$ (sharp-cutoff type), whereas LES runs with test filters of greater widths encountered numerical instabilities.
The filter-induced differences in the evaluated statistics for this model are primarily of quantitative nature. Typically, the LES results obtained with sharp-cutoff instead of top-hat-type test filters of the specified width are characterized by lower levels of subgrid energy and smaller absolute values of SGS stresses. Of the applied test filters $\widehat{G}_i \equiv$ f1, f2, f3a, f3b and the "exact" sharp-cutoff filter fsc, the latter was associated with the smallest mean subgrid-scale energy, while the trapezoidal-rule approximation to the top-hat filter, f1, gave the largest $<E_{SGS}>$-values. Comparing the sharp-cutoff approximations f3a and f3b in LES applications of model 4 (smagc) on the medium grid, f3a produced smaller SGS energies, whereas f3b seemed to more closely emulate the effect of the "exact" sharp-cutoff filter on the mean velocity profile.
As against experimental data, for the concerned model, $\widehat{G}_i \equiv$ f2 enabled the best results to be achieved, especially with respect to the mean axial velocity, which, mainly within $0.7 \leqslant r/R \leqslant 0.9$, was overpredicted with all the other test filters and those of sharp-cutoff type in particular.

Generally, in the present finite-difference LES computations, sharp-cutoff-type filters turned out to be more problematic from a numerical point of view and inferior to top-hat-type filters in reproducing experimental data for statistical turbulence characteristics.

V Final Model/Filter Evaluation

The common Smagorinsky **model 1 (smag)** gave a poor local performance in the *a priori* tests at all levels. This is especially manifested in an excessive peak located too close to the wall in the mean relevant SGS stress $<t_{rz}^{mod}>$ and hence in the vector-level subgrid term containing $d{<}t_{rz}^{mod}{>}/dr$ just as in the subgrid term at the scalar level. From the axis up to this near-wall peak, however, the absolute values of $<t_{rz}^{def}>$ are most strongly underestimated by this purely dissipative model. Globally, a reasonable approximation to the integral $\int_0^R <t_{rz}>dr$ was established by the Smagorinsky model. This result, considered in connection with the approximation to the corresponding integral of the GS part of the rz-Reynolds stress in the integrated shear-stress balance, gives, at least to some extent, an explanation of the model's satisfactory overall effect on the mean axial velocity profile computed in LES.

For the dynamic Smagorinsky-type **model 2 (lilly)** as distinguished from the nondynamic base parametrization, the *a priori*-test results indicated underestimated absolute values of the mean relevant SGS shear stress, $<t_{rz}>$, within the whole radial range as well as an underestimation of the extrema in the third component of the divergence of the mean SGS-stress tensor and of the peaks in the mean scalar-level subgrid term. For these quantities, the L_1-error norms are reduced, and the correlation coefficients are slightly increased against those resulting from model 1 (smag). In other respects, however, the *a priori* model performance is not considerably improved upon the Smagorinsky closure, and the dynamic SGS modelling potential appears to be not exhausted by the Lilly model. In LES, this parametrization gave a mean axial velocity profile in extremely close agreement with the measured curve along with slightly overpredicted rms values of this velocity component. Typically, the computed or estimated $<E_{GS}>$-, $<E_{SGS}>$- and $<t_{rz}>$-levels are mostly higher than those generated by the original nondynamic model.

A similar behaviour has been observed for the dynamic Smagorinsky-type **model 3 (pio)** with a localized coefficient. As compared with model 2 (lilly), it produced larger peak values of $<\nu_{SGS}>$, $<E_{SGS}>$ and $<t_{rz}>$ in both testing stages. Consequently, the *a priori* model performance is further improved primarily with respect to the test quantities t_{13}, $\sum_j \partial t_{3j}/\partial x_j$, $\sum_{ij} \overline{u}_i\, \partial t_{ij}/\partial x_j$ and also t_{23}, t_{12}. However, the simulation results, especially those for the mean axial velocity, suggest that the potential advantages of the localized coefficient formulation in this model are not equally reflected in improved LES predictions.

For the proposed generalized anisotropic Smagorinsky-type **model 4 (smagc)**, the *a priori*-test results revealed pronounced differences between the individual component-specific subgrid eddy viscosities and also against the scalar SGS turbulence viscosity of the known Smagorinsky-type closures. In comparison with models 1 (smag) to 3 (pio), mainly the local *a priori* performance at the tensor level and that with respect to the first and second components of the vector-level subgrid term is improved as can be seen from the correlation coefficients and L_1-error norms. The defined peak values of the mean dominant SGS normal stress, $<t_{zz}>$, of the mean subgrid-scale energy, $<E_{SGS}>$, and of the mean relevant SGS shear stress, $<t_{rz}>$, are, however, noticeably underestimated by this model. Likewise, in the *a posteriori* tests of model 4 (smagc), $<t_{rz}>$- and $<E_{SGS}>$-levels have been computed which lie below or slightly above, respectively, those given by the classical Smagorinsky model; and the largest near-wall peak values of grid-scale energy have resulted from LES applications of model 4 (smagc). Concerning energy transfer analyzed in the *a priori* tests, the defined "local" flux between subgrid scales and the adjacent range of the grid scales smaller than $\hat{\hat{\Delta}}$ is grossly overpredicted, while the defined "not-so-local" flux between subgrid and supertest ranges is underpredicted. As for the net flux between grid and subgrid scales, model 4 (smagc) turned out to be underdissipative in the *a priori* tests, and, due to the imposed clipping of the model coefficients according to nonnegative component-related total viscosities, the amount of backscatter is extremely reduced against its defined counterpart.

In the large-eddy simulations, this model combined with a top-hat filter of width $2\,\Delta x_i$ (Simpson's rule approximation) provided the best predictions for both mean and rms values of velocity among all the SGS models tested. For the mean axial velocity component, the computed radial profile is, apart from the underresolved near-wall region, in closest agreement with experimental data, and the reproduced rms values are improved upon those obtained with the Lilly model.

Model 6 (sc1), though of scale-similarity type, has a number of closure assumptions in common with model 4 (smagc), but no backscatter limitation is incorporated in its original formulation. Accordingly, in the *a priori*- and *a posteriori*-test results of model 6 (sc1), qualitative similarities have been observed yet also substantial differences in comparison with model 4 (smagc) and with the scale-similarity parametrizations 7 (sc2) to 12 (ss4). *A priori* tests of model 6 (sc1) showed an overestimation of the mean values of SGS normal stresses and hence of subgrid-scale energy as well as improvements upon closure 4 (smagc) with respect to $<t_{zz}>$, $<t_{rz}>$ and in the near-wall region in general. Compared with the latter model, the absolute values of the mean relevant shear stress, $<t_{rz}>$, in the *a priori* tests (and also in LES) are typically larger, and the modelled "local" flux between grid scales smaller than $\hat{\hat{\Delta}}$ and subgrid scales is less pronounced yet still greater than the defined one. As the most prominent feature of *a priori* model performance, a severely overestimated backscatter has been found along with the smallest peak of SGS dissipation among the results from all subgrid closures proposed. For this parametrization, remarkable further improvements in the *a priori* model performance have been achieved by applying the smaller variant of top-hat test-filtering. In LES, the particular effect of this model on the computed velocity field is manifested in a mean axial velocity profile that essentially lies above the values measured in experiment and those predicted by the other closures tested. In this respect, an increase in performance was observed for this model on the finest LES grid.

For the scale-similarity- and mixed-type **models 7 (sc2) to 13 (comb)**, a fairly good *a priori* performance with a substantially higher overall degree of correlation has been established showing these closures to be superior to the known models 1 (smag) to 3 (pio) and the parametrizations 4 (smagc) and 6 (sc1) in the first stage of evaluation. According to the *a priori*-test results at tensor, vector and scalar levels of comparison, the proposed models 7 to 13 were essentially subdivided into three groups: The group of the most promising parametrizations comprises the scale-similarity- and mixed-type closures 8 (sc3), 7 (sc2) and 13 (comb) with component-specific coefficients and is distinguished by an excellent qualitative and quantitative agreement between defined and modelled subgrid terms at all levels. This implies very small L_1-error norms and tensor-level correlation coefficients of nearly 1. As the second group, the parametrizations 12 (ss4) and 11 (ss3) in terms of the (modified) Leonard stresses with a scalar coefficient each follow, which are characterized by typical tensor-level correlations of about 0.95 and a marked decrease in correlation coefficients at vector and scalar levels. The third group contains the resolved-stress-related one-parameter closures 10 (ss2) and 9 (ss1) giving average stress-correlation coefficients roughly between 0.8 and 0.9 along with vector- and scalar-level correlations decreased to values between 0.3 and 0.6. In *a priori* reproducing subgrid terms, the mean absolute values of SGS normal stresses and thus of subgrid energy, of the relevant SGS shear-stress component, $<t_{rz}>$, and also the mean absolute values of subgrid terms at vector and scalar levels are typically slightly underpredicted by the considered models with only model 9 (ss1) resulting in overestimated absolute values of the mentioned tensor-level test quantities. Interscale energy transfer was found to be reasonably well approximated *a priori* by models 7 (sc2) to 13 (comb). Characteristically, the peaks of the absolute values of nearly all mean fluxes computed from the modelled SGS stresses are insignificantly lower than their defined counterparts. Backscatter is *a priori* at most slightly underpredicted in its absolute values and best reproduced by models 7 (sc2) and 12 (ss4), whereas the linear-combination model 13 (comb) gives rise to a somewhat excessive amount of backward energy flux. The closures 7 (sc2) to 13 (comb) tend to underestimate the forward scatter from grid to subgrid scales by a little greater amount than the backscatter and, accordingly, are considered to be somewhat underdissipative in the *a priori* tests. Differences between the models' *a priori*-test results are small yet most pronounced for the "local" flux between subgrid scales and the adjacent part of grid scales smaller than $\hat{\hat{\Delta}}$. For this quantity, the mixed model 13 (comb) provides the closest approximation.
With the backscatter modifications incorporated and along with the reference filter

combination, models 7 (sc2) to 13 (comb) yielded acceptable predictions of statistical quantities in LES. For the computed mean axial velocity profile, the quality of approximation provided by these parametrizations is partly inferior to that of model 4 (smagc). Within the radial subrange where the largest deviations from the measured $<w>$-curve were found, the linear-combination closure 13 (comb) gave slightly superior predictions among this group of models. For the single-coefficient models 9 (ss1) to 12 (ss4), the computed mean axial velocity values are generally smaller than their experimental counterparts, and both $<E_{GS}>$- and $<E_{SGS}>$-levels as well as the peak values of the mean relevant SGS shear stress, $<t_{rz}>$, are typically higher than those obtained with parametrizations 7 (sc2), 8 (sc3) and 13 (comb). In qualitative agreement with the *a priori*-test results, the peak values of $<E_{SGS}>$ and $<t_{rz}>$ are most pronounced in the predictions of model 9 (ss1).
Measured turbulence intensities, apart from the near-wall rms values, have been reproduced reasonably well by all the proposed scale-similarity- and combined-type models with a general tendency towards a slight underprediction.

With respect to the implemented **filters** of several types and widths, the effect of changing grid and test filters in the *a priori* tests was more striking than the influence of filter variations on the computed statistics in LES.
Both *a priori* and *a posteriori* tests indicated that, as compared with the top-hat filter of the same width, the spectral sharp-cutoff type is characteristically associated with smaller absolute values of (defined and generally also modelled) SGS stresses and thus smaller energies of subgrid motion together with smaller amounts of SGS dissipation yet larger amounts of backscatter. This is most pronounced for the "exact" sharp-cutoff filter of width $2\,\Delta x_i$. The latter has been approximated in physical space with comparable computational effort and, for the major part of the test quantities, more closely by the proposed discrete 5-point-implicit–7-point-explicit filter f3a as against f3b due to Spyropoulos and Blaisdell [90]. Here, the quality of approximation to the original spectral filter was found to be dependent on grid density. In applications along with models 4 (smagc) and 6 (sc1), the agreement between defined and modelled subgrid terms in the *a priori* tests as well as those between experimental data and the statistics evaluated in LES was clearly poorer for the sharp-cutoff than for the top-hat filters. With respect to numerical behaviour, too, the filters of top-hat type proved to be superior to those of sharp-cutoff type. Of the two adopted discrete versions of the top-hat filter, the approximation by means of Simpson's rule generally gave better *a priori*- and *a posteriori*-test results for all the models under investigation than the trapezoidal-rule approximation. Assuming equal filter widths, the former typically involves smaller absolute values of defined SGS stresses, subgrid energies, SGS dissipation and backscatter.
Considering the test-filter width, in the *a priori* tests for the majority of the proposed closures and for model 6 (sc1) most pronounced, the choice of the top-hat kernel of width $\widehat{\Delta}_i = \overline{\Delta}_i = 2\,\Delta x_i$ as against that of twice the grid-filter width turned out to be more favourable in terms of correlation coefficients and relative L_1-error norms. This is motivated in view of the amount of local informations utilized in modelling and the degree of similarity between $\overline{G}$- and $\widehat{\overline{G}}$-filtered quantities used to approximate subgrid and subtest-scale stresses.

Concerning LES, however, one has to take into consideration that the unknown "filter" inherent in the discretization method differs from the defined grid filter and that model performance is affected by truncation errors, which may produce strong effects near the grid scale.
The *a posteriori* tests also suggested to combine model 4 (smagc) with a test filter of width $2\,\Delta x_i$.
For the dynamic scale-similarity and mixed-type models, the mean axial velocity profiles predicted in LES were found to be comparatively insensitive to the adopted variations in test-filter width. Altogether, for the proposed models of scale-similarity and linear-combination types, the reference filter combination, i. e. Simpson's rule approximations to the top-hat filter with $\widehat{\Delta}_i = 2\,\overline{\Delta}_i = 4\,\Delta x_i$, generally produced LES results with the smallest absolute values of mean SGS stresses and subgrid energies and established the closest agreement with measured flow statistics available.

VI Summary and Conclusions

The advantages and potentialities offered by dynamic subgrid-scale modelling in general as contrasted with particular problems encountered in deriving, implementing and applying popular dynamic SGS closures as well as the need for further improvements in their performance formed the motivation of the present study.

Within the framework of the most common approach to dynamic subgrid modelling, refined principles of developing and evaluating SGS models were suggested, from which nine dynamic subgrid parametrizations of three types were derived. As the essence of modelling, it was proposed to use the Germano identity [2] in a more general sense including also consequences at vector and scalar levels to uniquely and efficiently determine model coefficients. This opens up the possibility of addressing the overspecification problem by selecting a proper subset of identities equal in number to that of the model coefficients to be evaluated dynamically.
Related to this, the most prominent feature of the proposed generalized anisotropic models consists in the use of component-specific coefficients assigned to the individual SGS stresses. These subgrid closures with additional degrees of freedom thus avoid overspecification in evaluating the model coefficients from the tensorial Germano identity and are intended to overcome some of the inherent limitations of the scalar-coefficient base parametrizations they originate from. Specifically, they enabled a more flexible capturing of the near-wall SGS-stress-tensor anisotropy to be achieved. In addition, the models with component-related coefficients aim at a proper approximation to local instantaneous backscatter energy transfer, which, however, turned out to be a serious problem in LES.
Proceeding from these generalized anisotropic closures, as another model group, versions with a scalar coefficient each were designed to fulfil strong realizability conditions for nonnegative filter functions in physical space. Here, the single model coefficient was evaluated from a physically meaningful scalar equation taking SGS dissipation into consideration.
Common to all the proposed subgrid parametrizations, their model coefficients are defined locally, i. e. essentially without using any kind of global averaging. These localized formulations are expected to improve the predictive capability on a local level and to offer a wider range of applicability beyond flows with homogeneous directions or statistically steady flows, by way of example. For numerical stabilization, a clipping of the model coefficients combined with a special procedure employed in case of small denominators was found to be appropriate.
To evaluate the SGS stresses or the involved model coefficients appearing inside the test-filtering operation of the Germano identity or related equations, the generally applicable and computationally efficient approximate localization approach due to Piomelli *et al.* [20] was mainly adopted, and the use of approximate values computed in the preceding time step proved successful.

Within the proposed modelling framework, the usual assumption of identical model coefficients assigned to both the subgrid- and subtest-scale stress parametrizations may, if required, be discarded in favour of a more general approach.
In addition, as distinguished from known SGS models for only the deviatoric part of the subgrid-stress tensor, the modelling principles introduced in the present paper permit a more comprehensive model evaluation including also GS pressure, SGS normal stresses and quantities derived therefrom. Particularly, realizability [49], [50], [51] of the modelled SGS-stress tensor is verifiable.
Useful further information for model evaluation in both *a priori* and *a posteriori* tests or for dynamically choosing among available SGS parametrizations in LES [13] can also be obtained from the tensorial Germano identity and consequences at vector and scalar levels, e. g. by analyzing the error in satisfying these equations with the subgrid- and subtest-scale stresses replaced by the models under study.

The dynamic closures presented comprise a generalized anisotropic Smagorinsky-type model, 4 (smagc); three scale-similarity models with component-specific coefficients, 6 (sc1) to 8 (sc3); four parametrizations of scale-similarity type with a scalar coefficient each, 9 (ss1) to 12 (ss4);

and a linear-combination model with component-related coefficients in the Smagorinsky part, 13 (comb). For each of the three base model types, a special motivation and particular aims were formulated.

Applied to a fully developed turbulent pipe flow described in cylindrical (r, φ, z)-coordinates, these models along with several filters were evaluated in a systematic two-stage testing procedure. Using a self-generated DNS database pertaining to a Reynolds number of $Re_\tau = u_\tau\, R/\nu = 180$, *a priori* tests as the first stage were performed. Their results, mainly via correlation coefficients and L_1-norms of the differences between defined and modelled subgrid terms at tensor, vector and scalar levels provided first informations on model performance and filter effects, from which to select model/filter combinations primarily designated for further studying.
In actual finite-difference large-eddy simulations ($Re_\tau = 1{,}050$) as the second testing stage, the models' predictive capability was examined as well as the sensitivity of simulation results to variations in filters and other input parameters. Models were evaluated against experimental and numerical pipe-flow data, and model performance was assessed in comparison with each other and with the classical Smagorinsky model 1 (smag) [63], the dynamic versions 2 (lilly) due to Lilly [18] and 3 (pio) by Piomelli *et al.* [20] together with a simple nondynamic Leonard-stress-based parametrization, 5 (leo) following [78].

As against these known SGS closures, considerable improvements in local *a priori* performance at all levels were demonstrated for the proposed subgrid models and particularly for those of scale-similarity and combined types with component-specific coefficients. In the *a posteriori* tests, the generalized anisotropic Smagorinsky-type model including coefficient clipping proved most successful and stood comparison with the known subgrid parametrizations, whereas problems were encountered with the scale-similarity and mixed models in their original formulation, and additional procedures were needed to limit excessive backscatter. In both testing stages, the top-hat filter approximated by means of Simpson's rule enabled the overall closest agreement with the relevant comparative data to be achieved.

Following this rough outline of the results, a more detailed model- and filter-related evaluation is presented subsequently.
Regardless of its deficiencies mainly with respect to reproducing the dominant SGS normal stress and the relevant SGS shear stress, subgrid dissipation and backscatter in the *a priori* tests, the generalized anisotropic Smagorinsky-type model 4 (smagc) with coefficient cutting provided the best LES predictions for velocity mean and rms values among all SGS closures tested.
As distinguished from model 4 (smagc), the dynamic scale-similarity- and combined-type closures 6 (sc1) to 13 (comb) gave a superior performance in the *a priori* tests. Their results led to a classification of these models into three groups with the group of the most promising parametrizations comprising models 8 (sc3), 7 (sc2) and 13 (comb) with component-specific coefficients. In addition, as the prime candidate of the second group and a representative of the single-coefficient models, the Leonard-stress-related closure 12 (ss4), which was derived from the scalar-level Germano identity, is designated for further studies. Especially these models offer a great potential for reproducing the subgrid terms at tensor, vector and scalar levels as well as interscale energy transfer including SGS dissipation and backscatter. Typically, these models only slightly underpredicted the various net energy fluxes computed from the DNS data and turned out to be somewhat underdissipative in the first stage of evaluation.
As contrasted with the appealing *a priori*-test results, the potential advantages of these models did, however, not produce adequate effects in LES. Instead, in the complex dynamics of GS/SGS interaction with these models, backscatter was found to be a crucial problem of the large-eddy simulations. Applied in their original formulation, the models typically resulted in clearly too flat mean axial velocity profiles and considerable amounts of SGS energy in the LES computations or even caused numerical instabilities in some simulations.
A quantitative backscatter analysis reveals that, with the reference filter combination on the medium grid mainly used in LES, the SGS stresses computed according to definition from DNS data give rise to a reverse energy flux in about 30 % to 31 % of the total number of grid points. That backscatter essentially doesn't exceed an intensity corresponding to a negative total viscosity. This is well captured by models 7 (sc2) to 13 (comb) in the consistent *a priori* tests. In LES

(at a greater Reynolds number), however, backscatter was established with these models in 32 % to 38 % of the nodes, and as much as over 20 % to 25 % of the discretization points experienced an amount of backscatter corresponding to a negative total viscosity. These facts indicate the need for further research into backscatter, whose importance, mechanisms and suitable modelling without the risk of generating numerical instabilities are still controversial. Though not satisfactory from a theoretical point of view, an artificial backscatter limitation via modified model coefficients proved to be feasible in the present LES computations.
With backscatter modifications similar to the imposed clipping of model coefficients according to nonnegative component-related total viscosities in closure 4 (smagc), these models generally yielded acceptable LES predictions of statistical one-point moments of the GS velocity field. Specifically for the computed mean axial velocity profile, the quality of approximation provided by these parametrizations is partly inferior to that achieved with the Smagorinsky-type model 4 (smagc). Here, among the SGS closures with scale-similarity part, the mixed model 13 (comb) produced slightly more favourable results.
Within the group of the proposed scale-similarity parametrizations, an exceptional behaviour was found for model 6 (sc1), which has a number of closure assumptions in common with model 4 (smagc) yet another parametrization tensor and no backscatter modification in its original formulation. As the most striking feature of *a priori* performance, an extremely overestimated amount of backscatter was observed along with the smallest SGS dissipation within this group of subgrid closures. The particular model effects on the computed statistics in LES were most evident from the mean axial velocity profile and spatial one-dimensional energy spectra in the mean flow direction.

With respect to the parametrization tensor of the scale-similarity closures, the (modified) Leonard stresses generally proved to be superior to the resolved-stress tensor in the *a priori* tests as can be concluded from the comparative evaluation of the models in conjunction with test filters of the usual (twice the grid filter) width and those equal in width to the grid filter. In the large-eddy simulations, the differences in the computed one-point statistics appeared to be less pronounced, and, for the Leonard-stress-related models, backscatter was observed in a greater fraction of the computational points.

As the base types of spatial filters involved in dynamic modelling, 3-point-explicit approximations to the top-hat kernel by means of trapezoidal and Simpson's rules as well as 5-point-implicit–7-point-explicit approximations to the spectral sharp-cutoff type were applied in physical space along with the "exact" sharp-cutoff filter implemented via FFT.
For models compatible with a spectrally sharp GS/SGS separation, their combination with spectral sharp-cutoff type filters resulted in typically smaller absolute values of mean subgrid stresses and SGS energies yet considerably larger amounts of backscatter and, generally, in a decline in model performance as against the top-hat filter of the same width. Both *a priori*- and *a posteriori*-test results suggest to prefer Simpson's rule approximation to the top-hat filter to be used in finite-difference large-eddy simulations.
A test filter of this type and equal in width to twice the grid size was most successfully combined in LES with the generalized anisotropic Smagorinsky-type model 4 (smagc). For the majority of the proposed scale-similarity- and mixed-type models 6 (sc1) to 13 (comb), the particular choice of a top-hat filter of width equal to twice the grid spacing and approximated by Simpson's rule as both grid and test filter yielded the overall closest qualitative and quantitative agreement between modelled and defined subgrid terms in the *a priori* tests. As against the usual choice of test-filter width, this produced smaller absolute values of defined subgrid stresses, SGS energy and energy fluxes of "local" nature. In LES applications, simulation results were rather insensitive to the adopted variations in test-filter width, and, in all, the choice of the reference filter combination (Simpson's rule approximation to the top-hat filter with the usual test-filter width) turned out to be more favourable with respect to reproducing experimental flow data.

In establishing these results by means of the applied two-stage approach, the *a priori* tests in the present study at least gave useful indications of the relative performance of the individual models of each of the three types, which were roughly confirmed in LES. The *a priori*-testing methodology failed, however more than expected, in capturing the effects of the different types of closure in their dynamical interactions with the GS field and with respect to backscatter in particular, which showed limitations of this approach.

Concerning numerical aspects, the proposed models are not substantially more complex than known dynamic SGS parametrizations. Obviously, model variants with component-related coefficients imply increased storage requirements in comparison with the traditional one-parameter models, and scale-similarity as against Smagorinsky-type closures are associated with additional computational effort according to the number of filtering operations involved. By way of example, for top-hat type filters and a grid with about 131,000 nodes, CPU times of LES are increased by factors of roughly 2 (model 4) up to 8 (models 7 and 8) as compared with the standard Smagorinsky model (simulations with 32 processors on a Parsytec GC/PowerPlus-128).
In both *a priori* and *a posteriori* tests, apart from reduced storage requirements, hardly any advantage of the one-parameter model versions with a scalar coefficient were seen in terms of results and computational efficiency.
In evaluating the fluctuating component-related model coefficients, the most appealing numerical behaviour as reflected in the smallest range of variations, the lowest frequence and smallest magnitude of peaks was observed with model 8 (sc3).
For these models with component-specific coefficients, the tested modifications to ensure realizability in case of top-hat type filters did not indicate a definite global increase in the *a priori* model performance and typically caused a rise in mean axial velocity values computed in LES, which implies improvements for model 4 (smagc).

In addition to backscatter treatment, filters and realizability modifications, other model parameters were varied which produced weaker effects or which are of minor importance within the scope of the present work.
Variations in grid resolution were also studied. The *a priori* tests were mainly performed using the original highly-resolved DNS raw data on a grid with approximately 3.15 million nodes. These investigations were supplemented by consistent *a priori* tests on a coarser (LES) grid, which, apart from some observable quantitative differences, gave similar qualitative results. In LES, the effect of spatial resolution on model performance was examined using three grid levels, and the sensitivity of the simulation results to grid density was noticed not only in the underresolved near-wall region. Simulations were focused on the medium LES grid with about 131,000 cells. Proceeding to the finest LES grid level with roughly 1.05 million nodes, a partial improvement in *a posteriori* performance was achieved for model 6 (sc1) with respect to the mean axial velocity profile. Local computer facilities, however, did not permit a thorough *a posteriori* testing of all the proposed models on this or even more refined grids. Consequently, further grid refinement studies for model evaluation are required to be made, and, particularly, a higher resolution of near-wall regions is desirable in the context with dropping artificial wall-boundary conditions.
On account of the complex interactions between the LES components, higher-order difference schemes have to be included in model testing, which is to be extended to other flow types and more irregular geometries.

Since all dynamic SGS models proposed in this paper proved to be superior to the known subgrid parametrizations in the *a priori* tests and largely came up to the expectations in the first stage of evaluation, our future research efforts will focus on LES applications of the most promising model versions 4 (smagc), 7 (sc2), 8 (sc3), 12 (ss4) and 13 (comb) to more fully exploit their potential *a posteriori*. Special attention will be paid to the discretization of the computational domain and of the governing differential equations as well as to the issue of backscatter.

Acknowledgments

The work reported here was supported by the Deutsche Forschungsgemeinschaft (DFG) under grant II D 5 – Me 1224/4-2. The authors also thank Professors A. Meyer, H. Herwig, and M. Hoffmeister for useful comments and suggestions and for reviewing the manuscript.

References

[1] COST Action F1: "Complex Three-Dimensional Viscous Flows: Prediction, Modelling, Manipulation, Control and Experiment"
European Cooperation in the Field of Scientific and Technical Research, Round II: September 1995 – September 1999.

[2] M. GERMANO, U. PIOMELLI, P. MOIN, and W. H. CABOT. A dynamic subgrid-scale eddy viscosity model. *Phys. Fluids A*, 3(7):1760 – 1765, July 1991. Erratum: *Phys. Fluids A*, 3(12):3128, December 1991.

[3] M. GERMANO. An algebraic property of the turbulent stress and its possible use in subgrid modeling. In *Proceedings 8th Symposium on Turbulent Shear Flows. Technical University of Munich, September 9 - 11, 1991*, pages 19–1–1 – 19–1–6, 1991.

[4] M. GERMANO. A statistical formulation of the dynamic model. *Phys. Fluids*, 8(2):565 – 570, February 1996.

[5] C. MENEVEAU, T. S. LUND, and W. H. CABOT. A Lagrangian dynamic subgrid-scale model of turbulence. *J. Fluid Mech.*, 319:353 – 386, July 1996.

[6] J. RÉVEILLON and L. VERVISCH. Response of the dynamic LES model to heat release induced effects. *Phys. Fluids*, 8(8):2248 – 2250, August 1996.

[7] Q. WANG and K. D. SQUIRES. Large eddy simulation of particle-laden turbulent channel flow. *Phys. Fluids*, 8(5):1207 – 1223, May 1996.

[8] X. WU and K. D. SQUIRES. Large eddy simulation of a canonical three-dimensional boundary layer. In F. DURST, B. E. LAUNDER, F. W. SCHMIDT, and J. W. WHITELAW, editors, *Proceedings 10th Symposium on Turbulent Shear Flows, Pennsylvania State University*, 1995.

[9] F. GAO and E. E. O'BRIEN. A large-eddy simulation scheme for turbulent reacting flows. *Phys. Fluids A*, 5(6):1282 – 1284, June 1993.

[10] K. HORIUTI. A new dynamic two-parameter mixed model for large-eddy simulation. *Phys. Fluids*, 9(11):3443 – 3464, November 1997.

[11] C. MENEVEAU and T. S. LUND. The dynamic Smagorinsky model and scale-dependent coefficients in the viscous range of turbulence. *Phys. Fluids*, 9(12):3932 – 3934, December 1997.

[12] C. RONCHI, M. YPMA, and V. M. CANUTO. On the application of the Germano identity to subgrid-scale modeling. *Phys. Fluids A*, 4(12):2927 – 2929, December 1992.

[13] C. MENEVEAU and J. KATZ. Dynamic testing of subgrid models in large eddy simulation based on the Germano identity. *Phys. Fluids*, 11(2):245 – 247, February 1999.

[14] D. CARATI and E. VANDEN EIJNDEN. On the self-similarity assumption in dynamic models for large eddy simulations. *Phys. Fluids*, 9(7):2165 – 2167, July 1997.

[15] J. O'NEILL and C. MENEVEAU. Subgrid-scale stresses and their modelling in a turbulent plane wake. *J. Fluid Mech.*, 349:253 – 293, 1997.

[16] P. MOIN. A new approach for large eddy simulation of turbulence and scalar transport. In T. DRACOS and A. TSINOBER, editors, *New Approaches and Concepts in Turbulence, Proc. Monte Verita Coll. on Turbulence.* Birkhäuser; Bale, 1991.

[17] P. MOIN and J. JIMENEZ. Large eddy simulations of complex turbulent flows. Paper 93-3099, AIAA, 1993. AIAA 24th Fluid Dynamics Conference, Orlando, 1993.

[18] D. K. LILLY. A proposed modification of the Germano subgrid-scale closure method. *Phys. Fluids A*, 4(3):633 – 635, March 1993.

[19] S. GHOSAL, T. LUND, P. MOIN, and K. AKSELVOLL. A dynamic localization model for large eddy simulation of turbulent flows. *J. Fluid Mech.*, 286:229 – 255, 1995. Corrigendum: *J. Fluid Mech.*, 297:402, 1995.

[20] U. PIOMELLI and J. LIU. Large-eddy simulation of rotating channel flows using a localized dynamic model. *Phys. Fluids*, 7(4):839 – 847, April 1995.

[21] A. ABBÀ, R. BUCCI, C. CERCIGNANI, and L. VALDETTARO. New Variants to the Dynamic Subgrid Scale Model. In A. MENEGUZZI, editor, *Small-scale structures in three-dimensional hydrodynamic and magnetohydrodynamic turbulence. Proceedings Workshop, Nice, France, 10 - 13 January 1995*, pages 231 – 237, 1995.

[22] W. CABOT and P. MOIN. Large Eddy Simulation of Scalar Transport with the Dynamic Subgrid-Scale Model. In B. GALPERIN and S. A. ORSZAG, editors, *Large Eddy Simulation of Complex Engineering and Geophysical Flows*, pages 141 – 158. Cambridge University Press; Cambridge, 1993.

[23] H. ZHAO and P. R. VOKE. A dynamic subgrid-scale model for low-Reynolds-number channel flow. *Int. J. Numer. Meth. Fluids*, 23(1):19 – 27, 1996.

[24] I. CALMET and J. MAGNAUDET. Large-eddy simulation of high-Schmidt number mass transfer in a turbulent channel flow. *Phys. Fluids*, 9(2):438 – 455, February 1997.

[25] K. AKSELVOLL and P. MOIN. Large Eddy Simulation of a Backward Facing Step Flow. In W. RODI and F. MARTELLI, editors, *Engineering Turbulence Modelling and Experiments 2*, pages 303 – 313. Elsevier Science Publishers; Amsterdam, 1993.

[26] M. BREUER and W. RODI. Large-Eddy Simulation of Turbulent Flow Through a Straight Square Duct and a 180^o Bend. In P. R. VOKE, L. KLEISER, and J.-P. CHOLLET, editors, *Direct and Large-Eddy Simulation I*, pages 273 – 285. Kluwer Academic Publishers, 1994.

[27] M. CIOFALO, G. LOMBARDO, and M. W. COLLINS. Large-Eddy Simulation of Flow and Heat Transfer in Compact Heat Exchangers. In P. R. VOKE, L. KLEISER, and J.-P. CHOLLET, editors, *Direct and Large-Eddy Simulation I*, pages 261 – 272. Kluwer Academic Publishers, 1994.

[28] K. D. SQUIRES and U. PIOMELLI. Dynamic Modeling of Rotating Turbulence. In F. DURST, N. KASAGI, B. E. LAUNDER, F. W. SCHMIDT, and J. H. WHITELAW, editors, *Turbulent Shear Flows 9*, pages 71 – 83. Springer; Heidelberg, 1995.

[29] Y. ZANG, R. L. STREET, and J. KOSEFF. A dynamic mixed subgrid-scale model and its application to turbulent recirculating flows. *Phys. Fluids A*, 5(12):3186 – 3196, December 1993.

[30] M. BREUER. Large Eddy Simulation of the Subcritical Flow Past a Circular Cylinder: Numerical and Modeling Aspects. *Int. J. Numer. Meth. Fluids*, 28:1281 – 1302, 1998.

[31] P. E. DESJARDIN and S. H. FRANKEL. Large eddy simulation of a nonpremixed reacting jet: Application and assessment of subgrid-scale combustion models. *Phys. Fluids*, 10(9):2298 – 2314, September 1998.

[32] P. G. WILSON and L. L. PAULEY. Two- and three-dimensional large-eddy simulations of a transitional separation bubble. *Phys. Fluids*, 10(11):2932 – 2940, November 1998.

[33] M. OLSSON and L. FUCHS. Significant Terms in Dynamic SGS-Modeling. In P. R. VOKE, L. KLEISER, and J.-P. CHOLLET, editors, *Direct and Large-Eddy Simulation I*, pages 73 – 83. Kluwer Academic Publishers, 1994.

[34] M. OLSSON and L. FUCHS. Large eddy simulations of a forced semiconfined circular impinging jet. *Phys. Fluids*, 10(2):476 – 486, February 1998.

[35] M. FATICA, P. ORLANDI, and R. VERZICCO. Direct and Large Eddy Simulations of Round Jets. In P. R. VOKE, L. KLEISER, and J.-P. CHOLLET, editors, *Direct and Large Eddy Simulation I*, pages 49 – 60. Kluwer Academic Publishers, 1994.

[36] F. M. NAJJAR and D. K. TAFTI. Study of discrete test filters and finite difference approximations for the dynamic subgrid-scale stress model. *Phys. Fluids*, 8(4):1076 – 1088, April 1996.

[37] P. SAGAUT, B. TROFF, T. H. LE, and T. P. LOC. Two-dimensional Simulations with Subgrid Scale Models for Separated Flow. In P. R. VOKE, L. KLEISER, and J.-P. CHOLLET, editors, *Direct and Large-Eddy Simulation I*, pages 109 – 120. Kluwer Academic Publishers, 1994.

[38] J. LIU, U. PIOMELLI, and P. R. SPALART. Interaction between a spatially growing turbulent boundary layer and embedded streamwise vortices. *J. Fluid Mech.*, 326:151 – 179, 1996.

[39] M. OLSSON and L. FUCHS. Large eddy simulation of the proximal region of a spatially developing circular jet. *Phys. Fluids*, 8(8):2125 – 2137, August 1996.

[40] D. CARATI, S. GHOSAL, and P. MOIN. On the representation of backscatter in dynamic localization models. *Phys. Fluids*, 7(3):606 – 616, March 1995.

[41] T. LUND, S. GHOSAL, and P. MOIN. Numerical experiments with highly variable eddy viscosity models. In S. A. RAGAB and U. PIOMELLI, editors, *Engineering Applications of Large Eddy Simulations*, volume 162 of *ASME-FED*, page 7. The American Society of Fluids Engineering, New York, 1993.

[42] T. GOUTORBE, D. LAURENCE, and V. MAUPU. A Priori Tests of a Subgrid Scale Stress Tensor Model Including Anisotropy and Backscatter Effects. In P. R. VOKE, L. KLEISER, and J.-P. CHOLLET, editors, *Direct and Large-Eddy Simulation I*, pages 121 – 131. Kluwer Academic Publishers, 1994.

[43] K. HORIUTI. Assessment of the Generalized Normal Stress and the Bardina Reynolds Stress Subgrid-Scale Models in Large Eddy Simulation. In P. R. VOKE, L. KLEISER, and J.-P. CHOLLET, editors, *Direct and Large-Eddy Simulation I*, pages 85 – 96. Kluwer Academic Publishers, 1994.

[44] S. LIU, C. MENEVEAU, and J. KATZ. Experimental study of similarity subgrid-scale models of turbulence in the far field of a jet. In P. R. VOKE, L. KLEISER, and J. P. CHOLLET, editors, *Direct and Large Eddy Simulation I*, pages 37 – 48. Kluwer Academic Publishers, 1994.

[45] M. V. SALVETTI and S. BANERJEE. A priori tests of a new dynamic subgrid-scale model for finite-difference large-eddy simulations. *Phys. Fluids*, 7(11):2831 – 2847, November 1995.

[46] B. VREMAN, B. GEURTS, and H. KUERTEN. On the formulation of the dynamic mixed subgrid-scale model. *Phys. Fluids*, 6(12):4057 – 4059, December 1994.

[47] S. LIU, C. MENEVEAU, and J. KATZ. On the properties of similarity subgrid scale models as deduced from measurements in a turbulent jet. *J. Fluid Mech.*, 275:83 – 119, 1994.

[48] V. C. WONG. A proposed statistical-dynamic closure method for the linear or nonlinear subgrid-scale stresses. *Phys. Fluids A*, 4(5):1080 – 1082, May 1992.

[49] J. L. LUMLEY. Computational modeling of turbulent flows. *Adv. Appl. Mech.*, 18:123 – 176, 1978.

[50] U. SCHUMANN. Realizability of Reynolds-stress turbulence models. *Phys. Fluids*, 20:721 – 725, 1977.

[51] B. VREMAN, B. GEURTS, and H. KUERTEN. Realizability conditions for the turbulent stress tensor in large-eddy simulations. *J. Fluid Mech.*, 278:351 – 362, 1994.

[52] F. UNGER. *Numerische Simulation turbulenter Rohrströmungen.* PhD thesis, Technical University of Munich, February 1994.

[53] H. BUNGARTZ and W. HUBER. First Experiments with Turbulence Simulation on Workstation Networks Using Sparse Grid Methods. In S. WAGNER, editor, *Computational Fluid Dynamics on Paralllel Systems*, volume 50 of *Notes on Numerical Fluid Mechanics*, pages 36 – 48. Vieweg; Braunschweig/Wiesbaden, 1995.

[54] J. G. M. EGGELS. *Direct and large eddy simulation of turbulent flow in a cylindrical pipe geometry.* PhD thesis, Delft University of Technology, The Netherlands, 1994.

[55] C. J. JIMENEZ-HÄRTEL. *Analyse und Modellierung der Feinstruktur im wandnahen Bereich turbulenter Scherströmungen.* PhD thesis, Technical University of Munich, June 1994.

[56] C. WAGNER. *Direkte numerische Simulation turbulenter Strömungen in einer Rohrerweiterung.* PhD thesis, Technical University of Munich, May 1995, VDI-Verlag, 1996.

[57] J. G. M. EGGELS, F. UNGER, M. H. WEISS, J. WESTERWEEL, R. J. ADRIAN, R. FRIEDRICH, and F. T. M. NIEUWSTADT. Fully developed turbulent pipe flow: a comparison between direct numerical simulation and experiment. *J. Fluid Mech.*, 268:175 – 209, 1994.

[58] J. WESTERWEEL, A. A. DRAAD, J. G. T. van der HOEVEN, and J. van OORD. Measurement of fully-developed turbulent pipe flow with digital particle image velocimetry. *Experiments in Fluids*, 20(3):165 – 177, January 1996.

[59] T. A. ZANG and U. PIOMELLI. Large Eddy Simulation of Transitional Flow. In B. GALPERIN and S. A. ORSZAG, editors, *Large Eddy Simulation of Complex Engineering and Geophysical Flows*, pages 209 – 227. Cambridge University Press; Cambridge, 1993.

[60] U. PIOMELLI, Y. YU, and R. J. ADRIAN. Subgrid-scale energy transfer and near-wall turbulence structure. *Phys. Fluids*, 8(1):215 – 224, January 1996.

[61] U. PIOMELLI. High Reynolds number calculations using the dynamic subgrid-scale stress model. *Phys. Fluids A*, 5(6):1484 – 1490, June 1993.

[62] S. CERUTTI and C. MENEVEAU. Intermittency and relative scaling of subgrid-scale energy dissipation in isotropic turbulence. *Phys. Fluids*, 10(4):928 – 937, April 1998.

[63] J. S. SMAGORINSKY. General circulation experiments with the primitive equations. I. The basic experiment. *Mon. Weather Rev.*, 91(3):99 – 164, March 1963.

[64] J. W. DEARDORFF. A numerical study of three-dimensional turbulent channel flow at large Reynolds numbers. *J. Fluid Mech.*, 41:453 – 480, 1970.

[65] A. SCOTTI, C. MENEVEAU, and D. K. LILLY. Generalized Smagorinsky model for anisotropic grids. *Phys. Fluids A*, 5(9):2306 – 2308, September 1993.

[66] A. SCOTTI, C. MENEVEAU, and M. FATICA. Dynamic Smagorinsky model on anisotropic grids. *Phys. Fluids*, 9(6):1856 – 1858, June 1997.

[67] D. K. LILLY. The representation of small-scale turbulence in numerical simulation experiments. In *Proceedings of the IBM Scientific Computation Symposium on Environmental Sciences 1967*, number 320-1951 in IBM Form, pages 195 – 210, 1967.

[68] J. H. FERZIGER. Subgrid-Scale Modeling. In B. GALPERIN and S. A. ORSZAG, editors, *Large Eddy Simulation of Complex Engineering and Geophysical Flows*, pages 37 – 54. Cambridge University Press; Cambridge, 1993.

[69] D. C. LESLIE and G. L. QUARINI. The application of turbulence theory to the formulation of subgrid modelling procedures. *J. Fluid Mech.*, 91 part 1:65 – 91, 1979.

[70] K. HORIUTI. A proper velocity scale for modeling subgrid-scale eddy viscosities in large eddy simulation. *Phys. Fluids A*, 5(1):146 – 157, January 1993.

[71] K. HORIUTI. Anisotropic Representation of Subgrid-Scale Reynolds Stress in Large Eddy Simulation. In B. GALPERIN and S. A. ORSZAG, editors, *Large Eddy Simulation of Complex Engineering and Geophysical Flows*, pages 193 – 208. Cambridge University Press; Cambridge, 1993.

[72] R. M. KERR, J. A. DOMARADZKI, and G. BARBIER. Small-scale properties of nonlinear interactions and subgrid-scale energy transfer in isotropic turbulence. *Phys. Fluids*, 8(1):197 – 208, January 1996.

[73] S. A. ORSZAG, I. STAROSELSKY, and V. Y. YAKHOT. Some Basic Challenges for Large Eddy Simulation Research. In B. GALPERIN and S. A. ORSZAG, editors, *Large Eddy Simulation of Complex Engineering and Geophysical Flows*, pages 55 – 78. Cambridge University Press; Cambridge, 1993.

[74] V. M. CANUTO and Y. CHENG. Determination of the Smagorinsky-Lilly constant C_S. *Phys. Fluids*, 9(5):1416 – 1529, May 1997.

[75] A. YOSHIZAWA, M. TSUBOKURA, T. KOBAYASHI, and N. TANIGUCHI. Modeling of the dynamic subgrid-scale viscosity in large eddy simulation. *Phys. Fluids*, 8(8):2254 – 2256, August 1996.

[76] X. HUAI, R. D. JOSLIN, and U. PIOMELLI. Large-eddy simulation of spatial development of transition to turbulence in a two-dimensional boundary-layer. *Theor. Comput. Fluid Dyn.*, 9:149 – 163, 1997.

[77] X. HUAI, R. D. JOSLIN, and U. PIOMELLI. Large-eddy simulation of boundary-layer transition on a swept wedge. *J. Fluid Mech.*, 381:357 – 380, 1999.

[78] J. BARDINA, J. H. FERZIGER, and W. C. REYNOLDS. Improved Subgrid Scale Models for Large Eddy Simulation. Paper 80-1357, AIAA, 1980.

[79] M. GERMANO. A proposal for a redefinition of the turbulent stresses in the filtered Navier-Stokes equations. *Phys. Fluids*, 29(7):2323 – 2324, July 1986.

[80] K. HORIUTI. The role of the Bardina model in large eddy simulation of turbulent channel flow. *Phys. Fluids A*, 1(2):426 – 428, February 1989.

[81] K. HORIUTI and N. N. MANSOUR. A normal SGS eddy viscosity model in LES. In *Proceedings 9th Symposium on Turbulent Shear Flows. August 16 - 18. 1993. Kyoto, Japan*, pages 17–1–1.

[82] J. A. DOMARADZKI and W. LIU. Approximation of subgrid-scale energy transfer based on the dynamics of resolved scales of turbulence. *Phys. Fluids*, 7(8):2025 – 2035, August 1995.

[83] J. A. DOMARADZKI and E. M. SAIKI. A subgrid-scale model based on the estimation of unresolved scales of turbulence. *Phys. Fluids*, 9(7):2148 – 2164, July 1997.

[84] M. V. SALVETTI, Y. ZANG, R. L. STREET, and S. BANERJEE. Large-eddy simulation of free-surface decaying turbulence with dynamic subgrid-scale models. *Phys. Fluids*, 9(8):2405 – 2419, August 1997.

[85] B. J. GEURTS. Inverse modeling for large-eddy simulation. *Phys. Fluids*, 9(12):3585 – 3587, December 1997.

[86] C. HÄRTEL, L. KLEISER, F. UNGER, and R. FRIEDRICH. Subgrid-scale energy transfer in the near-wall region of turbulent flows. *Phys. Fluids*, 6(9):3130 – 3143, September 1994.

[87] U. PIOMELLI, T. A. ZANG, C. G. SPEZIALE, and M. Y. HUSSAINI. On the large-eddy simulation of transitional wall-bounded flows. *Phys. Fluids A*, 2(2):257 – 265, February 1990.

[88] A. A. ALDAMA. *Filtering Techniques for Turbulent Flow Simulation*, volume 56 of *Lecture Notes in Engineering*. Springer-Verlag; Berlin, Heidelberg, 1990.

[89] S. K. LELE. Compact Finite Difference Schemes with Spectral-Like Resolution. *J. Comput. Phys.*, 103:16 – 42, 1992.

[90] E. T. SPYROPOULOS and G. A. BLAISDELL. Evaluation of the dynamic model for simulations of compressible decaying isotropic turbulence. *AIAA J.*, 34(5):990 – 998, May 1996.

[91] U. PIOMELLI, J. H. FERZIGER, P. MOIN, and J. KIM. New approximate boundary conditions for large eddy simulations of wall-bounded flows. *Phys. Fluids A*, 1(6):1061 – 1068, June 1989.

[92] E. LINDBORG. Kinematics of homogeneous axisymmetric turbulence. *J. Fluid Mech.*, 302:179 – 201, 1995.

[93] M. PESTER and S. RJASANOW. A Parallel Version of the Preconditioned Conjugate Gradient Method for Boundary Element Equations. *Numerical Linear Algebra with Applications*, 2(1):1 – 16, 1995.

[94] R. A. CLARK, J. H. FERZIGER, and W. C. REYNOLDS. Evaluation of subgrid-scale models using an accurately simulated turbulent flow. *J. Fluid Mech.*, 91 part 1:1 – 16, 1979.

[95] N. M. EL-HADY, T. A. ZANG, and U. PIOMELLI. Application of the dynamic subgrid-scale model to axisymmetric transitional boundary layer at high speed. *Phys. Fluids*, 6(3):1299 – 1309, March 1994.

[96] C. HÄRTEL and L. KLEISER. Comparative Testing of Subgrid-Scale Models for Wall-Bounded Turbulent Flows. In CH. HIRSCH, editor, *Computational Fluid Dynamics '92*, volume 1, pages 215 – 222. Elsevier; Amsterdam, 1992.

[97] H. G. IM, T. S. LUND, and J. H. FERZIGER. Large eddy simulation of turbulent front propagation with dynamic subgrid models. *Phys. Fluids*, 9(12):3826 – 3833, December 1997.

[98] Y. KANEDA and D. C. LESLIE. Tests of subgrid models in the near-wall region using represented velocity fields. *J. Fluid Mech.*, 132:349 – 373, 1983.

[99] O. J. McMILLAN and J. H. FERZIGER. Direct Testing of Subgrid-Scale Models. *AIAA J.*, 17(12):1340 – 1346, December 1979.

[100] O. J. McMILLAN, J. H. FERZIGER, and R. S. ROGALLO. Tests of New Subgrid-Scale Models in Strained Turbulence. Paper 80-1339, AIAA, 1980.

[101] T. MIYAUCHI, M. TANAHASHI, and K. MIYAKE. Verification of SGS-Stress Models by Direct Numerical Simulation of Compressible Homogeneous Isotropic Turbulence. *JSME Int. Journal, Series B (Fluids and Thermal Engineering)*, 39(4):685 – 691, November 1996.

[102] M. TANAHASHI and T. MIYAUCHI. Assessment of Subgrid Scale Models by a Direct Numerical Simulation of a Temporal Developing Turbulent Mixing Layer. *JSME Int. Journal, Series B (Fluids and Thermal Engineering)*, 39(4):676 – 684, November 1996.

[103] U. PIOMELLI, P. MOIN, and J. H. FERZIGER. Model consistency in large eddy simulation of turbulent channel flows. *Phys. Fluids*, 31(7):1884 – 1891, July 1988.

[104] C. MENEVEAU. Statistics of turbulence subgrid-scale stresses: Necessary conditions and experimental tests. *Phys. Fluids*, 6(2):815 – 833, February 1994.

[105] M. Y. HUSSAINI, C. SPEZIALE, and T. A. ZANG. The Potential and Limitations of Direct and Large Eddy Simulations. Comment 2. In J. L. LUMLEY, editor, *Whither Turbulence? Turbulence at the Crossroads. Proceedings of a Workshop Held at Cornell University, Ithaca, N. Y., 1989.* Springer-Verlag; Berlin, Heidelberg, 1990.

[106] P. MOIN, K. SQUIRES, W. CABOT, and S. LEE. A dynamic subgrid-scale model for compressible turbulence and scalar transport. *Phys. Fluids A*, 3(11):2746 – 2757, November 1991.

[107] M. V. SALVETTI and F. BEUX. The effect of the numerical scheme on the subgrid scale term in large-eddy simulation. *Phys. Fluids*, 10(11):3020 – 3022, November 1998.

[108] L. W. B. BROWNE and A. DINKELACKER. Turbulent pipe flow: Pressures and velocities. *Fluid Dynamics Research*, 15(3):177 – 204, March 1995.

[109] J. LAUFER. The structure of turbulence in fully developed pipe flow. Rep. 1174, NACA, 1954.

[110] J. SABOT. *Etude de la coherence spatiale et temporelle de la turbulence etablieau en conduite circulaire*. PhD thesis, Université Claude Bernard de Lyon, 1976. No d'Ordre 76-36.

Other titles in the SFB393 series:

97-01 P. Benner, V. Mehrmann, H. Xu. A new method for computing the stable invariant subspace of a real Hamiltonian matrix or Breaking Van Loan's curse? January 1997.

97-02 B. Benhammouda. Rank-revealing 'top-down' ULV factorizations. January 1997.

97-03 U. Schrader. Convergence of Asynchronous Jacobi-Newton-Iterations. January 1997.

97-04 U.-J. Görke, R. Kreißig. Einflußfaktoren bei der Identifikation von Materialparametern elastisch-plastischer Deformationsgesetze aus inhomogenen Verschiebungsfeldern. March 1997.

97-05 U. Groh. FEM auf irregulären hierarchischen Dreiecksnetzen. March 1997.

97-06 Th. Apel. Interpolation of non-smooth functions on anisotropic finite element meshes. March 1997

97-07 Th. Apel, S. Nicaise. The finite element method with anisotropic mesh grading for elliptic problems in domains with corners and edges.

97-08 L. Grabowsky, Th. Ermer, J. Werner. Nutzung von MPI für parallele FEM-Systeme. March 1997.

97-09 T. Wappler, Th. Vojta, M. Schreiber. Monte-Carlo simulations of the dynamical behavior of the Coulomb glass. March 1997.

97-10 M. Pester. Behandlung gekrümmter Oberflächen in einem 3D-FEM-Programm für Parallelrechner. April 1997.

97-11 G. Globisch, S. V. Nepomnyaschikh. The hierarchical preconditioning having unstructured grids. April 1997.

97-12 R. V. Pai, A. Punnoose, R. A. Römer. The Mott-Anderson transition in the disordered one-dimensional Hubbard model. April 1997.

97-13 M. Thess. Parallel Multilevel Preconditioners for Problems of Thin Smooth Shells. May 1997.

97-14 A. Eilmes, R. A. Römer, M. Schreiber. The two-dimensional Anderson model of localization with random hopping. June 1997.

97-15 M. Jung, J. F. Maitre. Some remarks on the constant in the strengthened C.B.S. inequality: Application to h- and p-hierarchical finite element discretizations of elasticity problems. July 1997.

97-16 G. Kunert. Error estimation for anisotropic tetrahedral and triangular finite element meshes. August 1997.

97-17 L. Grabowsky. MPI-basierte Koppelrandkommunikation und Einfluß der Partitionierung im 3D-Fall. August 1997.

97-18 R. A. Römer, M. Schreiber. Weak delocalization dueto long-range interaction for two electrons in a random potential chain. August 1997.

97-19 A. Eilmes, R. A. Römer, M. Schreiber. Critical behavior in the two-dimensional Anderson model of localization with random hopping. August 1997.

97-20 M. Meisel, A. Meyer. Hierarchically preconditioned parallel CG-solvers with and without coarse-matrix-solvers inside FEAP. September 1997.

97-21 J. X. Zhong, U. Grimm, R. A. Römer, M. Schreiber. Level-Spacing Distributions of Planar Quasiperiodic Tight-Binding Models. October 1997.

97-22 W. Rehm (Ed.). Ausgewählte Beiträge zum 1. Workshop Cluster-Computing. TU Chemnitz, 6./7. November 1997.

97-23 P. Benner, Enrique S. Quintana-Ortí. Solving stable generalized Lyapunov equations with the matrix sign function. October 1997

97-24 T. Penzl. A Multi-Grid Method for Generalized Lyapunow Equations. October 1997

97-25 G. Globisch. The hierarchical preconditioning having unstructured threedimensional grids. December 1997

97-26 G. Ammar, C. Mehl, V. Mehrmann. Schur-like forms for matrix Lie groups, Lie algebras and Jordan algebras. November 1997

97-27 U. Elsner. Graph partitioning - a survey. December 1997.

97-28 W. Dahmen, R. Schneider. Composite Wavelet Bases for Operator Equations. December 1997.

97-29 P. L. Levin, M. Spasojević, R. Schneider. Creation of Sparse Boundary Element Matrices for 2-D and Axi-symmetric Electrostatics Problems Using the Bi-orthogonal Haar Wavelet. December 1997.

97-30 W. Dahmen, R. Schneider. Wavelets on Manifolds I: Construction and Domain Decomposition. December 1997.

97-31 U. Elsner, V. Mehrmann, F. Milde, R. A. Römer, M. Schreiber. The Anderson Model of Localization: A Challenge for Modern Eigenvalue Methods. December 1997.

98-01 B. Heinrich, S. Nicaise, B. Weber. Elliptic interface problems in axisymmetric domains. Part II: The Fourier-finite-element approximation of non-tensorial singularities. January 1998.

98-02 T. Vojta, R. A. Römer, M. Schreiber. Two interfacing particles in a random potential: The random model revisited. February 1998.

98-03 B. Mehlig, K. Müller. Non-universal properties of a complex quantum spectrum. February 1998.

98-04 B. Mehlig, K. Müller, B. Eckhardt. Phase-space localization and matrix element distributions in systems with mixed classical phase space. February 1998.

98-05 M. Bollhöfer, V. Mehrmann. Nested divide and conquer concepts for the solution of large sparse linear systems. March 1998.

98-06 T. Penzl. A cyclic low rank Smith method for large, sparse Lyapunov equations with applications in model reduction and optimal control. March 1998.

98-07 V. Mehrmann, H. Xu. Canonical forms for Hamiltonian and symplectic matrices and pencils. March 1998.

98-08 C. Mehl. Condensed forms for skew-Hamiltonian/Hamiltonian pencils. March 1998.

98-09 M. Meyer. Der objektorientierte hierarchische Netzgenerator Netgen69-C++. April 1998.

98-10 T. Ermer. Mappingstrategien für Kommunikatoren. April 1998.

98-11 D. Lohse. Ein Standard-File für 3D-Gebietsbeschreibungen. – Definition des Fileformats V 2.1 –. April 1998.

98-13 L. Grabowsky, T. Ermer. Objektorientierte Implementation eines PPCG-Verfahrens. April 1998.

98-14 M. Konik, R. Schneider. Object-oriented implementation of multiscale methods for boundary integral equations. May 1998.

98-15 W. Dahmen, R. Schneider. Wavelets with complementary boundary conditions - Function spaces on the cube. May 1998.

98-16 P. Hr. Petkov, M. M. Konstantinov, V. Mehrmann. DGRSVX and DMSRIC: Fortran 77 subroutines for solving continuous-time matrix algebraic Riccati equations with condition and accuracy estimates. May 1998.

98-17 D. Lohse. Ein Standard-File für 3D-Gebietsbeschreibungen. - Datenbasis und Programmschnittstelle `data_read`. April 1998.

98-18 A. Fachat, K. H. Hoffmann. Blocking vs. Non-blocking Communication under MPI on a Master-Worker Problem. June 1998.

98-19 W. Dahmen, R. Schneider, Y. Xu. Nonlinear Functionals of Wavelet Expansions - Adaptive Reconstruction and Fast Evaluation. June 1998.

98-20 M. Leadbeater, R. A. Römer, M. Schreiber. Interaction-dependent enhancement of the localisation length for two interacting particles in a one-dimensional random potential. June 1998.

98-21 M. Leadbeater, R. A. Römer, M. Schreiber. Formation of electron-hole pairs in a one-dimensional random environment. June 1998.

98-22 A. Eilmes, U. Grimm, R. A. Römer, M. Schreiber. Two interacting particles at the metal-insulator transition. August 1998.

98-23 M. Leadbeater, R. A. Römer, M. Schreiber. Scaling the localisation lengths for two interacting particles in one-dimensional random potentials. July 1998.

98-24 M. Schreiber, U. Grimm, R. A. Römer, J. X. Zhong. Application of random matrix theory to quasiperiodic systems. July 1998.

98-25 V. Mehrmann, H. Xu. Lagrangian invariant subspaces of Hamiltonian matrices. August 1998.

98-26 B. Nkemzi, B. Heinrich. Partial Fourier approximation of the Lamé equations in axisymmetric domains. September 1998.

98-27 V. Uski, B. Mehlig, R. A. Römer, M. Schreiber. Smoothed universal correlations in the two-dimensional Anderson model. September 1998.

98-28 D. Michael, M. Meisel. Some remarks to large deformation elasto-plasticity (continuum formulation). September 1998.

98-29 V. Mehrmann, H. Xu. Structured Jordan Canonical Forms for Structured Matrices that are Hermitian, skew Hermitian or unitary with respect to indefinite inner products. October 1998.

98-30 G. Globisch. The hierarchical preconditioning on locally refined unstructured grids. October 1998.

98-31 M. Bollhöfer. Algebraic domain decomposition. (PhD thesis) March 1998.

98-32 X. Guan, U. Grimm, R. A. Römer. Lax pair formulation for a small-polaron chain. (Proceedings PILS'98, in: Ann. Physik, Leipzig 1998). November 1998.

98-33 U. Grimm, R. A. Römer, G. Schliecker. Electronic states in topologically disordered systems. (Proceedings PILS'98, in: Ann. Physik, Leipzig 1998). November 1998.

98-34 C. Villagonzalo, R. A. Römer. Low temperature behavior of the thermopower in disordered systems near the Anderson transition. (Proceedings PILS'98, in: Ann. Physik, Leipzig 1998). November 1998.

98-35 V. Uski, B. Mehlig, R. A. Römer. A numerical study of wave-function and matrix-element statistics in the Anderson model of localization. (Proceedings of PILS'98, in: Ann. Physik, Leipzig 1998) November 1998.

98-36 F. Milde, R. A. Römer. Energy level statistics at the metal-insulator transition in the Anderson model of localization with anisotropic hopping. (Proceedings of PILS'98, in: Ann. Physik, Leipzig 1998). November 1998.

98-37 M. Schreiber, U. Grimm, R. A. Römer, J. X. Zhong. Energy Levels of Quasiperiodic Hamiltonians, Spectral Unfolding and Random Matrix Theory. November 1998.

99-01 P. Kunkel, V. Mehrmann, W. Rath. Analysis and numerical solution of control problems in descriptor form. January 1999.

99-02 A. Meyer. Hierarchical preconditioners for higher order elements and applications in computational mechanics. January 1999.

99-03 T. Apel. Anisotropic finite elements: local estimates and applications (Habilitationsschrift). January 1999.

99-04 C. Villagonzalo, R. A. Römer, M. Schreiber. Thermoelectric transport properties in disordered systems near the Anderson transition. February 1999.

99-05 D. Michael. Notizen zu einer geometrisch motivierten Plastizitätstheorie. Februar 1999.

99-06 T. Apel, U. Reichel. SPC-PM Po 3D V 3.3, User's Manual. February 1999.

99-07 F. Tröltzsch, A. Unger. Fast solution of optimal control problems in the selective cooling of steel. March 1999.

99-08 W. Rehm, T. Ungerer (Eds.). Ausgewählte Beiträge zum 2. Workshop Cluster-Computing 25./26. März 1999, Universität Karlsruhe. März 1999.

99-09 M. Arav, D. Hershkowitz, V. Mehrmann, H. Schneider. The recursive inverse eigenvalue problem. March 1999.

99-10 T. Apel, S. Nicaise, J. Schöberl. Crouzeix-Raviart type finite elements on anisotropic meshes. May 1999.

99-11 M. Jung. Einige Klassen iterativer Auflösungsverfahren (Habilitationsschrift). Mai 1999.

99-12 V. Mehrmann, H. Xu. Numerical methods in control, from pole assignment via linear quadratic to H_∞ control. June 1999.

The complete list of current and former preprints is available via
`http://www.tu-chemnitz.de/sfb393/preprints.html`.